STUDIES ON GRAPHENE OXIDE BASED NANOCOMPOSITES AND THEIR APPLICATIONS

**Thesis submitted to the Delhi Technological University
for the award of the Degree of**

DOCTOR OF PHILOSOPHY

By

SAKSHI VERMA
(2K18/Ph.D./AC/06)

**DEPARTMENT OF APPLIED CHEMISTRY
DELHI TECHNOLOGICAL UNIVERSITY
BAWANA ROAD, DELHI-110042
INDIA**

JULY 2024

STUDIES ON GRAPHENE OXIDE BASED NANOCOMPOSITES AND THEIR APPLICATIONS

**Thesis submitted to the Delhi Technological University
for the award of the Degree of**

DOCTOR OF PHILOSOPHY

By

SAKSHI VERMA
(2K18/Ph.D./AC/06)

**DEPARTMENT OF APPLIED CHEMISTRY
DELHI TECHNOLOGICAL UNIVERSITY
BAWANA ROAD, DELHI-110042
INDIA**

JULY 2024

Dedicated
To
My Father

DECLARATION

I state that this Ph.D thesis titled "**Studies on Graphene Oxide Based Nanocomposites and their Applications**" was completed by me for the award of degree of Doctor of Philosophy under the supervision of Prof. D. Kumar, Department of Applied Chemistry, Delhi Technological University and Dr. Chandra Mouli Pandey, SGT University, Gurugram, Haryana.

This thesis presents the results of my original research work. Every effort has been made to indicate any contributions made by others with proper citation.

No degree or diploma has ever been awarded to me from this or any other University for the present thesis which I am submitting to the Delhi Technological University.

Place: **Ms. Sakshi Verma**

Date: Delhi Technological University

CERTIFICATE

This is to certify that the thesis entitled **"Studies on Graphene Oxide Based Nanocomposites and their Applications"** submitted by **Ms. Sakshi Verma** to **Delhi Technological University**, for the award of the degree of "Doctor of Philosophy" is a record of the work carried out by her. Ms. Sakshi Verma has worked under our guidance and has fulfilled the requirements for the submission of this thesis.

The results embodied in this thesis have not been submitted to any other university or institute for the award of any degree or diploma as per our knowledge and belief.

Prof. D. Kumar
Professor
Department of Applied Chemistry
Delhi Technological University
Bawana Road, Delhi- 110042

Dr. C. M. Pandey
Assistant Professor
Department of Chemistry
SGT University, Gurugram
Haryana- 122505

Prof. Anil Kumar
Head, Department of Applied Chemistry
Delhi Technological University
Bawana Road, Delhi- 110042

ACKNOWLEDGEMENT

ABSTRACT

The research work reported in this thesis states the fabrication of a biosensing electrode that provides quantitative information for the detection of water pollution phenolic compounds. Bio-sensing is achieved by utilizing a biological recognition element that must be in direct spatial contact with a transducer which in turn converts the biological signal to measurable electrical signal. Biosensors chiefly consist of two parts viz, bio-recognition element and sensing element. Generally, enzymes, antibodies, DNA, etc., are used for the specific detection of analyte. Biosensors used in multidisciplinary fields of science and technology still have a lot of space for innovation. Recently, a new generation of biosensors has become popular and designed to assist in combining biological molecules with a biocompatible nanotechnology conducting framework. Organic chemicals are being regressively used for development, modernization, and urbanization for industries and domestic purposes. There is always a considerable quantity of untreated effluents that run into the water system. Hydroquinone and catechol are some of the most widely used chemicals in industries and are the main constituents in photography, stabilizers in paints, dye intermediates, etc. However, even low concentration acquaintance with phenol derivatives in water reservoirs can cause numerous health issues.

Graphene oxide (GO) has attracted much attention in biosensor application. This is due to owing its distinct electrical features, high surface area, superior conductivity, excellent charge transfer capability, flexibility of functionalization and biocompatibility. Furthermore, due to its high electrocatalytic activity and potential to exhibit direct electron transfer property, GO has been investigated as a sensitive

platform in electrochemical biosensors. The incorporation of nanomaterials such as metal oxides and metal sulphides has sparked considerable attention due to possibility of tailoring the specific features of each component into single material.

Additionally synergetic effects of these materials have influenced the biosensor performance, resulting in the better sensitivity and selectivity. Thus, the present study focusses on the synthesis, characterization and application of rGO (reduced graphene oxide) based nanocomposites with MgO and MoS$_2$, in the development of efficient electrochemical biosensors for the sensitive and selective detection of hydroquinone using enzymatic and non-enzymatic approaches. The detection was carried out using amperometry technique wherein, synthesized nanocomposites were electrophoretically deposited onto ITO glass substrate. Under enzymatic approach, laccase enzyme has been immobilized onto modified ITO sheets. The fabricated platform was found suitable for detection of phenolic water pollutants under spiked river and tap water samples, proving its efficiency.

CONTENTS

Chapter 4: Enzymatic biosensor based on Graphene oxide/MoS₂ nanocomposite for Phenolic Compounds detection

LIST OF FIGURES

LIST OF TABLES

ABBREVIATIONS

CNms	Carbon nanomaterials
CNTs	Carbon nanotubes
MWCNTs	Multi-walled carbon nanotubes
SWCNTs	Single-walled carbon nanotubes
GO	Graphene oxide
rGO	Reduced graphene oxide
CVD	Chemical Vapor deposition
LPE	Liquid phase exfoliation
MMC	Micromechanical cleavage
EC-Red	Electrochemical reduction
PANI	Polyaniline
PEDOT:PSS	Poly(3,4-ethylenedioxythiphene) polystyrene
PC	Phenolic compounds
PhCs	Phenolic contaminents
Lac	Laccase enzyme
LEB	Laccase enzyme based biosensors
UV-Vis	Ultra Violet visible
FT-IR	Fourier transform Infrared spectroscopy
XRD	X ray diffraction
SEM	Scanning electron microscopy

TEM	Transmission electron microscopy
EDX	Energy dispersive X-ray Analysis
EIS	Electrochemical impedance spectroscopy
AC	Alternate currents
CPE	Constant phase element
CV	Cyclic voltammetry
SWV	Square wave voltammetry
LOD	Limit of detection
EDC	1-Ethyl-3-(3-dimethylaminopropyl)carbodiimide)
NHS	N-hydroxylsuccinimide
ITO	Indium tin oxide
FE-SEM	Field emission scanning electron microscopy
Hq	Hydroquinone
Ctl	Catechol

CHAPTER 1

INTRODUCTION

1.1. Carbonaceous Nanomaterials

The element Carbon, having atomic number 6, has taken its name from the Latin word 'carbo', which means 'coal'. This versatile element has been widely distributed in nature and is regarded as the 15th most abundant element on earth's crust. Carbon has a unique electronic structure allows it to undergo sp^3, sp^2, and sp hybridization, resulting in the formation of stable allotropes having a massive surface-to-volume ratio compared to other elements. The typical examples of allotropes of carbon are graphite, diamond, and fullerene [1]. Carbon nanomaterials (CNms) comprise pure carbon; subsequently, a major part of the human body contains carbon in one form or another; therefore, these materials are considered highly biocompatible [2]. CNms have significantly gained attention because of their low toxicity and superior optical, electronic, mechanical, thermal, and chemical properties. These materials are found to be highly accessible to electrolytes due to their excellent electrical conductivity, linear geometry, and large surface-to-volume ratio.

The popularity of CNms is increasing because of their applications in numerous fields, specifically in electronics. The combination of nano range diameter and micro range length of such materials, along with the optoelectronic properties, makes them promising candidates. It has been found that composites made by using such nanostructures give rise to new engineering outcomes in biomedical applications, chiefly drugs, biosensing, and pharmaceuticals. However, commercial viability for such applications is still limited [3].

Advanced technologies utilize CNms of zero, one, two and three dimensions, which offer new opportunities in the field of research. Fullerenes, graphene, carbon nanotubes (CNTs), carbon quantum dots, and carbon nanofibers are among the majorly benefiting CNms for various applications **(Fig. 1.1).**

Carbon nanomaterials
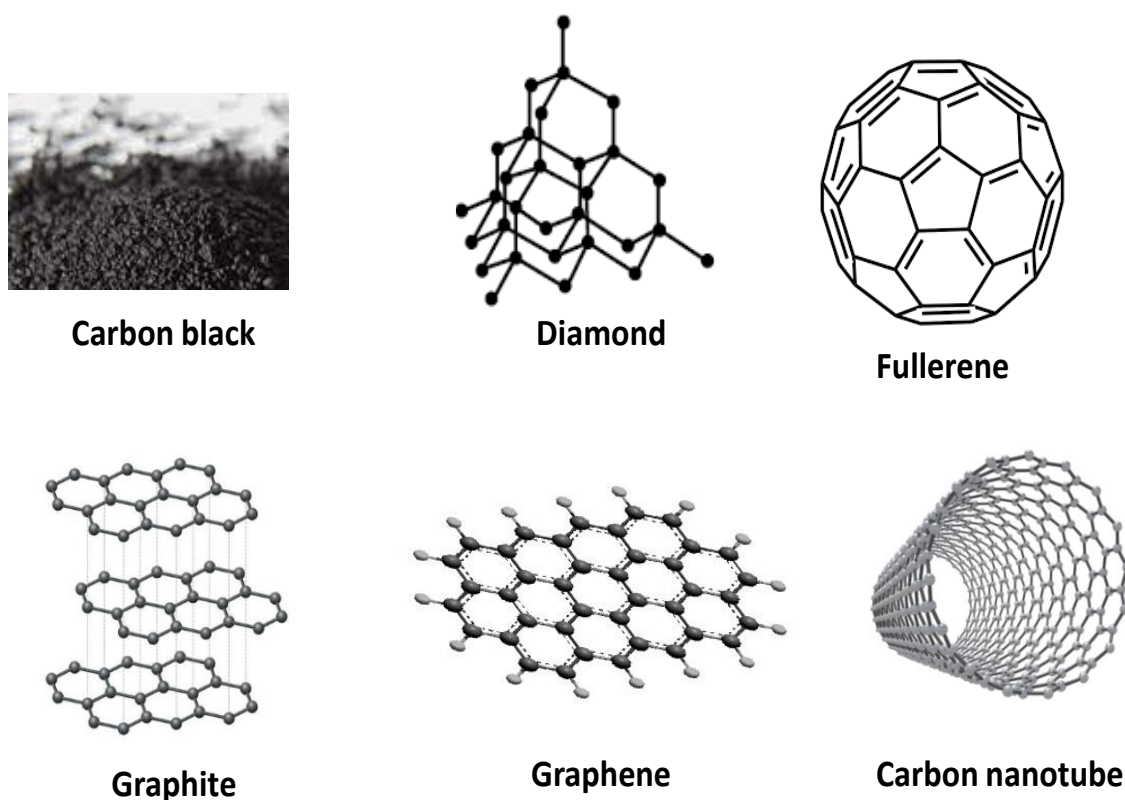
Fig. 1.1: Different carbon-based nanomaterials

1.2. Classification of CNms

CNms are among the most important categories of nanomaterials with variable entities and unique characteristics. This section deals with the detailed properties of different categories of CNms based on dimensionality: 0D (fullerenes, carbon dots, diamond), 1D (carbon nano tubes, carbon nano fibers), 2D (graphene) and 3D

(graphite). A brief comparison of important properties of which has been mentioned in **Table 1.1**.

Table 1.1: Comparative properties of different CNms

Carbonaceous Nanomaterials	Dimensions/ Hybridization	Experimental Specific surface area ($m^2 g^{-1}$)	Thermal Conductivity ($W m^{-1} K^{-1}$)	Electrical Conductivity ($S cm^{-1}$)
Graphite	3 / sp^2	~ 10- 20	1500-2000, 5-10	2 – 3 * 10^4
Graphene	2 / sp^2	~ 1500	4840 - 5300	~ 2000
CNTs	1 / generally sp^2	~ 1300	3500	Varies on the basis of structure
Fullerene	0 / generally sp^2	80 - 90	0.4	10^{-10}

1.2.1. Fullerene

Fullerene is an allotrope of carbon whose unique properties like electronic structure, solvent dispersibility and ease of modification make it a suitable nanomaterial for various applications. Among the various fullerene, Buckminsterfullerene (C60) is a 0D closed hollow cage-like material having 60 carbon atoms in sp^2 hybridization and was discovered in 1985 [4]. The average diameter of C60 has been found to be 1 nm [5]. Besides the well-known C60 structure, fullerene also exists in larger structures viz., C70, C76, and C78. Fullerenes possess remarkable mechanical characteristics, superior resisting pressure and the ability to retain their original structure even after dealing with a high pressure of more than 3000 atm. The theoretical bulk modulus for a single molecule of C60 (75% compressed) is 668 GPa, which signifies the hardness of fullerene [6]. Due to such properties and the delocalization of π electrons,

fullerenes are suitable for different biomedical applications such as antimicrobial activity, drug delivery, antioxidant activity, etc [7]. However, their poor solubility in polar solvents limits their application [8].

1.2.2. Carbon nanotubes (CNTs)

CNTs are widely explored cylindrical carbon nanostructures with a diameter of a few nanometers. The first tubular structure of carbon atoms arranged in a cage-like structure was observed in 1991 by Iijima [9]. The nano-sized tubes comprised of multiple graphitic sheets known as multi-walled CNTs (MWCNTs) separated by a distance of approximately 0.34 nm and a diameter of 1 nm. Two years later, Single-walled CNTs (SWCNTs) were also discovered [10]. The overall structure and properties of two types of CNTs depend on their shape, i.e., their length, small diameter and surface morphology. CNTs can be regarded as semiconductors or conductors/metals based on chirality. The theoretical electrical current density of metallic CNTs has been observed to be 1000 times better as compared to metals like copper. CNTs offer much greater tensile strength (SWCNTs – 50 times, MWCNTs-200 times) and one-sixth density when compared to steel, whereas their thermal conductivity is much higher than diamond. In addition, they offer a superior theoretical surface area of more than 1300 m^2/g. Compared to other semiconductors, one-dimensional semiconducting CNTs enable tubular ballistic transport, giving rise to high intrinsic mobility. This unique carbon structure has been found to be extremely light-weight and chemically stable. As a result, CNTs remain an ideal candidate for applications like batteries, supercapacitors, electrochemical biosensors, hydrogen storage cells etc. [11].

1.2.3. Graphite and Graphene

Graphite is the 3D, most versatile allotrope of carbon, which comprises layers of carbon atoms having sp^2 hybridization stacked by the weak Van Der Waals forces. Each layer is arranged in a 2D honeycomb-like lattice and is referred to as graphene. A single graphene sheet was first extracted using micromechanical cleavage of graphite in 2004 [12].

Graphene is the thinnest 2D material, which possesses excellent anisotropic behavior in terms of high thermal conductivity ($\sim 5,000$ W m^{-1} K^{-1}), electrical conductivity (6500 S m^{-1}) and mechanical stiffness (tensile strength ~ 130 GPa) [13]. Conductivity among graphene layers is in-plane, i.e., in the direction parallel to layers because of the overlapping of sp^2 hybrid orbitals. However, the p_z orbitals overlay to result in an occupied valence band of π orbitals and a vacant π^* orbitals conduction band, which is accountable for the planar conduction. It exhibits high electron mobility ($> 10^4$ cm^2 V^{-1} s^{-1}) at ordinary temperature and is a zero-band gap semiconductor. Also, it can sustain one million times more electrical current densities than copper [14].

Graphene possesses remarkable optical transparency and is impermeable to gases. Among various properties of graphene, its negligible effective mass and stretchability (20%) due to its incomparable large theoretical specific surface area (2391 m^2 g^{-1}) attracts special attention [15],[16]. In addition, graphene offers superior biocompatibility because of its unique surface properties. Due to such extraordinary properties, graphene-based materials can be utilized in biomedical applications, transistors, sensors, solar cells, catalysis, environmental remediation, energy production, and much more [17].

Graphene is comparatively hard to produce and lacks functionality; therefore, continuous efforts have been made to utilize the unique properties of graphene-based derivatives and related materials by finding effective and reasonable ways [18]. Plenty of work has been done on graphene-based materials to enhance their functionality and dispersibility in solvents so that they can be used for broad applications.

1.2.4. Derivatives of Graphene

Bottom-up synthesis, poor solubility, and excessive agglomeration limit pristine graphene use. Alternatively, compounds with an approximately similar arrangement to graphene have been produced using raw graphite or any carbon source through a top-down approach so that the advantages of pristine graphene could be retained and overcome the limitations **(Fig. 1.2).**

Graphite   **Graphene**   **Graphene oxide**   **Reduced graphene oxide**
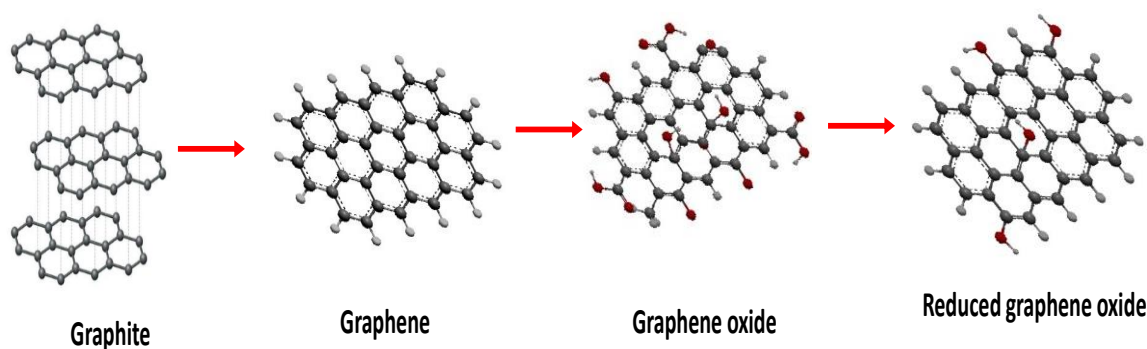
Fig. 1.2: Conversion from graphite to reduced graphene oxide

One such derivative is graphene oxide (GO), which is a carbonaceous structure arranged in a stacked layered fashion in which oxygenated functional groups, particularly hydroxyl (-OH), carbonyl (C=O), epoxy (C-O-C), the carboxylic acid (-COOH) etc., are attached to the surface and the edges of the plane. Oxidation of graphite leads to graphite oxide, which yields GO in protonated solvents on further exfoliation. Functional oxygen-containing groups make GO a hydrophilic material,

thus providing better solubility in water and organic solvent. In addition, the functionality of GO makes it possible to integrate with other nanomaterials [19].

The specific surface area of GO sheets has been observed to be around 890 $m^2 g^{-1}$, along with tensile strength of 120 MPa and Young's modulus of approximately 210 GPa. Broadly, the chemical compositions of GO rely on graphite or the method of synthesis. The conductivity of GO is highly dependent on the extent of oxidation and thermal conditions. Over-oxidized GO is a poor electrical conductor as the band gap is nearly 2.2 eV [20].

Another derivative of graphene is reduced graphene oxide (rGO); a number of approaches have been adopted for the synthesis of rGO so that the properties of graphene can be regenerated accompanied by the presence of functional groups. A general comparison of the general characteristics of graphene, GO and rGO has been depicted in Table 1.2 [20].

Table 1.2: Comparative general properties of Graphene, GO and rGO

Properties	Graphene	GO	rGO
Electron mobility at room temperature ($cm^2 V^{-1} s^{-1}$)	~2,00,000 – 2,50,000	0.1 -10	2 - 200
Thermal conductivity ($W m^{-1} K^{-1}$)	~5000	0.5 - 18	1390 - 2275
Surface area ($m^2 g^{-1}$)	2630	736.6	466 - 758
Specific capacitance ($F g^{-1}$)	550	215 - 255	210 - 425
Electrical conductivity ($S m^{-1}$)	~6 * 10^8	5.7 * 10^{-6}	10^2 - 10^5

The aim of reducing GO to rGO is to achieve characteristics of pristine graphene by diminishing oxygen groups from the surface of GO. The extent of oxygen reduction

from GO and the methods of reduction viz, thermal reduction, chemical reduction, electrochemical reduction and hydrothermal reduction, decides the characteristics of the sheets. The partially reduced form of GO i.e., rGO regains π conjugation of electrons in the system, thus leading to a drastic increase in properties such as thermal and electrical conductivity. With the exception of certain residual oxygen and structural flaws, the assembly of rGO is similar to that of graphene.

1.3. Synthesis of Graphene and its derivatives

The desired structure of graphitic materials depends on size, shape and functional group types aligned at the surface. Ideally, a single graphene layer's structure consists of one thick atom sheet with a sp^2 hybridized carbon network comprising negligible defects. A single sheet (graphene) is obtained only after exfoliation of a multi-layered structure with stacked sheets. Although for industrial applications, the synthesis of such structures, the bottom-up practice has been observed as a difficult approach. However, the top-down approach has been observed as a comparatively easier approach to synthesizing an oxidized form of graphene having both sp^2 and sp^3 carbon layers rich in oxygen groups. Further, on reduction of which maximum sp^3 hybridized carbon and oxygen-containing functional groups give rise to a graphene like environment (rGO) having highly enhanced properties as compared to GO [21]. This section discusses the detailed synthesis process of graphene, GO and rGO.

1.3.1. Synthesis of Graphene

Brodie and Schafhaeutl observed the very first successful isolation of graphene [22]. By the end of 1940, P.R. Wallace suggested various astonishing theoretical electronic and mechanical properties of isolated graphite sheets. However, in the diluted alkaline

medium along with hydrogen sulphide, hydrazine, or iron salts (reducing agents), a structure similar to that of graphene synthesized using graphite flakes was first described in 1962. Consequently, after 40 years, in 2004, Gein and Novoselov successfully produced thin carbon flakes using the micromechanical method and won the Nobel Prize in Physics in 2010. Later numerous graphene synthesis methods were reported [23].

The two most popular suggested routes for graphitic material synthesis have been categorized as top-down and bottom-up approaches **(Fig. 1.3).** In the top-down approach, graphite is used to produce graphene by dissociating it into the smallest possible constituents. Plasma etching, liquid phase exfoliation, electrochemical exfoliation, ball milling, and chemical reduction remain the chief top-down approaches. However, the bottom-up synthesis approach includes using basic carbon materials to synthesize graphene and assembling a hexagon-type arrangement of graphene layers. CVD, thermal pyrolysis, and epitaxial growth are often utilized bottom-up methods for synthesizing graphene.
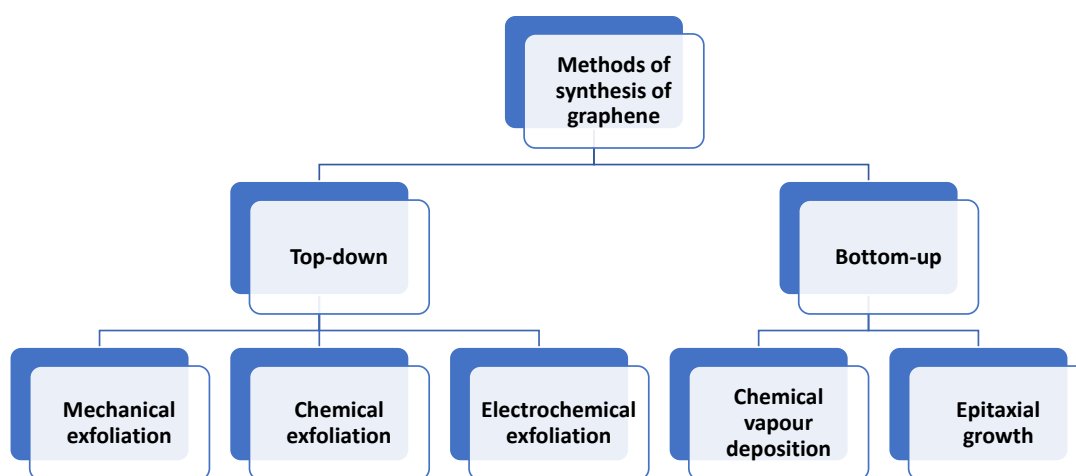
Fig. 1.3: Scheme representing the most popular methods of synthesis of graphene

Commonly implemented methods have been discussed in the subdivisions below and summarised in **Table 1.3**.

1.3.1.1. Chemical vapor deposition (CVD)

CVD is a very popular bottom-up synthesis approach for synthesizing high-quality graphene. In this approach, the synthesis of graphene is carried out either using carbonaceous gases such as methane by collecting their vapors or by the detachment of carbon from the surface of metal/metal carbide mixtures. Several factors affect the reactions involving the synthesis of graphene in a CVD reactor, some of which are the effect of temperature, proportion, and pressure of gases etc. Besides these factors, the time of deposition and type of substrate and material to be decomposed have also been found responsible. The major shortcoming of using the CVD technique is that it requires extremely high temperatures for operation and leads to the formation of toxic gases as byproducts. In addition, under this technique, the synthesized graphene has to be transferred from the substrate, which is challenging and gives rise to surface defects. Attempts to use this technique at lower temperatures are underway [24][25].

1.3.1.2. Epitaxial growth

Epitaxial growth of graphene is a bottom-up approach to produce single-layer graphene in bulk, and this takes place at silicon carbide (SiC) like substrate by thermal decomposition. Since the vapor pressure of Si is much higher than carbon, while subjecting to higher temperature (< 1400°C) and high Ar pressure on SiC substrate, early Si desorption occurs from the surface of SiC.

Therefore, a surface rich in carbon atoms is left behind on which the growth of graphene initiates. The graphene layers thus formed are known as epitaxial layers.

This approach has been found extremely promising to produce superior quality graphene layers comprising large surface areas and uniform thickness. In addition, one major ease and advantage of using this approach compared to CVD is that we do not need to transfer graphene to another substrate after synthesis [22].

1.3.1.3. Liquid phase exfoliation (LPE)

LPE has been considered an excellent technique for synthesizing graphene in bulk. This method is widely employed in both industrial as well as in research. The foremost successful LPE was performed by sonicating graphite powder in N-methyl pyrrolidone solvent. LPE by sonication is advantageous because the size and distribution of graphene flakes can be controlled using this method. However, its limitation remains low efficiency, inhomogeneous flakes, costly, and huge energy requirement. To overcome the limitations of sonicated assisted LPE, a microfluidizer LPE approach has been developed, which processes the graphene synthesis at ambient pressure and temperature to produce a good yield [26]. For even better performance, stabilizers like sodium salt of a styrene-maleic anhydride copolymer have also been utilized in the microfluidizer-based LPE method [27].

1.3.1.4. Mechanical exfoliation

Mechanical exfoliation embraces various top-down approaches such as micromechanical cleavage (MMC), sonication and ball milling to synthesize graphene. Out of which, the MMC has been extensively used to manufacture high-quality graphene with micro-scale dimensions. In 2004, Novoselov et al. were the first to execute MMC, also named by 'Scotch tape technique,' which was used to isolate graphene layers from a piece of exceedingly ordered pyrolytic graphite. Later, in

2010, a Nobel prize in Physics rewarded them for this discovery [28]. Yet research is needed for the betterment of this technique because of constraints like low yield, time-consuming exfoliations, unsustainable commercial application etc.

1.3.1.5. Chemical exfoliation

Chemical exfoliation is a top-down approach observed as an efficient, cost-effective method for synthesizing graphene-like structural sheets (GO/rGO). This method produces a large quantity of graphene layers via the isolation of graphite using either oxidation or reduction processes. In this method, the interspacing of sheets increases, thereby minimizing the van der Waals force of attraction between graphite sheets under harmful solvents like hydrazine hydrate, N-methyl pyrrolidone etc., or oxidizing agents like $H_2SO_4/KMnO_4$ and H_2SO_4/HNO_3 [29].

1.3.1.6. Electrochemical exfoliation

Electrochemical exfoliation is an attractive top-down approach for graphene synthesis as it does not use harmful chemicals since this method's driving force is exfoliation and the presence of controllable electromotive force. Also, it requires a very short time for synthesis, is a low-cost instrument and produces high-quality graphene. The mechanical approach for this process includes applying a constant voltage to the graphitic electrodes, reducing van der Waals forces existing among graphite; thus, layers get separated. One another attractive feature of this method is to extract graphene from used graphite electrodes, which is a greener recycling approach. Contrary to this, non-homogeneous thickness and uncontrolled oxidation of graphene layers are the limitations of this method [30].

Table 1.3: Summary of different methods for the synthesis of graphene

Technique	Advantages	Limitations
Chemical vapor deposition	High quality	Costly
	Bulk	Complicated procedure
	Scalable	Transfer of substrate required
	Excellent conductivity	
	Choice for carbon precursors	
Epitaxial growth	No need to transfer substrate	Costly
	Minimal defects	Uncontrolled thickness
	High in quality	Probability to have some multi-layered graphene
Chemical exfoliation	Cost efficient	High chances of defects
	Excellent yield	Well functionalised
	Scalable	
Electrochemical exfoliation	Scalable	Chances of oxidation
	High quality	
	Cost efficient	
	Eco-friendly	
	Short duration	
Liquid phase exfoliation	Cost efficient	Low yield of monolayer
	Scalable	Time taking
	High quality	Small in size
	A few experimental conditions	Lacs in homogeneity
Mechanical exfoliation	Monolayer product	Low yield
	High quality	Non-scalable
	Defect less	Intensive labour required
	Large in size	

1.3.2 Synthesis of Graphene oxide (GO)

The oxidation of graphite to GO is entirely based on solvent-dependent methods. In 1859, Brodie used 1:3 ratio of graphite and potassium chlorate ($KClO_3$) followed by the addition of fuming nitric acid (HNO_3) and reacted the mixture for 3-4 days,

maintaining the temperature of 60°C for the successful synthesis of GO. It was assumed that only this mixture could produce GO with graphitizable carbons at that time. However, being time-consuming and using hazardous solvents, the method was observed to be less popular. Afterward in 1898, Staudenmaier reported a better yield of GO using H_2SO_4, HNO_3, and $KClO_4$ as solvents with graphite powder reacted under a single vessel. Here, two-thirds of fuming HNO_3 was replaced by H_2SO_4 and the process was completed in nearly 4 days [31]. Later in 1958, Hummer and Offeman demonstrated a more straightforward method for synthesizing graphite oxide using H_2SO_4, HNO_3 and $KMnO_4$. They improved previously proposed methods by replacing $KClO_3$ with $KMnO_4$ as an oxidizing agent because of the evolution of toxic ClO_2 gas while using $KClO_3$ [32]. The reactions involving all three methods have been illustrated below.

(1) Brodie method

$$\text{Graphite + KClO}_3 \xrightarrow[\text{60 °C}]{\text{HNO}_3} \xrightarrow{\text{H}_2\text{O}} \xrightarrow{\text{Exfoliation}} \text{GO}$$

(2) Staudenmaier method

$$\text{Graphite} \xrightarrow[\text{5 °C}]{\text{+H}_2\text{SO}_4/\text{HNO}_3} \xrightarrow{\text{KClO}_4} \xrightarrow{\text{H}_2\text{O}} \xrightarrow{\text{Exfoliation}} \text{GO}$$

(3) Hummer-Offeman method

$$\text{Graphite} \xrightarrow[\text{5 °C}]{\text{+H}_2\text{SO}_4} \xrightarrow[\text{<20 °C}]{\text{KMnO}_4} \xrightarrow[\text{90 °C}]{\text{H}_2\text{O}} \xrightarrow{\text{H}_2\text{O}_2} \xrightarrow{\text{Exfoliation}} \text{GO}$$
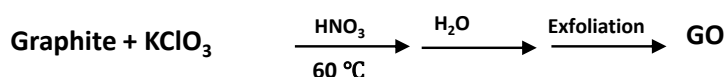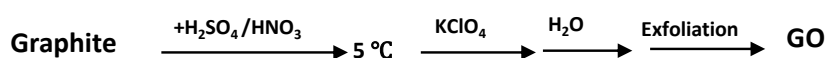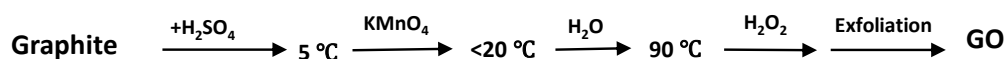
Amongst all methods, **Hummer's method has** gained maximum popularity and application. In this method, H_2SO_4 and $KMnO_4$ were used along with sodium nitrate ($NaNO_3$). The purpose of using $NaNO_3$ is to form in situ nitric acid to make the

process safer. Using Hummer's method, GO can be synthesized in bulk in just a few hours [33]. However, even Hummers' method is not green since it produces toxic gases like NO_2 and N_2O_4. [34]. Recently, an **improved Hummers' method** has been utilized as it excludes $NaNO_3$ while increasing the percentage of $KMnO_4$ in a mixture of solvents ($H_2SO_4:H_3PO_4 = 9:1$). The process is easy to perform (controllable temperature) and within few hours hydrophilic oxidized GO is being synthesized [35]. **Fig. 1.4** gives a brief overview of different Hummer's methods.
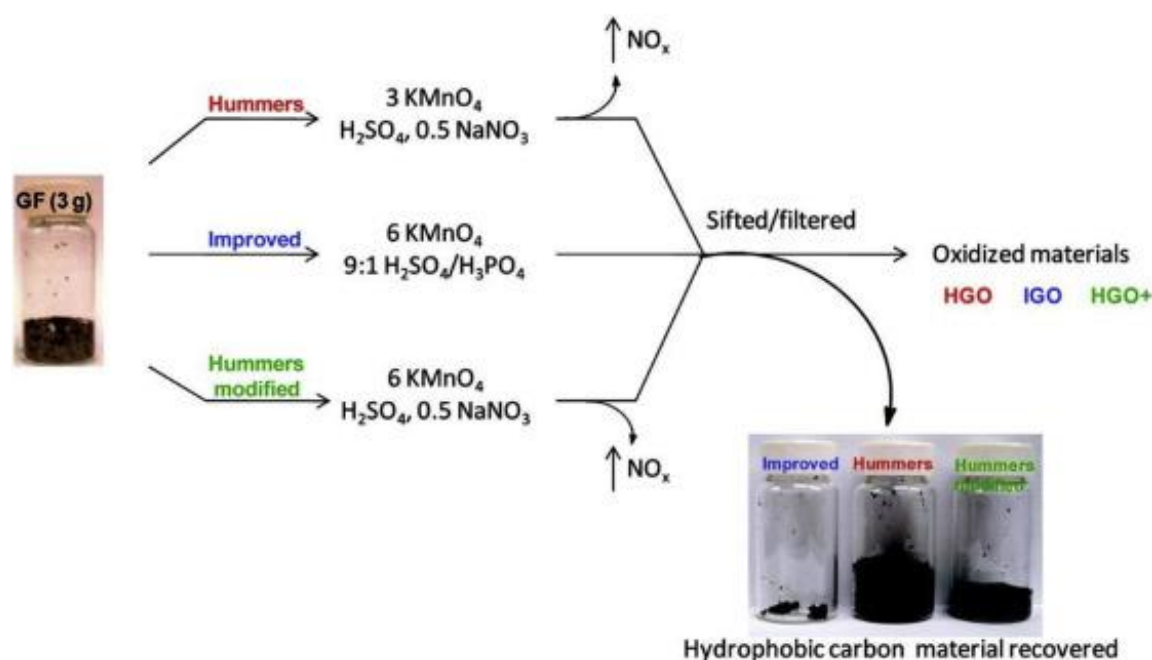
Fig. 1.4: Scheme representing development in Hummer's methods.

1.3.3. Synthesis of reduced Graphene oxide

The most common and simplified method for the reduction of GO is through its exfoliation in solvents. However, many more methods for reduction have been adopted by researchers, the major categories of which have been discussed in this section [36].

1.3.3.1 Chemical reduction

The most commonly used reducing agent is hydrazine monohydrate ($N_2H_4.H_2O$). rGO obtained using this method was observed to have the closest resemblance with pristine graphene in terms of conducting and structural properties. The very first reported hydrazine monohydrate-based reduction resulted in conductivity of nearly 200 S m^{-1} and had the indulgence of nitrogen upon rGO sheets and a C: N ratio of 16:1. However, the extent of reduction was carried out at different temperatures ranging from 15 – 95°C. Better yield has been obtained when the reaction was carried out at 95°C for 3 h, where a noteworthy increment in conductivity was observed [37]. Metals such as zinc and aluminum have been used as catalysts for vigorous GO reduction in an acidic medium within an hour. Zn and Al react with acid, e.g., HCl, to release H_2 gas, which on reaction with oxygenated functional groups of GO produces rGO. This method's electrical conductivity of rGO sheets obtained is nearly 2.1×10^3 S m^{-1} [38]. The chemical reduction has also been observed using various sodium metal-containing reducing agents such as sodium borohydride, sodium hypophosphite monohydrate, sodium tetraborate decahydrate, sodium bisulfite ($NaHSO_3$) and sodium sulfide (Na_2S). The most common reducing agent among these compounds is $NaBH_4$. For the reduction of GO, $NaBH_4$ has been found to be used with Ag nanoparticles, which were later observed to be colloidally unstable [39]. In another study, it was used merely in basic conditions, which offered conductivity of rGO around 10-1500 S m^{-1} on the basis of exposure time for reduction [40].

1.3.3.2. Biological reduction (Green reduction)

Ascorbic acid has been found to be the most commonly used low-cost, environment-friendly route for the reduction of GO. The reaction can occur in various solvents

such as water and N, N-dimethylformamide etc. This method offers rGO with electrical conductivity ranging from 4.13×10^{-7} to 0.28 S m^{-1} [39]. With the aim to adopt a greener approach for the reduction of GO so that cytotoxicity can be minimalized, a variety of plant extracts sourced from different parts of plants have been studied and experimented. For instance, green tea, pomegranate juice, marigold flower, spinach, caffeic acid, gallic acid, starch, rose water, orange peel extract, and many more. The principal component of roughly all plants remains polyphenol or flavonoids [41]. Besides plants, in particular, polysaccharides and proteins have found significance for the reduction of GO. For this, glucose (less efficient), sucrose, L-cysteine (common), glycine, bovine serum albumin, dopamine etc has been used [42][43]. The quality of rGO using such reduction compounds can be enhanced by adding metal-based catalysts or varying reaction conditions such as pH.

Another section of biocompatible reducing agents used so far includes microorganisms especially pathogens and yeast. The first bacteria which was extensively explored for this purpose was 'Shewanella'. It was utilized while keeping in mind its metal-reducing behavior. However, it is only able to reduce hydroxyl moieties, not the carbonyl ones [44]. Gram-negative bacteria Escherichia coli (E. coli) and yeast are among other microorganisms explored for reduction of GO, being cheap, abundant and biocompatible [45].

1.3.3.3. Electrochemical reduction (EC-Red)

Electrochemical techniques like cyclic voltammetry and linear sweep voltammetry have been utilized to reduce GO to rGO. For this, a constant optimized voltage is applied to the colloidal solution of GO, which is then used to form thin films of rGO

in a three-electrode set up at the surface of the electrode by supplying a constant optimized voltage. Moreover, EC-Red can also be processed after coating GO on the electrode, followed by its electrochemical reduction in buffer using a standard three-electrode set-up. The EC-Red has been found advantageous over chemical reduction techniques: quick, eco-friendly, low cost, works at room temperature, and most importantly, it offers access to regulate the size and thickness of rGO sheets [46].

1.3.3.4. Thermal reduction

Thermal annealing is a simple yet direct method for the reduction of GO. The extent of adsorption or the temperature to be applied depends on the requirement of application. In addition, several temperature-programmed desorption measurements have been performed to understand the kinetics and thermodynamics behind this reaction. Microwave irradiation is another thermal method used for very fast and direct reduction of GO. Using a standard microwave, Voiry et al. created large-size rGO sheets by irradiating GO with short pulses that lasted for a couple of seconds [47]. GO was also reduced in the solid state by Tang S. et al. utilizing a two-step pre-annealing and microwave irradiation procedure [48]. They observed that slightly reduced GO could minimize the loss of heat from the surface of GO and their temperature stability can be sustained while heating. Growing interest in quick, easy to use, non-destructive, and eco-friendly methods laid to cultivate interest in hydrothermal reduction in autoclaves. In this method, suspensions are placed in an autoclave and the hydrothermal reaction is commonly carried out at nearly 180-200°C for 6-8 h [49].

1.4. GO-based nanocomposite

GO-based nanocomposites have gained enormous attention due to their unique properties. Various efforts have been made to utilize GO for various applications by integrating GO with different nanomaterials, conducting polymers etc., to synergistically enhance their catalytic, electronic, magnetic, and optoelectronic behavior. Besides improving the properties of graphene, the added nanoparticles also act as a stabilizer that could protect the accumulation of distinct graphene layers held by strong van der Waals forces. Main group metals, transition metals, their oxides, and sulphide have been widely used to make nanocomposite with GO.

Bartolucci et.al fabricated Al-graphene using milling, hot isotactic pressing and hot extrusion for the first time [50]. They observed defects created in graphene using this method were responsible for increasing the interfacial binding. Other metals like Cu, Mg, Ni and Fe also replaced Al for synthesizing graphene-metal composite [51]. Coinage metals Au, Ag and Pt have also gained much attention with GO for use in numerous applications. Ag-doped graphene oxide possesses promising properties such as low resistance, high dispersibility, and advanced mechanical strength. Basically, Ag like metals get easily dispersed on layers of GO and effortlessly intercalate in between layers to enhance the electrochemical properties of GO [52]. On the other hand, metal oxide nanoparticles (ZnO, MgO, TiO_2, CuO, AgO, Al_2O_3, NiO and many more) have significantly gained attention to make nanocomposite with Gr-M. Their superior physical, chemical, thermal and mechanical properties have been explored to utilize them as electrode materials for electrical energy storage devices. Several rGO based nanocomposites such as ZnO/rGO, TiO_2/rGO, MoS_2/rGO

etc., have been synthesized by our group for electrochemical and photocatalytic applications [53][54][49]. All the nanocomposites show enhanced electron transfer ability with respect to pristine rGO. Metal graphene nanocomposites have transformed from basic to advanced level to offer the finest resolutions to industry and consumers.

Conducting polymers are a vast group of materials plentifully used in material chemistry. However, certain limitation in mechanical and physical properties of polymers can be removed to high extent by enforcing them with fillers. This can be done using graphitic materials; the interfacial interaction between polymers and GO improves the properties of both materials. These nanocomposites can be synthesized using melting, solution, in situ polymerization, and electrochemical methods [55]. The most common conducting polymer used with GO is polyaniline (PANI). PANI/GO nanocomposites have been extensively utilized for anti-corrosion activity [56], supercapacitor electrodes [57], electrochemical sensors [58] etc. In ultrahigh-molecular-weight polyethene, polypropylene, epoxy based GO nanocomposite, the strength and stiffness of polymers have been found to be greatly increased [55][59]. Poly(3,4-ethylenedioxythiophene) polystyrene sulfonate (PEDOT:PSS) is another popular polymer generally used in sensors, solar cells and supercapacitor as thin conducting electrode material. Various PEDOT:PSS and GO based nanocomposites are being studied frequently to make flexible devices. Geetu et.al, used PEDOT:rGO-TiO$_2$ conduction paper electrodes to electrochemically detect glucose with sensitivity of 94.98 μA mM^{-1} cm^{-2} and 0.01 mM limit of detection [60].

1.5. Applications of GO-based nanocomposites

This section briefs about most of the frequently used applications of such nanocomposites **(Fig. 1.5).**
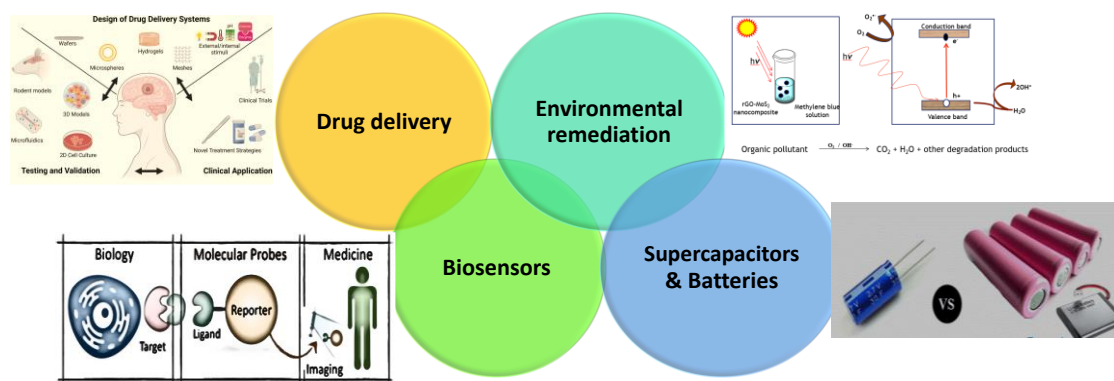
Fig. 1.5: Scheme showing applications of GO nanomaterials

1.5.1 Energy applications

GO-based nanomaterials can perform exceptionally well in terms of energy density, electrical conductivity, durability, flexibility and incomparable cyclic stability. These promising properties enable their use in energy storage and conversion applications. The various energy storage devices that can be fabricated using GO-based nanocomposites include lithium-ion batteries, supercapacitors etc., while for energy conversion, they are applicable for fuel cells, solar cells etc. [61].

1.5.2 Water treatment

Heavy metal ions and synthetic dyes have been found to be the most common pollutants in water bodies, which may cause life-threatening problems to flora and fauna. GO-based nanocomposite materials have been widely used to treat such contaminants due to their superior surface areas with respect to mass, excellent adsorption ability, and compliance with different functional groups makes them

suitable material for this application. This can be achieved either by the adsorption of contaminants from aqueous media or by the photo-degradation of industrially used dyes. GO-based nanocomposite materials have gained lots of attention serving as efficient adsorbents and photo-catalysts. Most GO nanocomposite have shown their applicability to make water get rid of such contaminants by 90% [62].

1.5.3 Membranes

Membrane separation technology is another useful application for resource recovery and industrial wastewater treatment. The evolving GO-based nanocomposite membranes offers exceptional resistance to organic solvents and oxidizers, additional hydrophilicity, controlled fouling and better separation performance for membrane separation in waste water treatment [63]. GO-based nanocomposite membranes have a huge scope for membrane-based desalination. Recently it has been stated that such membranes can offer a practical remedy for filtration by controlling pore size to result in 100% salt rejection [64].

1.5.4. Drug delivery

Another important application of GO-based nanocomposite under biomedical applications is drug delivery. Several studies have confirmed the effectiveness of these nanocomposite-based thin multilayer films to deliver or delay drugs in controlled amounts. Such nanocomposite offers a large surface area and prevents the drug from premature release outside the target [65].

1.6. GO for biosensing application

In biosensors, GO-based nanocomposites have emerged as a significant class of nanomaterials. Oxygen-containing functional groups make GO sheets highly available

for chemical functionalization. Also, GO-based nanocomposites have biocompatibility, exclusive morphology and conducting behavior enable their use in highly sensitive electrochemical biosensing applications [1]. Many analytes such as glucose, cholesterol, estradiol, cancer biomarkers, xanthine etc., have been detected using GO-based nanocomposites [66].

1.6.1. Biosensor

The first 'true' biosensor was introduced in 1956 to detect oxygen (using oxygen electrode) by Leland C. Clark, known as 'father of biosensor'. In 1962, the confirmation of an amperometric enzymatic electrode was put forward for efficient glucose concentration measurement. Thereafter in 1969, Guibault and Montalavo discovered the potentiometric biosensor for urea detection [67]. This can be considered the beginning for the era of biosensors which led to development of uncountable biosensing platforms till now worldwide. By then, the researchers have explored highly sensitive biorecognition entities [68]. The field of bioanalysis is rapidly expanding as different biorecognition elements accompanied by various transduction principles have been discovered to detect analytes used in innumerable applications. Biosensors offer to serve for a wide range of applications with the objective to advance the quality of life. This range covers their use for environmental monitoring, medical/clinical analysis, food safety, defense, veterinary and many more.

Basically, a biosensor is an analytical device that aims to detect biological / chemical substance in combination with a biological entity by help of a physiochemical detector. The device measures the biochemical reactions by producing electronic signals proportional to the analyte concentration in the reaction. Biosensors have certain specific

properties, the optimization of which indicates the performance of any biosensor. These properties include selectivity, reproducibility, stability, sensitivity and linearity.

1.6.2. Components of a biosensor

A biosensor consists of three major components **(Fig. 1.6)**:

❖ A bio-recognition element includes enzymes, DNA, antibody etc., which is used for the recognition of an analyte

❖ An immobilization matrix such as metal/metal chalcogenides, graphitic material-based nanoparticles, conducting polymers etc.

❖ A transducer which converts output received from biochemical reactions to electronic signals
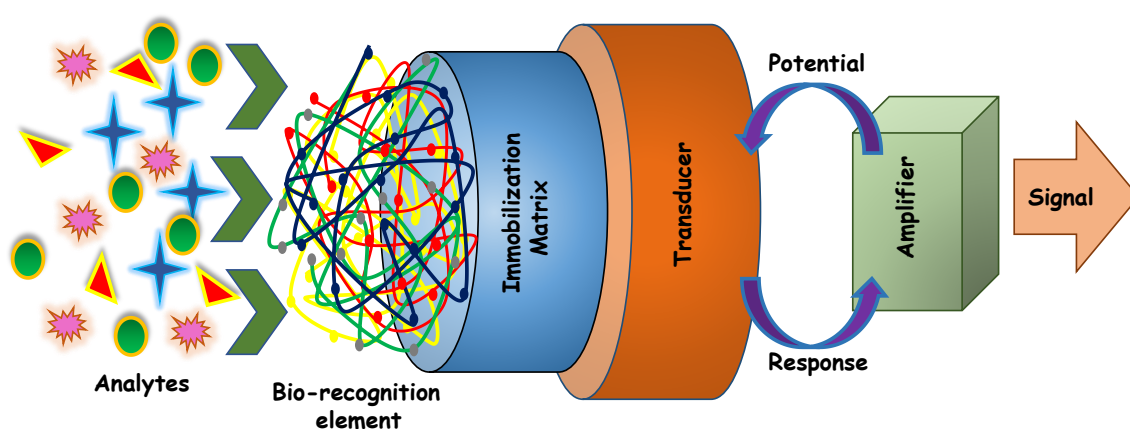
Fig. 1.6 Components of a biosensor

1.6.2.1. Biomolecular recognition element

For recognition of a target substance in a biosensing device, specific molecular assemblies have been selected, which can recognize the analyte and can forward the information to the electrical system. These specific entities are known as biomolecular recognition element. These are generally biologically derived materials or biomimetic

components that interact with a specific analyte including enzymes, antibodies, whole cells, DNA etc. The specificity of a biosensor depends majorly on the specificity of the biomolecule used as a recognition element [69].

1.6.2.2. Immobilization matrix

In order to enhance the stability of a biosensor, the recognition elements are required to be immobilized onto a solid support. Such solid support on which biorecognition entities can be attached through a number of forces can be regarded as an immobilization matrix. It has been widely observed that the activity of biomolecules increases drastically by support of an immobilization matrix. Additionally, the activity of biomolecules retains for a longer duration, resulting in more efficient sensing performance. However, the method of immobilization depends on the properties of the matrix. The most commonly used methods for immobilization can be cross-linking, physical adsorption, entrapment, covalent binding etc. [68]. Materials with large surface area, mechanical stability, thermal stability, electron mobility, biocompatibility, and rich in functional groups can serve as a good immobilization matrix [70].

1.6.2.3. Transducer

A transducer converts a bio-recognized signal obtained from the reaction of an analyte and biochemical component into a measurable electronic signal and forwards it to a detector system. Transducers can be categorized as optical, electrochemical, thermal, magnetic or piezoelectric based on the reaction type to produce the signal [71].

1.7. Non-enzymatic detection of phenolic compounds

Non-enzymatic biosensors can be regarded as third-generation biosensors under which reactions occur directly at the working electrode's surface. Direct

electrochemical detection of phenolic compounds (PC) on electrode's surface takes place via the formation of phenoxy radicals and their oxidation to quinones. In contrast, the radicals might further combine to form non-conducting polymers which may cause the deactivation of the electrode after multiple usage. In this context, Quynh et al., used a nanoporous gold electrode to detect phenol and catechol [72]. However, Y. Chen et al. used Au-Pd nanoflowers doped rGO film to efficiently detect Hq non-enzymatically [73].

1.8. Laccase enzyme for detection of PC

Laccase (Lac) is a multi-copper oxidase enzyme, which comprises of four Cu atoms. Cu atoms in the structure of Lac enzyme are found in different oxidation states. Lac enzyme has the ability to catalyze phenols (substrate) by their oxidation in the presence of O_2 by using a four-electron reduction. Further, the substrate in turn, gets reduced by Lac enzyme [74].

1.8.1. Sources of Lac

Plants	Fungi
• Fruits (apples, peaches, pears etc) • Vegetables (cabbage, potatoes, beets) • Other plants like tobacco, sycamore, maize's embryo and many more [75]	• Ascomycetes (*Polyporousvercicolor*, *Aspergillusnidulan*), • Deuteromycetes (Pestalotiopsis species) • Basidiomycetes (white rot fungi, Tremetes fungi etc.) are major sources [76].
Insects	**Bacteria**
• Azospirillumlipoferum (Ist reported) • Other insects such as *Bacillus subtilis*, *Streptomyces cyaneus*[77], *Streptomycesipomoeae* [78], and *Thermusthermophilus* [79].	• In particular *Azospirillumlipoferum*, *Pseudomonas putida F6*,*Bacillus licheniformis, Bacillus subtilis WPI* [78]

1.8.2. Classification of Lac

According to electron paramagnetic resonance (EPR), the Lac enzyme consists of four Cu atoms (**Fig. 1.7**) that can be separated into three groups [80] :
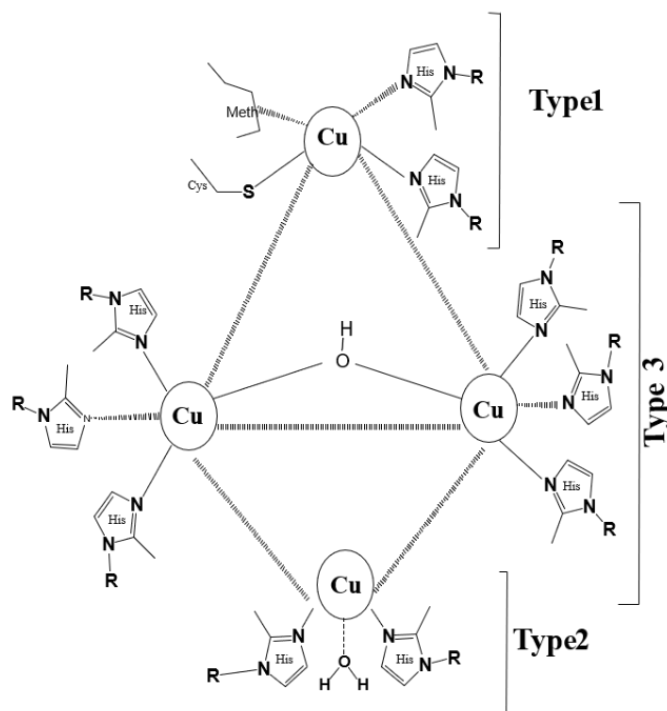
Fig.1.7. Structure of the Lac enzyme

- **Type I:** Cu is coordinated trigonally with an S of amino acid cysteine (Cys) and couple of N of histidine units. However, one more S of methionine has been attached axially as the fourth coordinate of Cu, at a larger distance than the other three. Therefore, the overall structure appears to be distorted tetrahedral with a triagonal elongation [80]. The intense blue color is observed in this case due to the absorbance under UV/visible region.

- **Type II:** Cu is coordinated to N of two histidine units and a H_2O molecule. However, its contrasting colored and paramagnetic characteristic has been proven

by EPR studies. The electron reduction of molecular oxygen and water discharge occurs at a tri-nuclear cluster.

- **Type III:** Comprises of two Cu atoms anti-ferromagnetically coupled, each attached to N of three histidine units and a bridging hydroxide group (O-H) tetragonally. Here, the oxidized form Cu depicts weak absorbance under the UV-visible spectrum, while EPR studies suggest it is diamagnetic.

1.8.3. Activity of the Lac Enzyme

Lac enzyme owe the ability to catalytically oxidize mono, di and polyphenols along with the associated four- electron reduction of oxygen to water. The different site of Cu atoms functions differently in Lac enzyme. The catalytic activity initiates through the donation of an electron to the substrate by Cu_I. The electron received then delivered from reduced Cu_I to trinuclear Cu cluster (Cu_{II} and Cu_{III}) through Cys-His pathway. Cu_{III} acts as a dual electron acceptor for which Cu_{II} must be accompanied. The Cu_{II} and Cu_{III} sites witness the reduction of molecular oxygen to water. It has been reported that H_2O_2 was not detected during the steady state [81]. This led to the generation of oxidized lac enzyme. Briefly, by reducing molecular oxygen to water and oxidizing the substrate, the Lac enzyme becomes oxidized. The catalytic mechanisms terminates when the oxidized Lac enzyme is reduced back to Lac **(Fig. 1.8).**

Besides phenolic substrates, the range of compounds to be oxidized by Lac enzyme can be drastically increased by oxidation of non-phenolic substrates which requires a mediator additionally [82]. The mediators behave as co-catalysts to improve the catalytic performance of the enzyme. For oxidation of non-phenolic compounds, mediator functions after oxidation of the substrate and mediator is then reduced to

original state, afterward, Lac oxidizes to oxidized Lac followed by reduction of oxygen to release water [83]. Low molecular weight mediators are preferred to confront the possible hindrance due to size for better efficiency. Besides this, the catalytic mechanism can be improved by using a high-potential mediator such as (2,2′-azino-bis-(3-ethylbenzothiazoline-6-sulfonic acid)) used for the analysis of non-phenolic compounds [84].
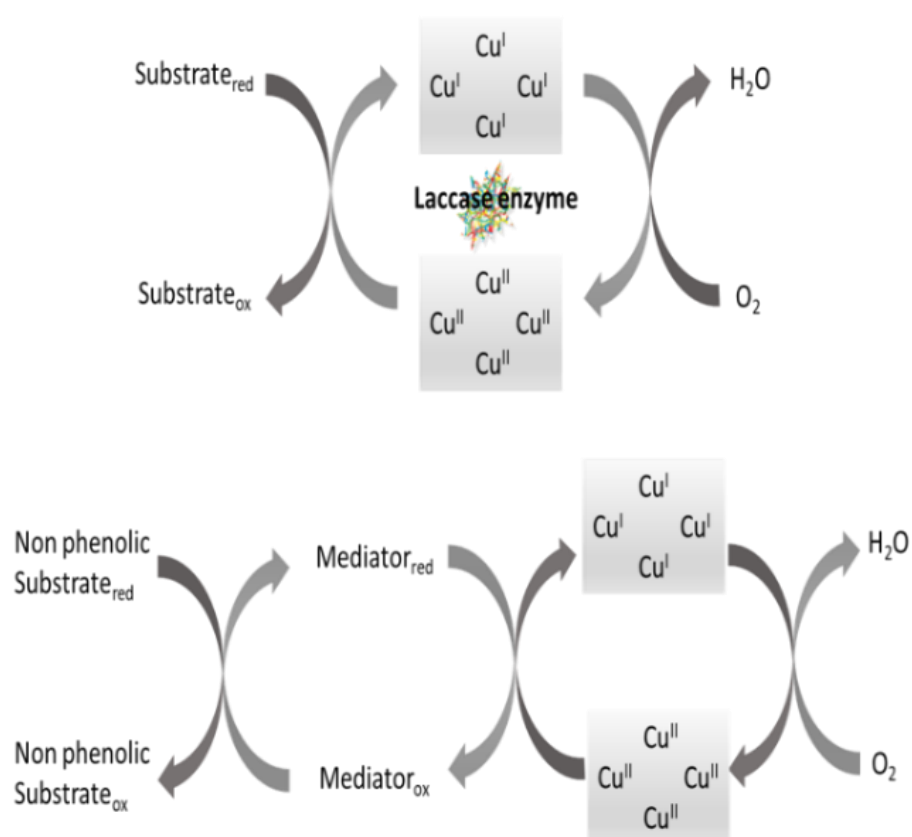
Fig. 1.8: Mechanism of action of the Lac enzyme for a phenolic and non-phenolic substrate

Enzymes other than laccase have also been studied for oxidation of PC, these include horseradish peroxidase and tyrosinase. However, Lac enzyme has been preferred for its better stability and higher catalytic activity than the other two. In addition, Lac enzyme-based biosensors (LEB) are among the latest in assembly compared to other

stated enzymatic biosensors because LEB generally require only O_2 as co-substarte not hydrogen peroxide (used in other enzymes) for the catalytic process [85].

1.8.4. Lac enzyme for biosensing application

1.8.4.1 Water pollutants detection

Water bodies suffer exposure of industrial waste, which may be toxic chemicals, synthetic dyes, etc., and that is one of the serious problems to address (**Fig. 1.9).** PC are one of the major contributors found to contaminate natural water systems when exposed untreated from plastic, textile, rubber and paper industries into water bodies. Before their removal using conventional techniques, their monitoring is important to save water and reduce the cost and timing for water purification.

Dihydroxy benzene isomers (hydroquinone and catechol) have been considered highly toxic compounds with poor degradability, which become one of the reasons for water pollution when these pollutants run off into waterbodies without prior treatment. The maximum permissible limit of such phenolic derivatives is 0.001 ppm in natural water and 1 ppm in inland surface water [86]. The excessive discharge of these compounds into water bodies has been found risky to human health as it leads to toxicity in soil microbial, causes skin irritation, may damage chromosomes and DNA, etc. [87],[88]. Conventional analytical techniques such as chemiluminescence, fluorescence, chromatography, advanced oxidation and capillary electrophoresis have been used to detect such pollutants [89]–[91]. However, these techniques are efficient but time-consuming, expensive, and complex [92]. A brief summary of sources and harmful effects of phenolic compounds have been mentioned in **Table 1.4 .**

Another class of water-polluting agents includes pesticides, insecticides, fungicides or herbicides, which leach easily to the water streams. LEB has been found to perform superior catalytic activity for detecting water-polluting phenols such as hydroquinone, catechol, bisphenol-A and pesticides such as carbamates [93],[94]. In this context, Thiago et.al detected primicarb in the micromolar range using MWCNTs [95]. Very recently, catechol has been detected using reusable Lac immobilized COOH-MWCNTs with excellent stability [96].

Table 1.4: Summary of phenolic contaminants (PhCs) and their sources [86]

PhCs	Effects	Sources
Catechol	Protein destruction in the body Damage to DNA	Coal conversion process Crude wood tar Coal tar production
Bisphenol A	Endocrine troublesome effects Interruption of the onset of puberty	Food and beverage packaging Flame retardants Building materials and electronic components Paper coatings
Caffeic and dihydrocaffeic acids	Damages DNA in the presence of copper Antioxidant property Prevents cardiovascular disease Reduces stress	Wine Coffee Spices and herbs
Chlorophenol	Mouth scorching Necrotic gashes in the respiratory canal	Bleaching Iron and steel industries Paper pulp and paper board mills Dye and pharmaceutical industries
Hydroquinone	Damages chromosome Toxic to soil microbial activities Skin irritation	Food and Rubber industries as an antioxidant Paint and fuel industries as a stabilizer Cosmetic industries
Para-cresol	Central nervous system disease Cardiovascular system Lungs and kidneys diseases	Fumigants Disinfectant Explosives
Estrogen	Endocrine disability Breast cancer	Urine
Dopamine	Enhance brain functions and memory Regulates blood pressure	Brain
Galliac acid	Antioxidant Reduce the risk of cardiovascular diseases Prevent certain cancer	Wine Chestnut Berries
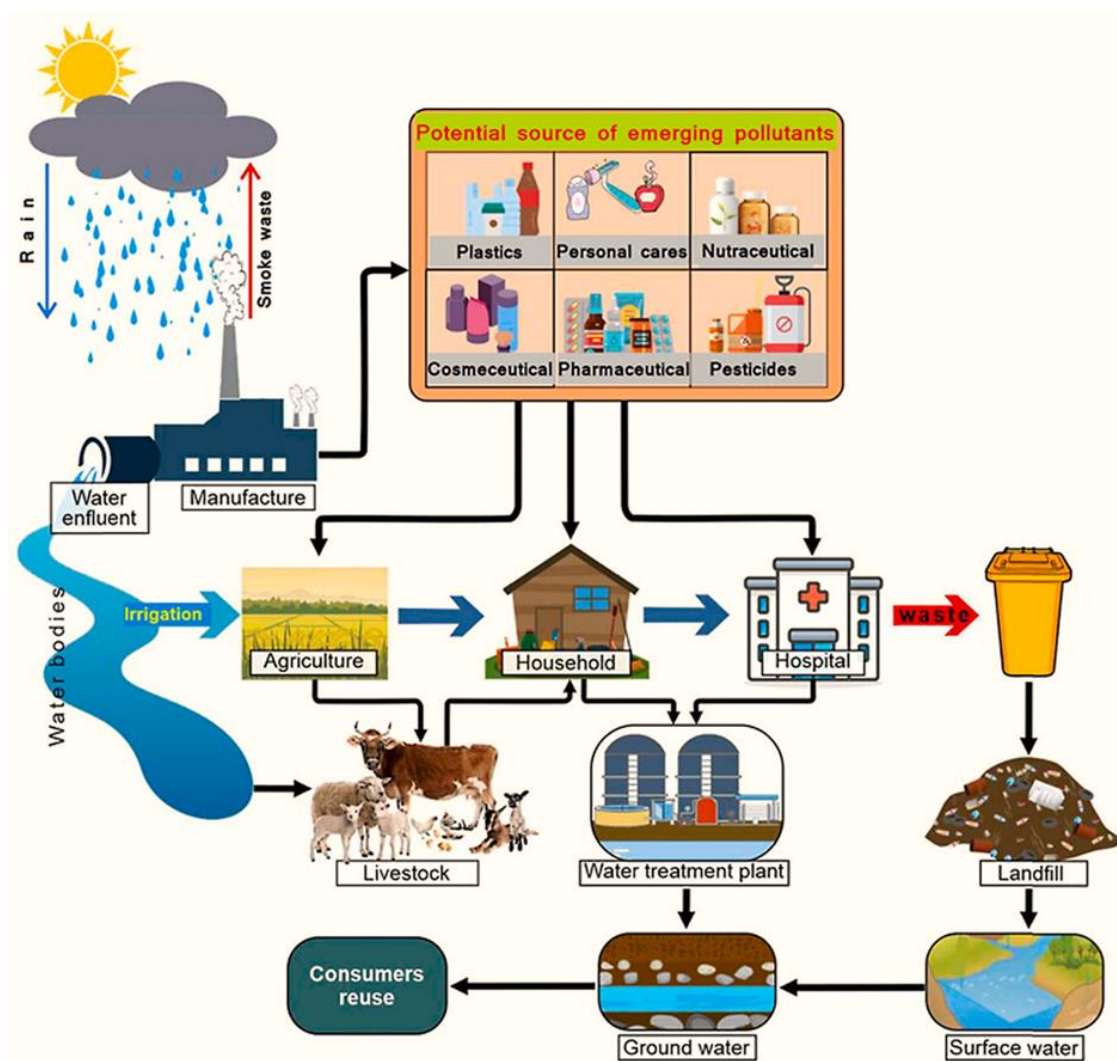
Fig. 1.9: Schematic representation of contamination of water by phenolic pollutants [97]

1.8.4.2. Antioxidant activity in food and beverages

Fruits, vegetables, cereals, beverages, and red wine contain certain PC. The presence of PC in such eatables can be used to check their antioxidant activity by monitoring their phenol content using LEB. In the past, this has been applied to check the antioxidant activity of dry extracts of red fruits, honey, caffeic acid in tea, chlorogenic acid in coffee and gallic acid in wines [86]. Macêdo et al. used LEB to estimate the total phenolic content in fruits using graphite electrodes [98]. However, Yongli Ye et al., reviewed all the recent advances in quantifying antioxidant activity in food items

utilizing LEB. They claimed that electrochemical biosensing can be successfully used for food analysis [99].

1.8.4.3. Body fluids analysis

Patients having Parkinson's disease, schizophrenia and dementia-like disease lack in dopamine concentration. Dopamine is another PC that plays a vital role as a neurotransmitter. Our brain requires a normal concentration of dopamine in the body to balance blood pressure and daily physical activities regulated by the brain such as learning [100]. Dopamine being PC can be monitored using LEB in clinical samples. Another important highly detected PC in urine and water samples are estrogen. The release of an inaccurate amount of estrogen in the environment leads to diseases related to fertility and tumors in females. LEB has been used to detect sensitively in clinical and water samples [101].

1.9. Objectives of the studies

The work's objective is to develop a biosensor using GO-based nanocomposites (rGO-MgONf, rGO-MoS$_2$, and MgO@rGO-MoS$_2$) to detect phenolic water pollutants. With the aim of attaining this objective, the following procedures have been undertaken.

➢ Synthesis and modification of GO nanostructures and studies on the factors influencing the electrochemical parameters.

➢ Structural and morphological characterization of GO-based nanocomposites.

➢ Electrophoretic deposition of synthesized GO-based nanocomposites onto ITO-coated glass substrate.

➢ Immobilization of enzyme onto coated matrices for enzymatic biosensing.

➤ Characteristic response studies of the biosensing electrodes using various electrochemical techniques for detection of phenolic pollutants in buffer solutions.

➤ Studies on specificity, reproducibility and shelf life of biosensors,

➤ Validation of results using real water samples spiked with synthetic phenolic pollutants.

1.10. Thesis organization

The present thesis deals with the preparation, characterization, and application of GO, GO-based nanocomposite (MgO and MoS_2), used in the fabrication of efficient electrochemical biosensors for sensitive and specific detection of phenolic pollutants **The six chapters that make up this thesis's research are grouped as follows.**

Chapter 1 will cover the literature survey on the research work concerned with enzymatic and non-enzymatic detection of phenolic water pollutants using biosensing technique and highlight the detailed description of GO in terms of its synthetic strategies, characteristic properties, and applications, with a special emphasis on biosensors.

Chapter 2 will briefly overview experimental techniques used to characterize GO, GO-based nanocomposite-modified electrodes and perform electrochemical biosensing applications. Attempts have also been made to describe the procedures and protocols used to estimate various parameters related to the performance of the GO nanocomposite-based biosensor for phenolic pollutant detection.

Chapter 3 presents studies relating to fabricating a sensitive and efficient electrochemical biosensor for hydroquinone (Hq) detection using reduced GO-MgO

nanoflakes (rGO-MgONf). Electrochemical studies have been performed to compare rGO-MgONf/ITO, GO/ITO and MgO/ITO electrode performance. Further, the fabricated biosensor (Lac/rGO-MgONf/ITO) was analyzed to detect Hq in tap and river water samples.

Chapter 4 described the findings of the research on the development of an ultrasensitive, electrochemical biosensor using rGO-MoS$_2$ nanocomposite. Under optimized conditions, Lac/rGO-MoS$_2$/ITO bioelectrode was used for Hq detection in real water (tap and river) samples with an excellent recovery rate. The proposed biosensor was also discovered to be reliable, reusable, and maybe useful as a platform for the effective detection of phenolic contaminants.

Chapter 5 investigates results pertaining to the development of electrochemical biosensors based on reduced GO-MoS$_2$ modified with MgO nanoparticles (MgO@rGO-MoS$_2$). The fabricated MgO@rGO-MoS$_2$/ITO electrode has been used for rapid non-enzymatic detection of water-polluting phenol derivatives i.e. Hq and catechol (Ctl). The performance of the biosensor was validated with tap and river water samples.

Chapter 6 summarises the findings concerning applications of GO nanocomposites-based biosensors for phenolic pollutant detection. Efforts have also been made to emphasize the potential of the rGO nanocomposite-based biosensor for future biosensing applications.

References

[1]   G. Maduraiveeran and W. Jin, "Carbon nanomaterials: Synthesis, properties and applications in electrochemical sensors and energy conversion systems," *Mater. Sci. Eng. B*, vol. 272, p. 115341, 2021.

[2]   D. Maiti, X. Tong, X. Mou, and K. Yang, "Carbon-Based Nanomaterials for Biomedical Applications: A Recent Study   ," *Frontiers in Pharmacology* , vol. 9, 2019.

[3]   J. R. Siqueira and O. N. Oliveira, "9 - Carbon-Based Nanomaterials," A. L. Da Róz, M. Ferreira, F. de Lima Leite, and O. N. B. T.-N. Oliveira, Eds. William Andrew Publishing, p. 233–249, 2017.

[4]   H. Kroto, "The Birth of C60: Buckminsterfullerene BT - Electronic Properties of Fullerenes," p. 1–7, 1993.

[5]   R. Qiao, A. P. Roberts, A. S. Mount, S. J. Klaine, and P. C. Ke, "Translocation of C60 and Its Derivatives Across a Lipid Bilayer," *Nano Lett.*, vol. 7, no. 3, p. 614–619, 2007.

[6]   J. R. Siqueira Jr and O. Oliveira, "Carbon-Based Nanomaterials," p. 233–249, 2017.

[7]   H. Kazemzadeh and M. Mozafari, "Fullerene-based delivery systems," *Drug Discov. Today*, vol. 24, no. 3, p. 898–905, 2019.

[8]   D. A. Heredia, A. M. Durantini, J. E. Durantini, and E. N. Durantini, "Fullerene C60 derivatives as antimicrobial photodynamic agents," *J. Photochem. Photobiol. C Photochem. Rev.*, vol. 51, p. 100471, 2022.

[9]   S. Iijima, "Helical microtubules of graphitic carbon," *Nature*, vol. 354, no. 6348, p. 56–58, 1991.

[10]   S. Iijima and T. Ichihashi, "Single-shell carbon nanotubes of 1-nm diameter," *Nature*, vol. 363, no. 6430, p. 603–605, 1993.

[11] T. Maruyama, "Chapter 6 - Carbon nanotubes," in *Micro and Nano Technologies*, S. Thomas, C. Sarathchandran, S. A. Ilangovan, and J. C. B. T.-H. of C.-B. N. Moreno-Piraján, Eds. Elsevier, p. 299–319, 2021.

[12] M. I. Katsnelson, "Graphene: carbon in two dimensions," *Mater. Today*, vol. 10, no. 1, p. 20–27, 2007.

[13] B. Alemour, M. Yaacob, H. Lim, and M. R. Hassan, "Review of electrical properties of graphene conductive composites," *Int. J. Nanoelectron. Mater.*, vol. 11, p. 371–398, 2018.

[14] J. H. Gosling *et al.*, "Universal mobility characteristics of graphene originating from charge scattering by ionised impurities," *Commun. Phys.*, vol. 4, no. 1, p. 30, 2021.

[15] D. G. Papageorgiou, I. A. Kinloch, and R. J. Young, "Mechanical properties of graphene and graphene-based nanocomposites," *Prog. Mater. Sci.*, vol. 90, p. 75–127, 2017.

[16] S. Zhang, H. Wang, J. Liu, and C. Bao, "Measuring the specific surface area of monolayer graphene oxide in water," *Mater. Lett.*, vol. 261, p. 127098, 2020.

[17] J. Aravind Kumar, T. Krithiga, D. Venkatesan, S. Sathish, and D. J. Amarnath, "Synthesis, Properties, and Applications of Graphene Nanocomposite BT - Handbook of Polymer and Ceramic Nanotechnology," C. M. Hussain and S. Thomas, Eds. Cham: Springer International Publishing, p. 1–21, 2020.

[18] V. B. Mbayachi, E. Ndayiragije, T. Sammani, S. Taj, E. R. Mbuta, and A. ullah khan, "Graphene synthesis, characterization and its applications: A review," *Results Chem.*, vol. 3, p. 100163, 2021.

[19] S. K. Sarkar, K. K. Raul, S. S. Pradhan, S. Basu, and A. Nayak, "Magnetic properties of graphite oxide and reduced graphene oxide," *Phys. E Low-dimensional Syst. Nanostructures*, vol. 64, p. 78–82, 2014.

[20] M. Husien Fahmy Taha, H. Ashraf, and W. Caesarendra, "A Brief Description of Cyclic Voltammetry Transducer-Based Non-Enzymatic Glucose Biosensor Using Synthesized Graphene Electrodes," *Appl. Syst. Innov.*, vol. 3, p. 32, Aug. 2020.

[21] A. T. Smith, A. M. LaChance, S. Zeng, B. Liu, and L. Sun, "Synthesis, properties, and applications of graphene oxide/reduced graphene oxide and their nanocomposites," *Nano Mater. Sci.*, vol. 1, no. 1, p. 31–47, 2019.

[22] G. R. Yazdi, T. Iakimov, and R. Yakimova, "Epitaxial Graphene on SiC: A Review of Growth and Characterization," *Crystals*, vol. 6, no. 5. 2016.

[23] Q. Abbas *et al.*, "Graphene Synthesis Techniques and Environmental Applications," *Materials*, vol. 15, no. 21. 2022.

[24] Y. Zhang, L. Zhang, and C. Zhou, "Review of Chemical Vapor Deposition of Graphene and Related Applications," *Acc. Chem. Res.*, vol. 46, no. 10, p. 2329–2339, 2013.

[25] I. Kondrashov, P. Rusakov, M. Rybin, and A. Pozharov, "Chemical Vapor Deposition of Graphene on Nickel from Different Gaseous Atmospheres," *J. Nanoelectron. Optoelectron.*, vol. 8, p. 83–86, 2013.

[26] Z. Li *et al.*, "Mechanisms of Liquid-Phase Exfoliation for the Production of Graphene," *ACS Nano*, vol. 14, no. 9, p. 10976–10985, 2020.

[27] Y. Wang, X. Zhang, H. Liu, and X. Zhang, "SMA-Assisted Exfoliation of Graphite by Microfluidization for Efficient and Large-Scale Production of High-Quality Graphene," *Nanomaterials*, vol. 9, no. 12. 2019.

[28] K. E. Whitener and P. E. Sheehan, "Graphene synthesis," *Diam. Relat. Mater.*, vol. 46, p. 25–34, 2014.

[29] G. G. Gebreegziabher, A. S. Asemahegne, D. W. Ayele, M. Dhakshnamoorthy, and A. Kumar, "One-step synthesis and characterization of reduced graphene oxide using chemical exfoliation method," *Mater. Today Chem.*, vol. 12, p. 233–239, 2019.

[30] F. Liu *et al.*, "Synthesis of graphene materials by electrochemical exfoliation: Recent progress and future potential," *Carbon Energy*, vol. 1, no. 2, p. 173–199, 2019.

[31] H. L. Poh, F. Šaněk, A. Ambrosi, G. Zhao, Z. Sofer, and M. Pumera, "Graphenes prepared by Staudenmaier, Hofmann and Hummers methods with consequent thermal exfoliation exhibit very different electrochemical properties," *Nanoscale*, vol. 4, no. 11, p. 3515–3522, 2012.

[32] K. Sheoran, H. Kaur, S. S. Siwal, A. K. Saini, D.-V. N. Vo, and V. K. Thakur, "Recent advances of carbon-based nanomaterials (CBNMs) for wastewater treatment: Synthesis and application," *Chemosphere*, vol. 299, p. 134364, 2022.

[33] N. I. Zaaba, K. L. Foo, U. Hashim, S. J. Tan, W.-W. Liu, and C. H. Voon, "Synthesis of Graphene Oxide using Modified Hummers Method: Solvent Influence," *Procedia Eng.*, vol. 184, p. 469–477, 2017.

[34] M. Sohail *et al.*, "Modified and improved Hummer's synthesis of graphene oxide for capacitors applications," *Mod. Electron. Mater.*, vol. 3, no. 3, p. 110–116, 2017.

[35] D. C. Marcano *et al.*, "Improved Synthesis of Graphene Oxide," *ACS Nano*, vol. 4, no. 8, p. 4806–4814, 2010.

[36] V. Agarwal and P. B. Zetterlund, "Strategies for reduction of graphene oxide – A comprehensive review," *Chem. Eng. J.*, vol. 405, p. 127018, 2021.

[37] C. K. Chua and M. Pumera, "The reduction of graphene oxide with hydrazine: elucidating its reductive capability based on a reaction-model approach," *Chem. Commun.*, vol. 52, no. 1, p. 72–75, 2016.

[38] Z. Fan, K. Wang, T. Wei, J. Yan, L. Song, and B. Shao, "An environmentally friendly and efficient route for the reduction of graphene oxide by aluminum powder," *Carbon N. Y.*, vol. 48, no. 5, p. 1686–1689, 2010.

[39] M. Ayán-Varela *et al.*, "Highly efficient silver-assisted reduction of graphene oxide dispersions at room temperature: mechanism, and catalytic and electrochemical performance of the resulting hybrids," *J. Mater. Chem. A*, vol. 2, no. 20, p. 7295–7305, 2014.

[40] L. G. Guex *et al.*, "Experimental review: chemical reduction of graphene oxide (GO) to reduced graphene oxide (rGO) by aqueous chemistry," *Nanoscale*, vol. 9, no. 27, p. 9562–9571, 2017.

[41] Z. Ismail, "Green reduction of graphene oxide by plant extracts: A short review," *Ceram. Int.*, vol. 45, no. 18, Part A, p. 23857–23868, 2019.

[42] D. Tran, S. Kabiri, and D. Losic, "A green approach for the reduction of graphene oxide nanosheets using non-aromatic amino acids," *Carbon N. Y.*, vol. 76, p. 193–202, Sep. 2014.

[43] J. Ma *et al.*, "Reduction of graphene oxide with L-lysine to prepare reduced graphene oxide stabilized with polysaccharide polyelectrolyte," *J. Mater. Chem. A*, vol. 1, p. 2192–2201, 2013.

[44] B. A. E. Lehner *et al.*, "Creation of Conductive Graphene Materials by Bacterial Reduction Using Shewanella Oneidensis," *ChemistryOpen*, vol. 8, no. 7, p. 888–895, Jul. 2019.

[45] M. Ponzelli, S. Zahedi, K. Koch, J. E. Drewes, and J. Radjenovic, "Rapid biological reduction of graphene oxide: Impact on methane production and micropollutant transformation," *J. Environ. Chem. Eng.*, vol. 10, no. 5, p. 108373, 2022.

[46] D. Karačić *et al.*, "Electrochemical reduction of thin graphene-oxide films in aqueous solutions – Restoration of conductivity," *Electrochim. Acta*, vol. 410, p. 140046, 2022.

[47] D. Voiry *et al.*, "High-quality graphene via microwave reduction of solution-exfoliated graphene oxide," *Science (80-.).*, vol. 353, no. 6306, p. 1413–1416, 2016.

[48] S. Tang *et al.*, "Effective reduction of graphene oxide via a hybrid microwave heating method by using mildly reduced graphene oxide as a susceptor," *Appl. Surf. Sci.*, vol. 473, p. 222–229, 2019.

[49] S. Verma, C. M. Pandey, and D. Kumar, "A highly efficient rGO grafted MoS2 nanocomposite for dye adsorption and electrochemical detection of hydroquinone in wastewater," *New J. Chem.*, vol. 46, no. 44, p. 21190–21200, 2022.

[50] S. F. Bartolucci *et al.*, "Graphene–aluminum nanocomposites," *Mater. Sci. Eng. A*, vol. 528, no. 27, p. 7933–7937, 2011.

[51] W. Chen *et al.*, "Advances in graphene reinforced metal matrix nanocomposites: Mechanisms, processing, modelling, properties and applications," *Nanotechnol. Precis. Eng.*, vol. 3, no. 4, p. 189–210, 2021.

[52] S. Kumari *et al.*, "A Novel Synthesis of the Graphene Oxide-Silver (GO-Ag) Nanocomposite for Unique Physiochemical Applications," *ACS Omega*, vol. 5, no. 10, p. 5041–5047, 2020.

[53] O. Jalil, C. M. Pandey, and D. Kumar, "Electrochemical biosensor for the epithelial cancer biomarker EpCAM based on reduced graphene oxide modified with nanostructured titanium dioxide," *Microchim. Acta*, vol. 187, no. 5, p. 275, 2020.

[54] P. Garg, D. Thakur, S. Verma, O. Jalil, C. M. Pandey, and D. Kumar, "Biosynthesized rGO@ZnO-based ultrasensitive electrochemical immunosensor for bovine serum albumin detection," *J. Appl. Electrochem.*, vol. 53, p.1449–1459, 2023.

[55] M. Safdari and M. Al-Haik, "A Review on Polymeric Nanocomposites," in *Carbon-Based Polymer Nanocomposites for Environmental and Energy Applications*, p. 113–146, 2018.

[56] S. Yang, S. Zhu, and R. Hong, "Graphene Oxide/Polyaniline Nanocomposites Used in Anticorrosive Coatings for Environmental Protection," *Coatings*, vol. 10, no. 12. 2020.

[57] A. Maddu, R. A. Nugroho, E. Rustami, S. Arjo, and M. Hidayat, "Synthesis of graphene/polyaniline nanocomposite for supercapacitor electrodes," *J. Phys. Conf. Ser.*, vol. 1171, no. 1, p. 12043, 2019.

[58] R. S. Alruwais, W. A. Adeosun, H. M. Marwani, M. Jawaid, A. M. Asiri, and A. Khan, "Novel Aminosilane (APTES)-Grafted Polyaniline@Graphene Oxide (PANI-GO) Nanocomposite for Electrochemical Sensor," *Polymers*, vol. 13, no. 15. 2021.

[59] Y. Pang *et al.*, "Exfoliated Graphene Leads to Exceptional Mechanical Properties of Polymer Composite Films," *ACS Nano*, vol. 13, no. 2, p. 1097–1106, 2019.

[60] G. Paul, S. Verma, O. Jalil, D. Thakur, C. M. Pandey, and D. Kumar, "PEDOT: PSS-grafted graphene oxide-titanium dioxide nanohybrid-based conducting paper for glucose detection," *Polym. Adv. Technol.*, vol. 32, no. 4, p. 1774–1782, 2021.

[61] D. Singh, S. Kumar, and A. Thakur, "Graphene Based Nanocomposites for Energy Applications,", p. 159–178, 2021.

[62] M. Yusuf, F. M. Elfghi, S. A. Zaidi, E. C. Abdullah, and M. A. Khan, "Applications of graphene and its derivatives as an adsorbent for heavy metal and dye removal: a systematic and comprehensive overview," *RSC Adv.*, vol. 5, no. 62, p. 50392–50420, 2015.

[63] G. Memisoglu, R. C. Murugesan, J. Zubia, and A. G. Rozhin, "Graphene Nanocomposite Membranes: Fabrication and Water Treatment Applications," *Membranes*, vol. 13, no. 2. 2023.

[64] Y. You, V. Sahajwalla, M. Yoshimura, and R. K. Joshi, "Graphene and graphene oxide for desalination," *Nanoscale*, vol. 8, no. 1, p. 117–119, 2016.

[65] Z. Wang, L. Colombi Ciacchi, and G. Wei, "Recent Advances in the Synthesis of Graphene-Based Nanomaterials for Controlled Drug Delivery," *Applied Sciences*, vol. 7, no. 11. 2017.

[66] A. N. Banerjee, "Graphene and its derivatives as biomedical materials: future prospects and challenges," *Interface Focus*, vol. 8, no. 3, p. 20170056, 2018.

[67] G. G. Guilbault and J. G. J. Montalvo, "Urea-specific enzyme electrode," *J. Am. Chem. Soc.*, vol. 91, no. 8, p. 2164–2165,1969.

[68] P. Bhattarai and S. Hameed, "Basics of Biosensors and Nanobiosensors," in *Nanobiosensors*, p. 1–22, 2020.

[69] M. A. Morales and J. M. Halpern, "Guide to Selecting a Biorecognition Element for Biosensors," *Bioconjug. Chem.*, vol. 29, no. 10, p. 3231–3239, 2018.

[70] M. Holzinger, A. Le Goff, and S. Cosnier, "Nanomaterials for biosensing applications: a review ," *Frontiers in Chemistry*, vol. 2. 2014.

[71] E. O. Polat *et al.*, "Transducer Technologies for Biosensors and Their Wearable Applications," *Biosensors*, vol. 12, no. 6. 2022.

[72] B. T. P. Quynh, J. Y. Byun, and S. H. Kim, "Non-enzymatic amperometric detection of phenol and catechol using nanoporous gold," *Sensors Actuators B Chem.*, vol. 221, p. 191–200, 2015.

[73] Y. Chen *et al.*, "Ultrasensitive and simultaneous detection of hydroquinone, catechol and resorcinol based on the electrochemical co-reduction prepared Au-Pd nanoflower/reduced graphene oxide nanocomposite," *Electrochim. Acta*, vol. 231, p. 677–685, 2017.

[74] H. Claus, "Laccases: Structure, reactions, distribution," *Micron*, vol. 35, no. 1–2, pp. 93–96, 2004.

[75] V. Kumar and P. Sonkar, "LACCASES: SOURCES AND THEIR Environmental Application," *Int. J. Bioassays*, vol. 2, pp. 909–911, 2013.

[76] B. Viswanath, B. Rajesh, A. Janardhan, A. P. Kumar, and G. Narasimha, "Fungal Laccases and Their Applications in Bioremediation," *Enzyme Res.*, vol. 2014, p. 163242, 2014.

[77] S. Ece, C. Lambertz, R. Fischer, and U. Commandeur, "Heterologous expression of a Streptomyces cyaneus laccase for biomass modification applications," *AMB Express*, vol. 7, no. 1, p. 86, 2017.

[78] A. Blánquez *et al.*, "Laccase SilA from Streptomyces ipomoeae CECT 3341, a key enzyme for the degradation of lignin from agricultural residues?," *PLoS One*, vol. 12, no. 11, p. e0187649, Nov. 2017.

[79] K. Miyazaki, "A hyperthermophilic laccase from Thermus thermophilus HB27," *Extremophiles*, vol. 9, p. 415–425, Dec. 2005.

[80] U. N. Dwivedi, P. Singh, V. P. Pandey, and A. Kumar, "Structure–function relationship among bacterial, fungal and plant laccases," *J. Mol. Catal. B Enzym.*, vol. 68, no. 2, p. 117–128, 2011.

[81] M. C. Castrovilli *et al.*, "The convergence of forefront technologies in the design of laccase-based biosensors – An update," *TrAC Trends Anal. Chem.*, vol. 119, p. 115615, Oct. 2019.

[82] M. M. Rodríguez-Delgado *et al.*, "Laccase-based biosensors for detection of phenolic compounds," *TrAC - Trends Anal. Chem.*, vol. 74, p. 21–45, 2015.

[83] P. Chaurasia, R. Yadav, and S. Yadava, "A review on mechanism of laccase action," vol. 7, p. 66–71, 2013.

[84] A. Tarasov, N. Stozhko, M. Bukharinova, and E. Khamzina, "Biosensors Based on Phenol Oxidases (Laccase, Tyrosinase, and Their Mixture) for Estimating the Total Phenolic Index in Food-Related Samples," *Life*, vol. 13, no. 2. 2023.

[85] M. M. Rodríguez-Delgado *et al.*, "Laccase-based biosensors for detection of phenolic compounds," *TrAC - Trends Anal. Chem.*, vol. 74, p. 21–45, 2015.

[86] S. Verma, D. Thakur, C. M. Pandey, and D. Kumar, "Recent Prospects of Carbonaceous Nanomaterials-Based Laccase Biosensor for Electrochemical Detection of Phenolic Compounds," *Biosensors*, vol. 13, no. 3. 2023.

[87]   F. Enguita and A. Leitão, "Hydroquinone: Environmental Pollution, Toxicity, and Microbial Answers," *Biomed Res. Int.*, vol. 2013, p. 542168, 2013.

[88]   A. A. Aghapour, G. Moussavi, and K. Yaghmaeian, "Biological degradation of catechol in wastewater using the sequencing continuous-inflow reactor (SCR)," *J. Environ. Heal. Sci. Eng.*, vol. 11, no. 1, p. 3, 2013.

[89]   P. V Rodionov, I. A. Veselova, and T. N. Shekhovtsova, "A solid-phase fluorescent biosensor for the determination of phenolic compounds and peroxides in samples with complex matrices," *Anal. Bioanal. Chem.*, vol. 406, no. 5, p. 1531–1540, 2014.

[90]   J. An *et al.*, "Revealing Decay Mechanisms of H2O2-Based Electrochemical Advanced Oxidation Processes after Long-Term Operation for Phenol Degradation," *Environ. Sci. Technol.*, vol. 54, no. 17, p. 10916–10925, Sep. 2020.

[91]   L. Shu, J. Zhu, Q. Wang, P. He, and Y. Fang, "Electrophoresis–chemiluminescence detection of phenols catalyzed by hemin," *Luminescence*, vol. 29, no. 6, p. 579–585, 2014.

[92]   N. Mohammed Modawe Alshik Edris, J. Abdullah, S. Kamaruzaman, and Y. Sulaiman, "Voltammetric determination of hydroquinone, catechol, and resorcinol by using a glassy carbon electrode modified with electrochemically reduced graphene oxide-poly(Eriochrome black T) and gold nanoparticles," *Microchim. Acta*, vol. 186, no. 4, p. 261, 2019.

[93]   N. Huang, M. Liu, H. Li, Y. Zhang, and S. Yao, "Synergetic signal amplification based on electrochemical reduced graphene oxide-ferrocene derivative hybrid and gold nanoparticles as an ultra-sensitive detection platform for bisphenol A," *Anal. Chim. Acta*, vol. 853, p. 249–257, 2015.

[94]   T. M. B. F. Oliveira *et al.*, "Laccase-Prussian blue film-graphene doped carbon paste modified electrode for carbamate pesticides quantification," *Biosens. & Bioelectron.*, vol. 47, p. 292–299, 2013.

45

[95] T. M. B. F. Oliveira *et al.*, "Biosensor based on multi-walled carbon nanotubes paste electrode modified with laccase for pirimicarb pesticide quantification," *Talanta*, vol. 106, p. 137–143, 2013.

[96] A. M. Othman and U. Wollenberger, "Amperometric biosensor based on coupling aminated laccase to functionalized carbon nanotubes for phenolics detection," *Int. J. Biol. Macromol.*, vol. 153, p. 855–864, 2020.

[97] R. Kumar *et al.*, "A review on emerging water contaminants and the application of sustainable removal technologies," *Case Stud. Chem. Environ. Eng.*, vol. 6, p. 100219, 2022.

[98] I. Macêdo *et al.*, "Electroanalytical Tools for Antioxidant Evaluation of Red Fruits Dry Extracts," *Food Chem.*, vol. 217, 2016.

[99] Y. Ye, J. Ji, Z. Sun, P. Shen, and X. Sun, "Recent advances in electrochemical biosensors for antioxidant analysis in foodstuff," *TrAC Trends Anal. Chem.*, vol. 122, p. 115718, 2020.

[100] S. Baluta, K. Malecha, D. Zając, J. Sołoducho, and J. Cabaj, "Dopamine sensing with fluorescence strategy based on low temperature co-fired ceramic technology modified with conducting polymers," *Sensors Actuators B Chem.*, vol. 252, 2017.

[101] A. Pavinatto, L. Mercante, R. Bartz Pena, R. Sanfelice, L. Mattoso, and D. Correa, "Ultrasensitive biosensor based on polyvinylpyrrolidone/ chitosan/reduced graphene oxide electrospun nanofibers for 17α – Ethinylestradiol electrochemical detection," *Appl. Surf. Sci.*, vol. 458, 2018.

CHAPTER 2

MATERIALS AND METHODS

2.1. Introduction

In the current chapter, we discuss all methodologies and strategies employed to characterize the synthesized GO and GO nanocomposites, followed by the fabrication of biosensing electrodes to electrochemically detect phenolic water pollutants. Further, electrodes fabricated using synthesized GO, rGO-MgO, rGO-MoS$_2$, and MgO@rGO-MoS$_2$ nanomaterials were subjected to various analytical techniques. Several characterization techniques used to characterize the synthesized nanomaterials have also been briefed. An attempt has also been done to explain the selection of enzymes to analyze the presence of phenolic water pollutants and to justify the specificity of fabricated electrodes. In addition, various protocols that have been utilized for the estimation of several parameters and factors responsible for justifying the reliability of a biosensor have also been discussed.

2.2. Materials

Materials used while experimentations are detailed as follows:

2.2.1. Chemicals

Graphite powder (size<20 µm) CAS:7782-42-5, thiourea (CH$_4$N$_2$S) ($\geq$99.0%) CAS:62-56-6, ammonium molybdate ((NH$_4$)$_6$Mo$_7$O$_{24}$.4H$_2$O; $\geq$99.0%) CAS:12054-85-2, D-(+)-Glucose ($\geq$99.5%) CAS:50-99-7, H$_2$SO$_4$ (~ 98%) CAS:7664-93-3, Hydroquinone (Hq; $\geq$99.0%) CAS:123-31-9, Catechol (ctl, $\geq$99.0%) CAS:120-80-9, ,

Magnesium nitrate hexahydrate (($Mg(NO_3)_2.6H_2O$, ~99%), CAS:13446-18-9, Laccase (≥50 units/mg; Rhus vernicifera) CAS:80498-15-3, Potassium permanganate ($KMnO_4$, ≥99.0%) CAS:7722-64-7 have been procured from Sigma-Aldrich, India. Hydrogen peroxide (H_2O_2 30% w/w) CAS:7722-84-1 from Fischer Scientific and Sodium hydroxide (NaOH) from Qualikems. All the purchased chemicals were used without any further purification.

Indium tin oxide coated glass (ITO) (TIX005, resistivity: ≤ 10 ohms/sq., Transmittance: ≥ 90%) was purchased from TECHINSTRO. Deionized water (Mili-Q, 18.2 MΩ cm) was used in solution preparation. Borosil glassware was used after getting autoclaved.

2.2.2. Buffers and solutions

- 100 mM Phosphate buffer saline (PBS) of pH 7.0 containing 0.9 % NaCl

- 5 mM $[Fe(CN)_6]^{3-}$ / $[Fe(CN)_6]^{4-}$ in PBS as redox indicator

2.3. Characterization techniques

The present thesis comprises work involving:

- Synthesis of GO, rGO-MgO, rGO-MoS$_2$, and MgO@rGO-MoS$_2$ nanomaterials

- Fabrication of films on electrodes using synthesized nanomaterials onto ITO-coated glass substrate

- Immobilization of enzyme for fabricating enzymatic biosensing electrode in case of enzymatic biosensor

- Application of fabricated electrode for detection of water-polluting phenolic compounds

At different stages of the synthesis of nanomaterials and while using the fabricated electrode for performing applications, the nanomaterials and electrodes have been characterized using a series of multiple characterizations. The following sub-section gives a brief overview of all the structural, morphological, and electrochemical characterization techniques that have been used in the entire thesis work.

2.3.1. Ultraviolet-Visible spectroscopy (UV-Vis)

UV-Vis spectroscopy is a powerful analytical practice that uses ultraviolet and visible ranges electromagnetic radiations to study the electronic transitions between atoms, ions, and molecules. When UV-Vis light is absorbed by a molecule, the electronic transition taking place leads to the displacement of the electrons from one energy level to another energy level. Each molecule absorbs specific wavelengths of light which become its characteristic. By measuring this specific wavelength, the energies of this electronic transition can be determined, which further gives an identification to suggest the structure and properties of molecules [1]. This spectroscopy has been extensively utilized in the fields of biotechnology, biochemistry, and material science. This spectroscopy is a valuable tool used to characterize the optical properties of materials, such as polymers and nanoparticles. The current thesis involves UV-Vis spectroscopy for the characterization of GO and rGO-MoS_2 nanocomposite (Chapter-4). The instrument used to study the electronic transitions was UV-Vis spectrophotometer (Perkin-Elmer) **(Fig. 2.1).**
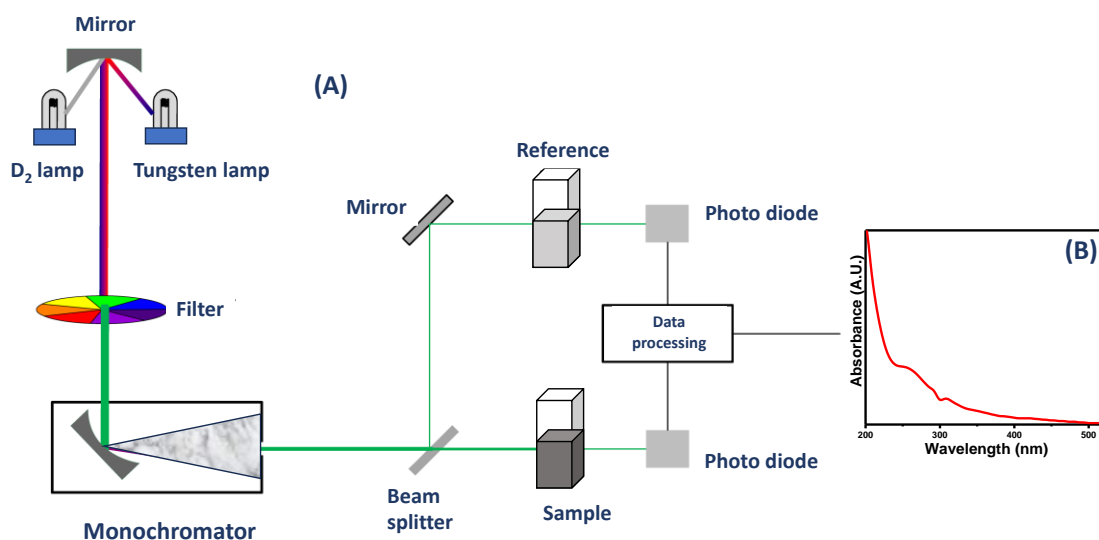
Fig. 2.1: **(A)** Diagrammatic representation of working of UV-Visible spectrophotometer and **(B)** UV-Visible spectrum of GO.

2.3.2. Raman spectroscopy

Raman spectroscopy is another analytical advanced technique which found its emergence from the discovery of the well-known Raman effect. It is based on phenomena occurring due to the inelastic scattering of monochromatic light with the compound and inelastic scattering results in light with different wavelengths as compared to incident light. The effect of light on molecular vibrations significantly gives ideas to elucidate molecular structure or helps to identify functional groups. In this spectroscopy, the laser is used as a source of light, the bandwidth of the laser decides the radiation of the spectrum. The sample molecule is placed in a sample chamber that accepts laser light, afterward the transmitted dispersed light passes through filters. High-quality filters are aligned to separate Rayleigh scattered light (elastic scattering) and Raman scattered light (inelastic scattering) and to avoid extra excitation by laser [2]. The light is then directed through a grating to focus on

detectors. Several different weak and strong bands (signals) are generally obtained from the spectra of a compound which reflects their characteristic properties. Factors such as chemical compositions as well as polymorphism, crystallinity/amorphous behavior, tacticity, etc. can be discovered by analyzing the spectra. This spectroscopy is widely used in several fields of nanotechnology, especially for biotechnology applications[3]. Raman spectroscopy is a significant tool for giving information about the presence of structural defects while characterizing carbon nanomaterials. In this thesis, the Horiba LabRam HR evolution spectrometer was used to record Raman spectra of GO and rGO-MoS$_2$ nanocomposites, and a 633 nm He-Ne laser was used to excite upon the samples **(Fig. 2.2)**.
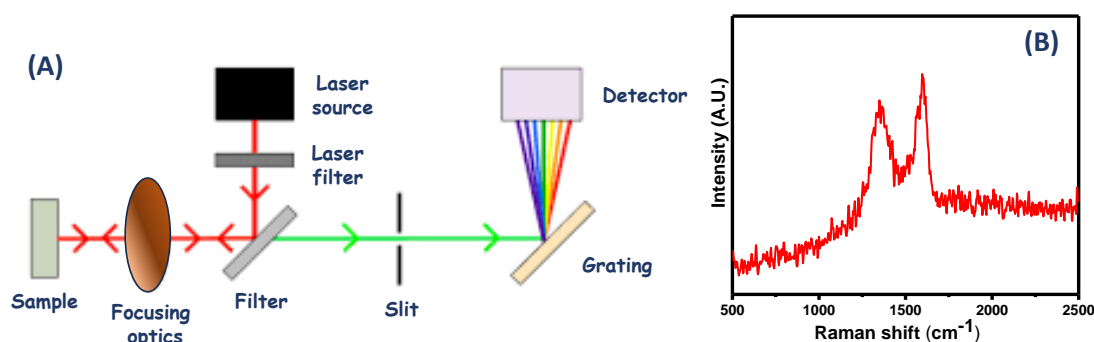
Fig. 2.2: (A) Illustration for the working of Raman spectrometer and **(B)** Raman spectra of synthesized GO

2.3.3. Fourier Transform Infrared spectroscopy (FT-IR)

FT-IR is based on infrared radiations to study the interaction of infra-red electromagnetic radiation with the material. It is highly used for structural characterization due to its high accuracy, fast analysis, simple process for handling, and enhanced sensitivity. This technique is non-destructive and can be employed to study samples of any nature. The fundamentals of FT-IR is based on the molecule's

atomic vibration, which absorbs specific energies and frequencies of infrared radiation. The material or chemical substance produces various spectral lines after absorbing the electromagnetic radiations from the light beam at each wavelength, which further determines the chemical composition of any material or chemical substance [4].

In FT-IR spectroscopy, the Michelson interferometer (**Fig. 2.3 A**) is used to determine the chemical composition of any material. Its basic setup involves four components (a) source of light (filament) (b) beam splitter (c) two mirrors as arranged in Figure 2.3 (d) detector. The source emits infrared radiation, which passage through the beam splitter. The beam-splitter divides the infrared radiation into two parts. The two separate beams of light further travel along two different paths and reflecting by mirrors at the end of each path. After reflection, these separate beams recombine and create an interference, further, the interference pattern is analyzed by the detector. FT-IR is a powerful characterization technique, which provides numerous advantages over dispersive measurements including wider spectral range, higher sensitivity, faster data acquisition, less sample requirement, higher spectral resolution, better signal-to-noise ratio, etc. [5]. This thesis involves the use of Perkin Elmer spectrometer Model Spectrum 2 for analysis of GO-based nanocomposites, especially involving the existence of C-H, C=C, C=O, C-O-C, -OH functional groups and also metal-oxygen stretching frequencies. Individually, Chapter 3 involves the FT-IR spectrum of GO (**Fig. 2.3 B**) and rGO-MgO nanoflakes, Chapter 4 uses FT-IR for determining functional groups and stretching-bending vibrations of GO and rGO-MoS$_2$ nanocomposites while Chapter 5 reveals FT-IR spectra for MgO@rGO-MoS$_2$ nanocomposite.
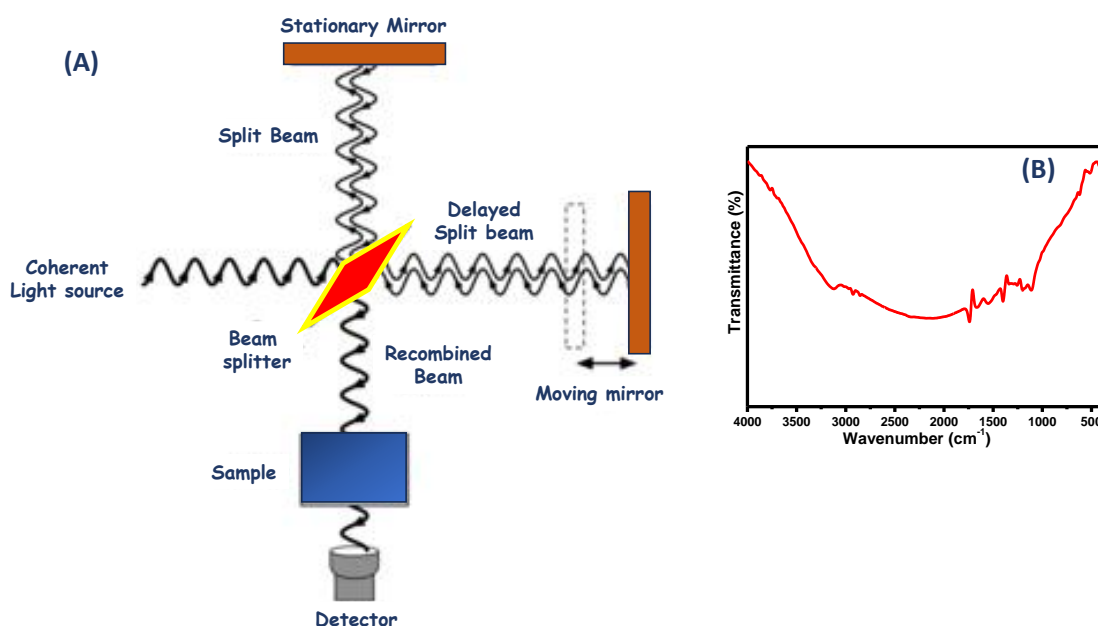
Fig. 2.3: (A) FTIR instrumentation scheme (B) FTIR spectra of GO

2.3.4. X-ray diffraction (XRD)

XRD is a characterization technique that provides primary identification of any unknown crystalline material. XRD has been highly utilized for the analysis of nanostructures of any size, and it basically helps to observe the changes in the positioning of diffraction peaks. Thus, conclusions can be made on how the structure of different crystals and cell parameters changes with the change in size and shape of nanoparticles. The crystallographic structure, orientation of the polycrystalline sample, and crystallite size are also determined by this technique. The working of this technique is based on Bragg's law, which explains how a beam of X-ray incident on a crystal lattice of a sample is reflected at certain angles, providing information about the structure and composition of the sample. X-ray diffractometer is used to record the XRD patterns. The schematic diagram of X-ray diffractometer is represented in **Fig. 2.4**.
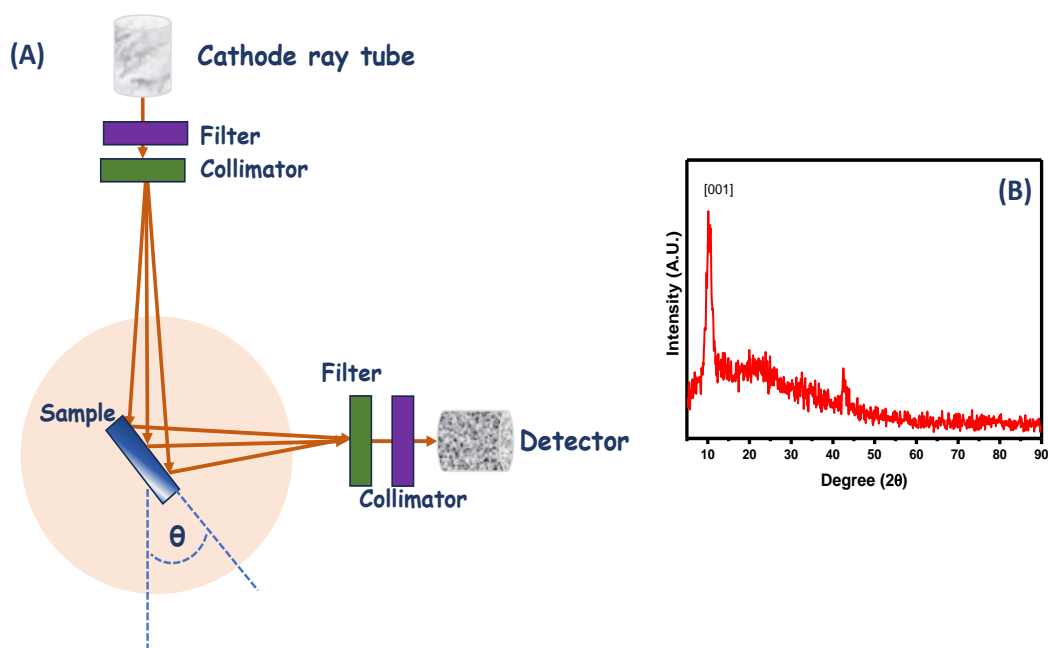
Fig. 2.4: **(A)** Schematic illustration for XRD, **(B)** XRD pattern of GO

The average peak broadening is measured using the most substantial diffraction peaks to obtain the peak broadening data. This data can then be used to analyze the material's structural properties. The Debye-Scherrer equation uses peak broadening in the X-ray diffraction pattern to determine any material's size. In this thesis, the average particle size of all materials has been evaluated by the use of the Debye-Scherrer equation (Eq. 2.1)

$$D = K\lambda / \beta\cos\Theta \tag{2.1}$$

In this equation, K represents the shape factor its value is 0.9, λ represents X-ray wavelength, Θ is Braggs angle in degree and the β represents full-width at half maxima [6]. In this thesis, the structural characterization using X-ray diffraction of all prepared materials (GO and GO based nanocomposites materials) has been recorded using Bruker D-8 Advance X-ray diffractometer having monochromatic radiation (1.5406 Å), diffraction angle ($2\Theta = 10\text{-}80^{\circ}$) and speed of 2°/min.

2.3.5. Scanning electron microscopy (SEM)

SEM is a special category of electron microscope designed to study surface morphologies. The SEM utilizes electrons rather than light to observe the image of the sample. SEM is advantageous with respect to other microscopes as SEM offers a comparatively larger depth of field in order to access more specimens at one time. Also, specimens are focused to give a higher degree of magnification suggesting a higher resolution of SEM. The main components of SEM include- Source of electrons, a column through which the electron beam travels via electromagnetic lenses, an electron detector, a specimen chamber, a computer, and a display unit to watch the images. The SEM has the ability to create plenty of signals at the surface of solids by focusing a beam of high energy electrons [7].

As shown in the scheme of SEM is shown in **Fig. 2.5**. The high-energy electrons are generated at the uppermost part of the column and accelerate in a downward direction, crossing through multiple lenses to result in a focused beam of electrons striking the surface of the specimen. In addition, SEM makes use of vacuum conditions in the specimen chamber by the use of a combination of pumps to result in images of the specimen. As a result of the interaction between the specimen and the electron, signals are produced which are then detected by detectors [8].

In this thesis work, surface morphologies of synthesized rGO-MgO (Chapter 3) and MgO@rGO-MoS$_2$ nanocomposites (Chapter 5) have been inspected using FESEM: FEI Quanta 200F integrated with Oxford-EDS system IE 250 X Max 80, Netherlands instruments, whereas SEM of GO and rGO-MoS$_2$ nanocomposite (Chapter 4) has been examined using EmCrafts Co. Ltd., South Korea instrument. In the same work, a

Lac enzyme-immobilized rGO-MoS$_2$/ITO electrode has also been subjected to undergo the influence of high energy electrons to analyze the morphology of the electrode in addition to raw nanocomposite.
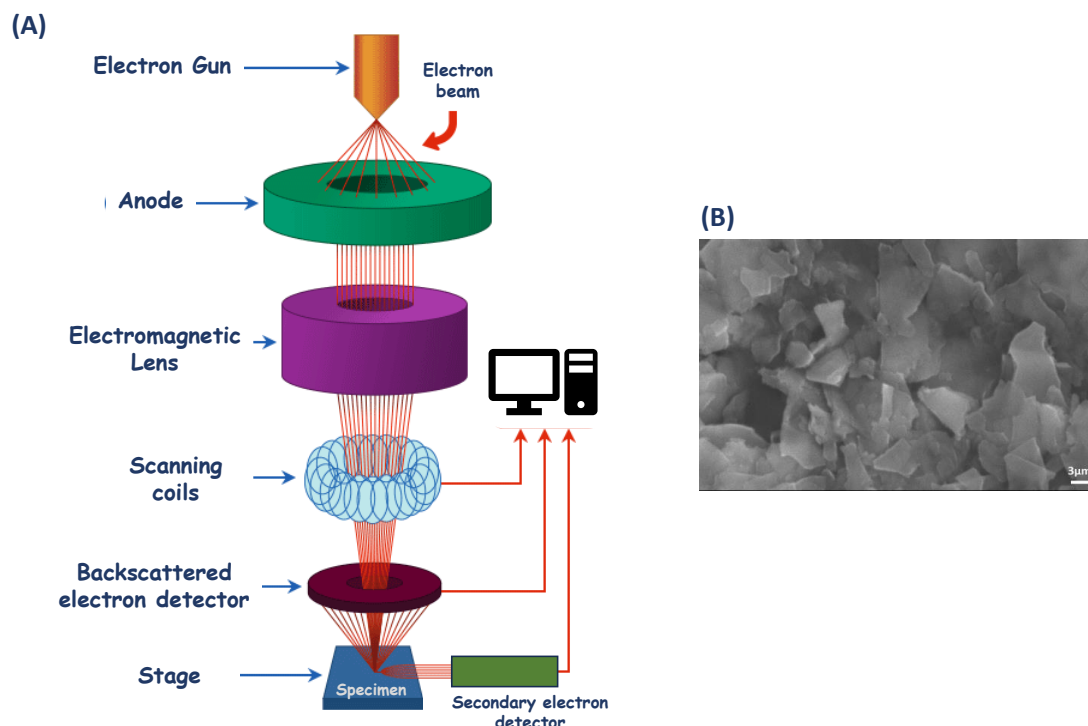
Fig. 2.5: Schematic illustration of SEM instrumentation (B) SEM image of GO

2.3.6. Transmission electron microscopy (TEM)

TEM offers application to study the image of the smallest structure in matter. Under this microscope, high-energy electrons are used to provide information related to the specimens' morphology, composition, and crystallography. TEM has the ability to visualize the detailing of the nanometer range of the specimen and also to magnify it up to a million times. Compared to other microscopes, TEM uses an electron beam of very short wavelength with respect to the wavelength of visible light which leads to an increase in the resolution of this microscope. This is the reason for the immense significance of TEM in the biological and medical fields [9].

56

The image visualization in TEM follows a slightly similar pathway to that of SEM. A high-energy electron beam arising from the electron gun placed at the topmost part of the TEM unit ejects electrons that transport through the microscope's vacuum tube. An electromagnetic lens placed in between focuses the electrons traveling through the tube in a fine beam which then strikes at the thin specimen **(Fig. 2.6).** This led to either scattering of electrons or hitting the electrons on a fluorescent screen placed at the lowermost part of the microscope. Thereafter, the specimen's image is reflected on the display unit, the image basically comprises shades of assorted parts of the specimen's depending upon the density of the specimen which appears on the screen [10]. In the present work, EVO-18, ZEISS TEM instrument has been used to study the morphology of MgO-rGO@MoS$_2$ nanohybrid in Chapter 5.
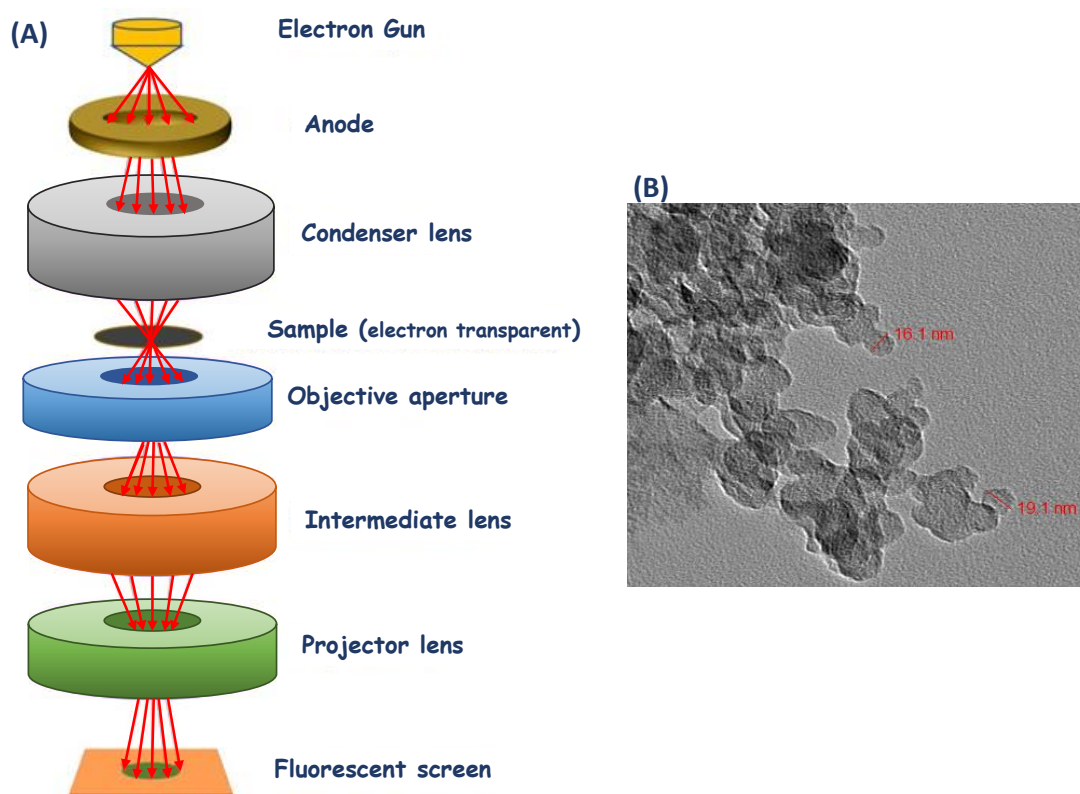
Fig. 2.6 (A) Schematic illustration of TEM instrumentation (B) TEM image of MgO-rGO@MoS$_2$

2.3.7. Energy Dispersive X-ray Analysis (EDX)

EDX examines near-surface elements and calculates the elemental proportion at various points to provide an overall sample mapping. The basic fundamentals of SEM and the EDX concept are conjoined. An electron beam with an energy of 10–20 keV impacts the surface, causing material to release X-rays; the energy of the emitted X-rays is dependent on the substance being studied. EDX does not qualify as a surface science method because the X-rays are produced in a zone that is only a few microns deep. The electron beam is moved across it to create an image of the elements present in the sample during EDX analysis. The composition and quantity of the heavy metal ions of the nanoparticles that are positioned close to or at the surface of a sample can be detected using the EDX. However, EDX has difficulty detecting atoms with atomic numbers below 11 [11]. As the X-ray intensity is low, it typically takes many hours to obtain the photographs. Silver, gold, and palladium nanoparticles on the surface are simple to recognize with EDX [12]. In the thesis work, EDX has been used in Chapter 3 to evaluate the presence of Mg, O, and C among rGO-MgO nanoflakes whereas in Chapter 5 it has been used to analyze the purity of nanohybrid $MgO@rGO-MoS_2$.

2.3.8. Electrochemical Techniques

Electrochemistry is an electroanalytical technique that measures responses occurring in an electrochemical cell in terms of potential or current. For biosensors, generally, electric potential is applied and the technique is used to ascertain the chemical reactivity of an analyte by recording data for changes in current or potential with respect to the concentration of an analyte. The majority of electrochemical methods' own assemblies have three electrodes set up, comprising a working electrode (nanocomposite), the reference electrode, and the counter/auxiliary electrode. These

electrodes are effectively coupled to a Potentiostat, which is a device that regulates the working electrode's voltage and detects the accompanying current response. In some electrochemical investigations, the working electrode is generally subjected to a suitable optimized potential to study the obtained current vs time response, while in other cases, the linear altered potential results in current vs applied potential responses. In an electrolytic solution, Nernst's equation gives a quantitative aspect of potential (E) for known concentrations of oxidized and reduced forms of the redox system, depicted by Eq. 2.2.

$$E = E_o + \frac{RT}{nF} \ln \frac{[oxi]}{[red]} \tag{2.2}$$

Here, E_o = electrode potential of electrodes, [oxi] and [red] = equilibrium concentrations of redox species while F and T represent Faraday's constant and temperature. The working of three electrodes relies on the applied potential, the redox species reacting at the electrodes regulate the proportion of concentrations ([oxi] and [red]) on the basis to satisfy the Nernst equation. Autolab (EcoChemie, Netherlands) Potentiostat/Galvanostat instrument has been used to perform all electrochemical characterization (Cyclic voltammetry, Chronoamperometry, Square wave voltammetry) in the present thesis. Here, the most common Ag/AgCl electrode has been used (E = +0.197 V) as the reference electrode whereas, platinum has been used as an auxiliary electrode. DC power source is used to obtain precise, regulated, and stable potential using the Potentiostat to produce an even fraction of current at a constant voltage.

2.3.8.1. Electrochemical impedance spectroscopic (EIS) measurements

EIS is a powerful method aimed at studying the electrochemical properties of conducting materials and the interfaces between electrodes. For an ideal resistor, the well-known Ohm's law defines the power of a single element of an electrical circuit to resist the flow of current (Resistance, R) in terms of the ratio between voltage (E) and current (I) which also remains completely in phase with each other. But in a realistic world, such properties of such circuits cannot be applied and utilized as they possess much complex behavior, and thus the concept of resistance is overtaken by impedance. The most common method for determining an electrochemical impedance is by applying AC potential and monitoring the current passing through the electrochemical cell. The generated AC current signals are analyzed sinusoidally on which excitation potential was most likely excited. A small excitation pulse is typically used to measure electrochemical impedance with the aim to obtain a pseudo-linear response from the electrochemical cell [13].

In a linear system with an applied sinusoidal potential, the matching current has a phase shift but is otherwise sinusoidal at the same frequency. It is possible to physically derive significant characteristics of the electrochemical system by modeling the impedance data in terms of R_s (solution resistance), R_{ct} (charge transfer resistance), CPE (constant phase element) and Cdl (double-layer capacitance). Z_w (Warburg element) is also used to display the cell's diffusion or mass transport impedance. For electrochemical cells, the equivalent circuit model EIS data are displayed using the Nyquist plot at a particular frequency. Under Nyquist plots, Z_w comprises both real and imaginary parts plotted either on X or Y axis[14].

For an electrochemical cell, Nyquist plot displays capacitive and inductive properties corresponding to the imaginary impedance. The mass transports of the reactant and product play a important part in determining the electron transfer rate, which is dependent on the consumption of the oxidants and reductants released near the surface of the electrode during charge transfer at the interface. Due to the presence of a current plateau in a polarogram or a peak current in a voltammogram, mass transfer of the reactants and products results in a different class of impedance (Z_W), which is investigated by electroanalytical chemists. In this thesis, EIS has been used to calculate R_{ct} of the obtained EIS spectra derived by fitting the obtained impedance spectra with an equivalent Randles and Ershler circuit model. Based on the obtained R_{ct} values, the exchange current per geometric unit area (I_o) and heterogeneous electron transfer rate constant (k_o) of the different electrodes has been calculated using equation (2.3) and (2.4):

$$I_o = nRT/R_{ct}F \tag{2.3}$$

$$k_o = RT/ n^2F^2AR_{ct}C \tag{2.4}$$

where R is the universal gas constant, F is Faraday's constant, n is the number of electrons transferred, A is the geometrical area of electrodes, T is the temperature in Kelvin and C is the concentration of the electro-active redox probe [15].

2.3.8.2. Cyclic Voltammetry (CV)

CV is among the most utilized electrochemical techniques to describe the electrochemical response of electroactive species. In a CV study, the voltage of the working electrode is swept across time in one direction and brought back in the opposite direction to its initial value after reaching the fixed point. For the purpose of

creating a CV graph, these potential cycles can be swept as needed at different scan rates. CV is used to obtain information about electrochemical reactions involving species with known redox potential. The counter electrode transports electrons from the source to the working electrode, afterwards, the current at the working electrode is used to record the potential scans against the potential of a stationary reference electrode (Illustration **Fig. 2.7**). Additionally, an electrolyte solution is required to provide an ionic medium to the electrodes during the redox process [16].
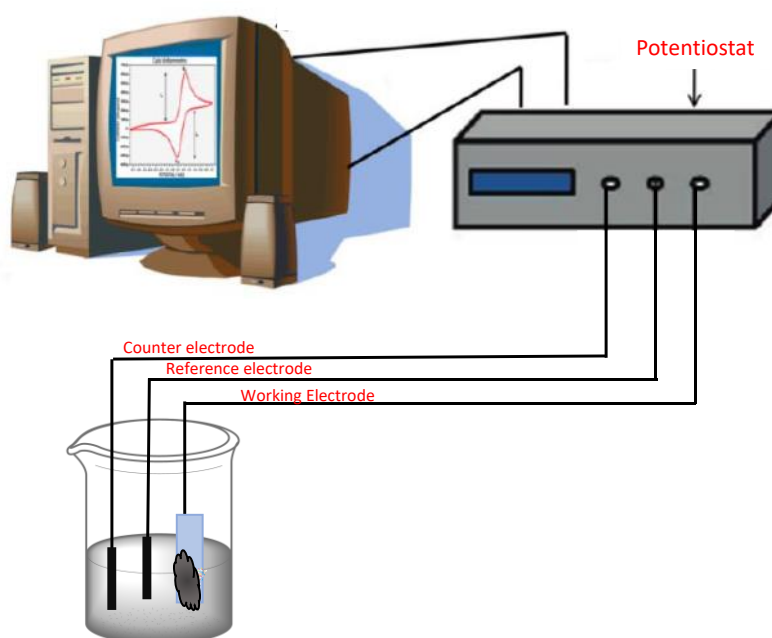
Fig. 2.7: Potentiostat workstation illustration with three-electrode set up

The obtained peak current during CV studies can be used to calculate seve.ral physical parameters that predict the efficiency of the electrode.

Based on Laviron's theory, α (charge transfer coefficient) and K_α (heterogeneous electron transfer rate constant) can be calculated using equations 2.5 to 2.7.

$E_{pa} = 2.303RT/(1-\alpha)nF$ and $E_{pc} = -2.303RT/\alpha n F$ **(2.5)**

$$\Delta E_p = E_{pa} - E_{pc} \tag{2.6}$$

$$\ln K_\alpha = \alpha \ln (1 - \alpha) + (1 - \alpha) \ln \alpha - \ln (R\,T/n\,F\,\upsilon) - \alpha\,(1 - \alpha)\,n\,F\,\Delta E_p\,/\,R\,T \tag{2.7}$$

Where E_{pa} is anodic and E_{pc} is cathodic peak potentials respectively [17], R is universal gas constant, F is Faraday's constant, and υ is scan rate [15].

Other parameters such as D (Diffusion coefficient) and Γ (surface concentration) of modified material on ITO electrode can be evaluated using the Randles–Ševčík equation [18]:

$$I_p = (2.69 \times 10^5)\, n^{3/2} AcD^{1/2} \upsilon^{1/2} \tag{2.8}$$

$$I_p = n^2 F^2 A \Gamma \upsilon / 4RT \tag{2.9}$$

where I_p= anodic peak current, c = molar concentration of $[Fe(CN)_6]^{3-/4-}$ in mol/cm^3 and n = electron per molecule oxidized or reduced [19]. In this thesis work, CV studies ranging from scan rate of 10 mV/s to 300 mV/s has been performed in potential window: -0.6 V to 0.6 V in Chapter 3, 4 and 5.

2.3.8.3. Chronoamperometry

Chronoamperometry is the simplest well established amperometric electrochemical analysis technique. It is basically a time-dependent step technique in which square wave potential is applied to the working electrode. This technique leads to either oxidation or reduction (faradaic process) in the electrolytic solution at the surface of the electrode. It is then used to record the relationship between current with respect to time for an electrode to monitor the diffusion of the substrate from the electrolytic bulk solution (buffer and analyte) [20]. The current fluctuates as the concentration of

substrate is subjected to any change due to rise and fall in diffuse layers of the substrate in the vicinity of the electrode. Chronoamperometry has been regarded as a sensitive technique that is independent of the classification of substrate or biological recognition element used for electrochemical biosensing [21]. In this thesis chronoamperometry technique has been used in Chapter 3 and Chapter 4 for electrochemical detection of analyte.

2.3.8.4. Square wave voltammetry (SWV)

SWV is a rapid and advanced large amplitude differential technique, wherein combination of ordered square waveforms overlying on staircase potential are operated onto a working electrode. SWV offers benefits over other differential techniques as it makes use of differential current plots rather than reverse current plots. Additionally, the negligible influence of non-faradaic currents in SWV also enhances the sensitivity of the working electrode and offers high rejection to capacitive currents [22]. SWV combines the characteristics of various pulse voltametric methods, most importantly background suppression and sensitivity of differential pulse voltammetry and diagnostic value of normal pulse voltammetry [23]. In this thesis SWV has been performed in Chapter 5 for detection of water pollutants using non-enzymatic approach.

2.4. Immobilization of enzyme to the GO-based matrix

The effective immobilization of the Lac enzyme onto suitable matrices is crucial for improving the stability, longevity, effectiveness, and reusability of fabricated biosensors for the detection of PC as well as equating their cost. Furthermore, unique bonding, entrapment, and crosslinking are likewise involved, which lengthens the duration of life

of enzymes. By properly adhering to the surface of the suitable matrix, immobilization preserves the structural stability and functional properties of the immobilized enzyme, allowing for the retention of the enzyme's necessary activity after repeated use of the sensor. There are several methods of immobilization, including covalent bonding, adsorption, cross-linking, entrapment, and encapsulation. Recently, immobilization matrices made of nanomaterials have received greater attention. Sofia et al. demonstrated numerous techniques for covalently immobilizing lactose onto various matrices (**Fig. 2.8**). For carbonaceous matrices, they observed two major methods to covalently attach those matrices i.e., Lac bonded with the -NH2 group and supported by glutaraldehyde and Lac bonded with the COOH by using EDC/NHS [24].
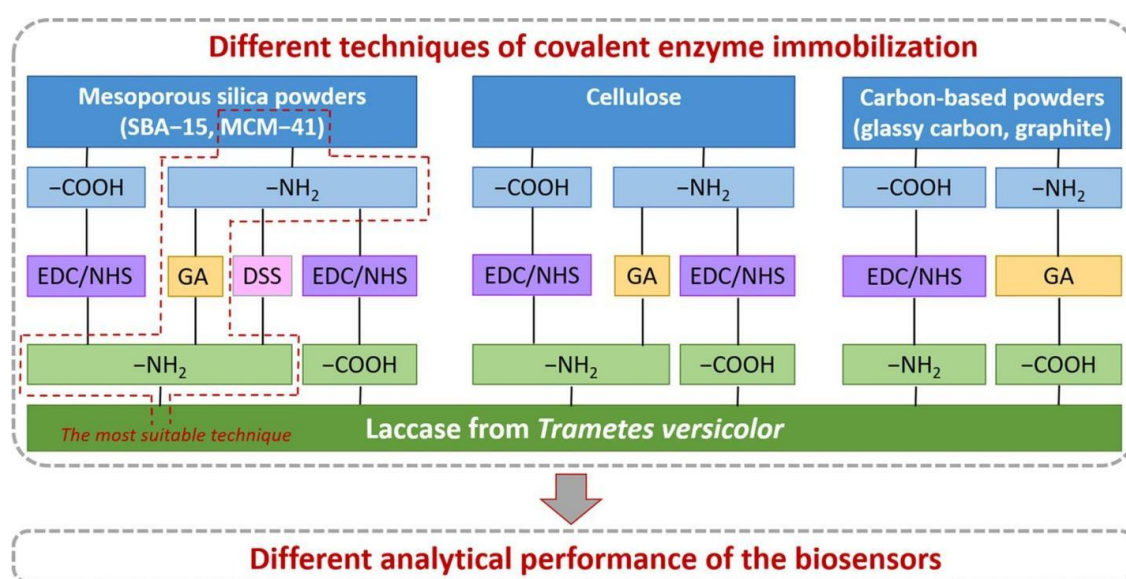
Fig. 2.8 Demonstration of various laccase covalent immobilization techniques on various matrices, Adapted with Permission from [24]. Copyright © 2022 Elsevier.

In this thesis, for GO-based nanocomposites in Chapter 3 and Chapter 4, EDC/NHS has been used as a crosslinker to form a bond in between the -COOH group of GO based matrix and -NH$_2$ group of lac enzyme.

2.5. Protocols for estimating different performance-related parameters for rGO nanocomposites-based immuno-biosensors

2.5.1. Linear Range, Sensitivity, and Detection Limit

The biosensor's linear detection range (LOD) is the range of concentration over which current response varies proportionally as a function of analyte's concentration. This thesis work used chromatoamperometry (Chapters 3 and 4) and SWV (Chapter 5) techniques to determine the linear range.

$$LOD = 3\sigma/S \tag{2.11}$$

where σ is the standard deviation of the electrode, S is the slope of the linearity plot)

The relationship between the change in analyte concentration and the strength of the signal produced by the transducer is known as the sensitivity of a biosensor. A biosensor should ideally produce a signal in response to even the smallest changes in the target analyte's concentration.

$$Sensitivity = slope/active \ surface \ area \ of \ electrode \tag{2.12}$$

2.5.2. Shelf-Life and reproducibility of the bioelectrodes

The shelf life and repeatability of the biosensor have been used to determine its lifespan. Shelf life refers to the duration a sensor considers suitable while maintaining its maximum activity level during storage. This can be achieved by measuring the current response of the bioelectrodes at regular intervals of time. Meanwhile, reproducibility refers to the measurement of the drift or scatter in a sequence of observations or findings made over time. The number of times the bioelectrode can be used is crucial for estimating repeatability. Some of the parameters that affect the stability of the bioelectrode include the material used for the sensor production, the morphology of the matrices, and the technique used to immobilize biomolecules.

References

[1]   L. D. S. Yadav, "Ultraviolet (UV) and Visible Spectroscopy BT - Organic Spectroscopy," L. D. S. Yadav, Ed. Dordrecht: Springer Netherlands, p. 7–51, 2005.

[2]   L. A. Woodward, "General Introduction BT - Raman Spectroscopy: Theory and Practice," H. A. Szymanski, Ed. Boston, MA: Springer US, p. 1–43, 1976.

[3]   J. R. Ferraro, K. Nakamoto, and C. W. Brown, "Chapter 4 - Materials Applications," J. R. Ferraro, K. Nakamoto, and C. W. B. T.-I. R. S. (Second E. Brown, Eds. San Diego: Academic Press, p. 207–266, 2003.

[4]   D. Peak, "FOURIER TRANSFORM INFRARED SPECTROSCOPY," D. B. T.-E. of S. in the E. Hillel, Ed. Oxford: Elsevier, p. 80–85, 2005.

[5]   P. Griffiths, "Handbook of Vibrational Spectroscopy," vol. 1, 2006.

[6]   R. A. Dunlap, "X-ray diffraction techniques," *Novel Microstructures for Solids*. Morgan & Claypool Publishers, p. 2–16, 2018.

[7]   M. de Assumpção Pereira-da-Silva and F. A. Ferri, "1 - Scanning Electron Microscopy," in *Micro and Nano Technologies*, A. L. Da Róz, M. Ferreira, F. de Lima Leite, and O. N. B. T.-N. T. Oliveira, Eds. William Andrew Publishing, p. 1–35, 2017.

[8]   M. K. Singh and A. Singh, "Chapter 17 - Scanning electron microscope," in *The Textile Institute Book Series*, M. K. Singh and A. B. T.-C. of P. and F. Singh, Eds. Woodhead Publishing, p. 387–419, 2022.

[9]   D. B. Williams and C. B. Carter, "The Transmission Electron Microscope BT - Transmission Electron Microscopy: A Textbook for Materials Science," D. B. Williams and C. B. Carter, Eds. Boston, MA: Springer US, p. 3–22, 2009.

[10]   H. Saka, "Chapter 14 - Transmission Electron Microscopy," E. YASUDA, M. INAGAKI, K. KANEKO, M. ENDO, A. OYA, and Y. B. T.-C. A. TANABE, Eds. Oxford: Elsevier Science, p. 223–238, 2003.

[11] D. Titus, E. James Jebaseelan Samuel, and S. M. Roopan, "Chapter 12 - Nanoparticle characterization techniques," in *Micro and Nano Technologies*, A. K. Shukla and S. B. T.-G. S. Iravani Characterization and Applications of Nanoparticles, Eds. Elsevier, p. 303–319, 2009.

[12] T. Roodbar Shojaei, S. Soltani, and M. Derakhshani, "Chapter 6 - Synthesis, properties, and biomedical applications of inorganic bionanomaterials," in *Micro and Nano Technologies*, A. Barhoum, J. Jeevanandam, and M. K. B. T.-F. of B. Danquah, Eds. Elsevier, p. 139–174, 2022.

[13] H. H. Hernández *et al.*, "Electrochemical Impedance Spectroscopy (EIS): A Review Study of Basic Aspects of the Corrosion Mechanism Applied to Steels," M. El-Azazy, M. Min, and P. Annus, Eds. Rijeka: IntechOpen, p. Ch. 1, 2020.

[14] Y. Bavafa-Toosi, "6 - Nyquist plot," Y. B. T.-I. to L. C. S. Bavafa-Toosi, Ed. Academic Press, p. 533–640, 2019.

[15] D. Thakur, C. M. Pandey, and D. Kumar, "Highly Sensitive Enzymatic Biosensor Based on Polyaniline-Wrapped Titanium Dioxide Nanohybrid for Fish Freshness Detection," *Appl. Biochem. Biotechnol.*, vol. 194, no. 8, p. 3765–3778, 2022.

[16] F. Marken, A. Neudeck, and A. M. Bond, "Cyclic Voltammetry BT - Electroanalytical Methods: Guide to Experiments and Applications," F. Scholz, Ed. Berlin, Heidelberg: Springer Berlin Heidelberg, p. 51–97, 2002.

[17] D. Cheng and X. Kan, "Simultaneous determination of dihydroxybenzene isomers based on gold dendritic/pEDOT electrochemical sensor," *J. Electroanal. Chem.*, vol. 857, p. 113741, 2020.

[18] S. Verma, C. M. Pandey, and D. Kumar, "A highly efficient rGO grafted MoS2 nanocomposite for dye adsorption and electrochemical detection of hydroquinone in wastewater," *New J. Chem.*, vol. 46, no. 44, p. 21190–21200, 2022.

[19] S. Paneru and D. Kumar, "A Novel Electrochemical Biosensor Based on Polyaniline-Embedded Copper Oxide Nanoparticles for High-Sensitive Paraoxon-Ethyl (PE) Detection," *Appl. Biochem. Biotechnol.*, vol. 195, p. 4485–4502 2023.

[20] R. J. Mortimer, "Spectroelectrochemistry, Methods and Instrumentation," J. C. Lindon, G. E. Tranter, and D. W. B. T.-E. of S. and S. (Third E. Koppenaal, Eds. Oxford: Academic Press, p. 172–177, 2017.

[21] G. Ghosh, "Chapter 27 - Graphene oxide-nanocomposite-based electrochemical sensors for the detection of organophosphate pesticides," S. Das, S. Thomas, and P. P. B. T.-S. of D. T. C. W. A. Das Nerve Agent Simulants, and their Toxicological Aspects, Eds. Elsevier, p. 635–658, 2023.

[22] A. Tolun and Z. Altintas, "Chapter 16 - Chemical sensing of food phenolics and antioxidant capacity," A. Barhoum and Z. B. T.-A. S. T. Altintas, Eds. Elsevier, p. 593–646, 2023.

[23] F. R. Simões and M. G. Xavier, "6 - Electrochemical Sensors," in *Micro and Nano Technologies*, A. L. Da Róz, M. Ferreira, F. de Lima Leite, and O. N. B. T.-N. and its A. Oliveira, Eds. William Andrew Publishing, p. 155–178, 2017.

[24] S. Tvorynska, J. Barek, and B. Josypcuk, "Influence of different covalent immobilization protocols on electroanalytical performance of laccase-based biosensors," *Bioelectrochemistry*, vol. 148, p. 108223, 2022.

CHAPTER 3

GRAPHENE OXIDE/MgO NANOFLAKES-BASED BIOSENSOR FOR THE DETECTION OF PHENOLIC COMPOUNDS

3.1. Introduction

In this work, we propose an ultrasensitive and stable graphene-magnesium oxide nanoflakes (rGO-MgONf) based electrode to achieve highly precise analysis of Hq (a water-polluting phenol) using Lac enzyme **(Fig. 3.1)**. Metal oxide nanostructures when combined with rGO, increase the biocompatibility, conductivity and catalytic activity of GO-based nanocomposites, making them more suitable for enzyme loading and electrochemical applications [1]. Among various materials, magnesium oxide (MgO) is chemically stable, environmentally friendly, electroconductive, and has a wide band gap [2],[3]. In the following segments all the details regarding the synthesis of rGO-MgONf, along with structural, morphological, elemental and electrochemical characterization results.
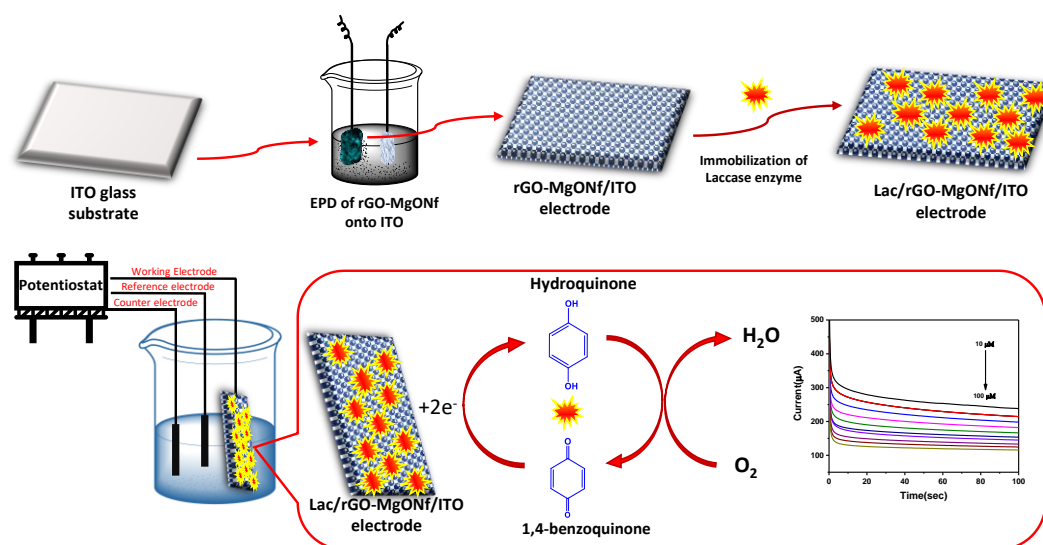
Fig. 3.1: Schematic diagram for the fabrication of Lac/rGO-MgONf based biosensing electrode for detection of Hq.

3.2. Experimental Section

3.2.1. Synthesis of GO

Synthesis of GO has been done using an improvised Modified Hummer's method [4]. Briefly, under an ice bath, 3 g of graphite powder was mixed in 70 mL of concentrated H_2SO_4 while constantly stirring for 2 h. $KMnO_4$ (9 g) was then suspended in the suspension, and the solution was kept below 20 °C while stirring. Further, the reaction progressed with the slow addition of 200 mL of DI water to the beaker nearly at 90 °C. After half an hour, the color of the solution turned intense yellow from brown. Afterward, 0.5 L of DI water and 15 mL of H_2O_2 (30%) was added. 1:1 mixture of HCl (10% v/v) and DI water was then used to remove impurities from the stagnant. The centrifuged solid precipitate (5000 rpm, 15 min) was separated and dried in an oven overnight at 60 °C.

3.2.2. Synthesis of MgO

MgO was synthesized using the sol-gel method [5], using $MgN_2O_6 \cdot 6H_2O$ (0.2 M, 10 mL) and subsequent dropwise addition of 0.5 M NaOH (pH 12) while continuously stirring for half an hour, resulting in a white precipitate of $Mg(OH)_2$. The crystal white precipitate was then centrifuged and washed using DI water-methanol to eliminate unwanted impurities. To obtain pure MgO powder, it was left overnight at 60 °C and thereafter annealed at 400 °C for 3 h in a muffle furnace. The following reactions are involved in this process:

$$Mg(NO_3)_2 + 2NaOH \rightarrow Mg(OH)_2 + 2NaNO_3$$

$$Mg(OH)_2 \rightarrow MgO + H_2O$$
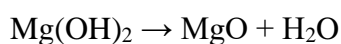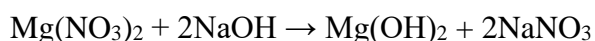
3.2.3. Synthesis of rGO-MgONf

rGO-MgONf was synthesized using the precipitation method with slight modifications [6]. Synthesized GO powder (1 mg/mL) was added to DI water (10 mL) and then ultrasonicated for 2 h. Thereafter, the colloidal solution of GO and pure $MgN_2O_6 \cdot 6H_2O$ (0.3 M, 100 mL DI) were mixed while constant stirring on a magnetic stirrer set at a temperature equivalent to 70 °C for 2 h. Hydrazine hydrate was then added dropwise to the solution as a reducing agent to obtain a pH of around 10.0. The solution was then left to cool at room temperature, washed several times using a water-ethanol solution, and centrifuged. The resulting grey product was further dried at 60 °C in an oven and then annealed at 400 °C for 3 h.

3.2.4. Electrophoretic deposition of rGO-MgONf

The rGO-MgONf was electrophoretically deposited onto a glass substrate with ITO coating. Pt was used as a counter electrode for the EPD and was positioned at a distance of 1 cm from the ITO glass substrate. The rGO-MgONf (0.25 mg mL^{-1}) was ultrasonicated in DI water to create a colloidal suspension and the deposition was conducted at an optimized DC potential of 10 V for 8 s for GO, MgO and rGO-MgONf.

3.2.5. Fabrication of rGO-MgONf nanocomposite-based biosensing electrode

The biosensing electrode was fabricated by drop-casting 10 µL EDC-NHS onto rGO-MgONf/ITO electrode, followed by incubation in a humid chamber for 2 h. The electrodes were washed using PBS and then 20 µL of Lac enzyme (1 mg/mL) was drop-casted onto a functionalized rGO-MgONf/ITO electrode. The Lac/rGO-

MgONf/ITO electrode was kept in a refrigerator (4 °C) prior to being used for biosensing applications.

3.3. Results And Discussion

3.3.1. Structural and morphological studies

Fig. 3.2A displays the XRD pattern of GO, MgO and rGO-MgONf. The (001) planes of GO (curve (i)) corresponds to the intense peak at 10.4º. The XRD of MgO nanoparticles illustrates crystalline cubic structure with peaks at 37° (111), 42° (200), 62° (220), 74° (311) and 78° (222), matching with JCPDS card number 75-1525 [7]. The disappearance of the peak at 10.4° in curve (iii) shows a reduction of GO to rGO, while other peaks were found similar to that of pure MgO in curve (iii) with a slight change in 2θ value, indicating the successful formation of rGO-MgONf. Using Debye Scherer's equation, it was determined that the average crystallite size of MgO is 20.26 nm.
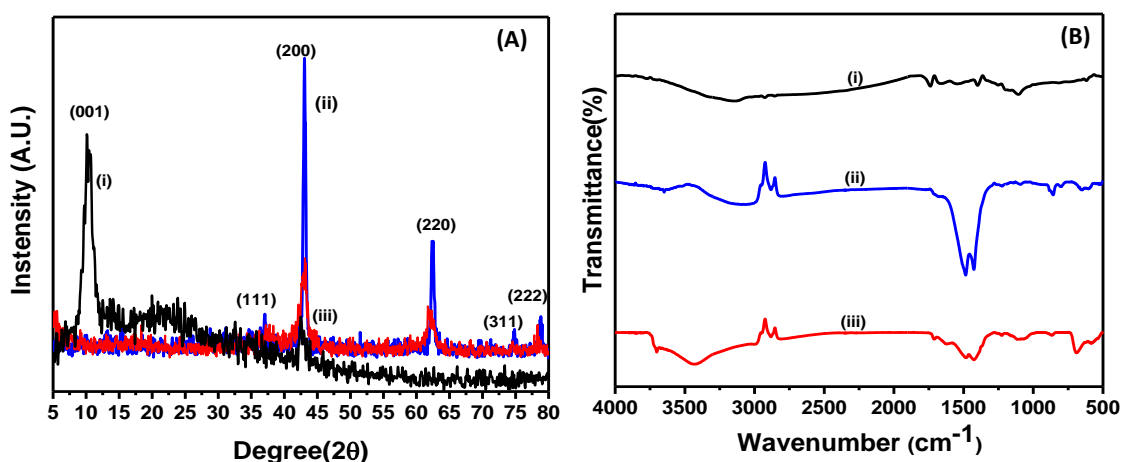
Fig. 3.2: (**A**) XRD patterns of (i) GO, (ii) MgO and (iii) rGO-MgONf (**B**) FT-IR spectra of (i) GO, (ii) MgO and (iii) rGO-MgONf.
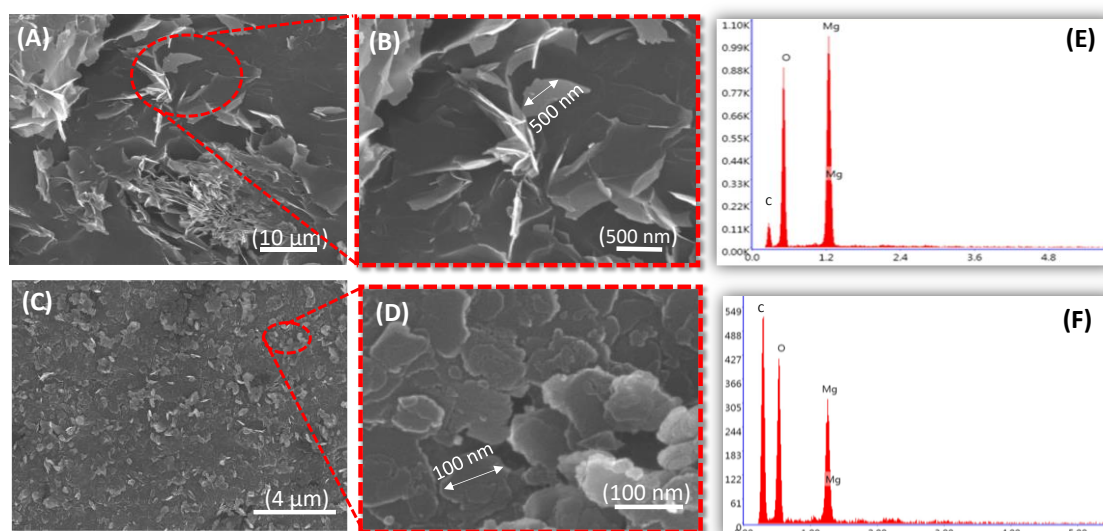
Fig. 3.3 FESEM image of **(A), (B)** MgO nanoparticles, **(C), (D)** rGO-MgONf and EDX spectra of **(E)** MgO and **(F)** rGO-MgONf

Fig. 3.2B shows the FTIR spectra of GO (curve (i)), primarily consisting of a broad peak at 3200 cm^{-1}, which corresponds to O-H vibration, while the other sharp peaks at 1738 cm^{-1}, 1666 cm^{-1}, 1401 cm^{-1} and 1102 cm^{-1} are due to C=O, C=C, C-H and C-O stretching vibrations respectively. FTIR spectra of MgO (curve (ii)) and rGO-MgONf (curve (iii)), show the O-H peak at 3500 cm^{-1}, whereas a peak at 2882 cm^{-1} denotes C-H vibration[8]. The small peak near 3600 cm^{-1} in MgO shows the formation of MgO from Mg(OH)$_2$; however, it becomes slightly sharp in the case of rGO-MgONf due to a partially hydroxylated surface [9]. The peak intensity for C=O and C=C bonds in the FTIR spectra of rGO-MgONf has been reduced and shifted. It may be due to the reduction of GO to rGO. The Mg-O-Mg stretching vibrations appear at 862 cm^{-1} and 682 cm^{-1} [10].

The surface morphology of the synthesized MgO shows a flake-like structure, where the flakes are densely packed and intercalated **(Fig. 3.3A)**. However, the SEM image

of rGO-MgONf **(Fig. 3.3C)** illustrates a clear, smooth, well-distributed, evenly sized flaked structure with an average diameter~100 nm, thus named nanoflakes that could provide better surface area for the enzymatic reaction. The EDX of MgO NPs shows intense peaks of Mg and O **(Fig. 3.3E)**. Whereas, the EDX of rGO-MgONf shows the presence of C, O and Mg, which shows the purity of synthesized nanomaterial **(Fig. 3.3F)**.

3.3.2. Electrochemical Characterization

Electrochemical impedance spectroscopy (EIS) was carried out in the 0.01-10^5 Hz frequency range with a set potential of 0.01V. It has been used to study the interfacial behavior of the electrode surface on modification. **Fig. 3.4** shows the Nyquist plot for the different fabricated electrodes. The inset **Fig. 3.4** represents an equivalent circuit that comprises of R_{ct}, R_s, *CPE*, and Z_w. The R_{ct} value of GO/ITO, MgO/ITO, rGO-MgONf/ITO electrodes analysed using curves (i), (ii) and (iii) respectively was found to be 70.79 kΩ, 35.25 kΩ, and 29.03 kΩ, respectively. The reduction in the R_{ct} value of the rGO-MgONf/ITO electrode compared to GO/ITO electrode and MgO/ITO electrode is attributed to a strong cohesion between MgO–rGO interface. The I_o (exchange current per geometric unit area) for GO/ITO electrode, MgO/ITO and rGO-MgONf/ITO electrode calculated using using the equations (2.3) was found to be 1.47 µA cm^{-2}, 2.96 µA cm^{-2}, and 3.66 µA cm^{-2}, respectively. Furthermore, the value of K_o (heterogeneous electron transfer rate constant) for the respective electrode was found using equation 2.4 was 30.2 nm s^{-1}, 60.6 nm s^{-1} and 73.5 nm s^{-1}. The advanced values of I_o and K_o for rGO-MgONf/ITO is due to synergistic interaction between MgO NPs and GO sheets [6].
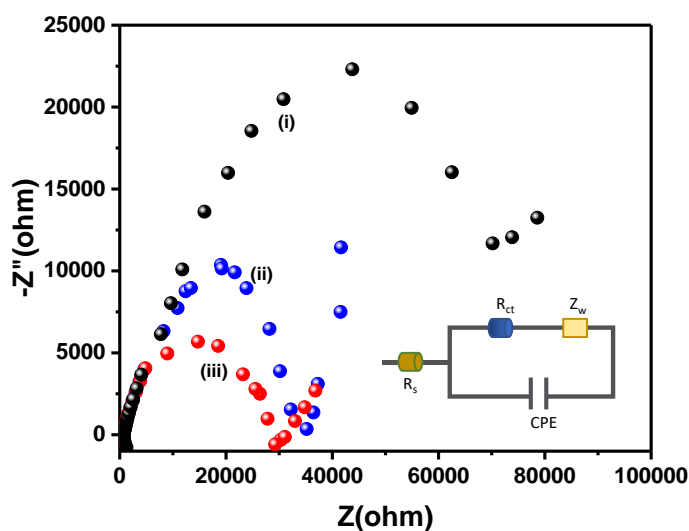
Fig. 3.4; (i) GO/ITO, (ii) MgO/ITO and (iii) rGO-MgONf/ITO electrode's Nquist diagrams (inset-circuit fit)

The CV studies performed at a scan rate of 50 mV/s depict that the rGO-MgONf/ITO electrode shows maximum current response (462.81 µA) as compared to MgO/ITO (339.21 µA), GO/ITO (273.01 µA) and bare ITO electrode (202.90 µA) **(Fig. 3.5A)**. This enhanced conductivity of the rGO-MgONf/ITO electrode may be due to the increased surface area that helps transfer electrons. The scan rate studies (10-300 mV/s) using CV have been performed for GO/ITO, MgO/ITO, and rGO-MgONf/ITO electrodes **(Fig. 3.5 B)**. It has been observed that redox potential plotted against log (scan rate) increases linearly for modified rGO-MgONf/ITO electrode **(Fig. 3.5 C)** and follows equations 3.1 and 3.2.

$E_{pa}(V)$ [rGO-MgONf/ITO] $= 0.1754$ (V) $+ 0.0380$ (V) $*$ Log [v (mV/s)]; $R^2 = 0.976$ **(3.1)**

$E_{pc}(V)$ [rGO-MgONf/ITO] $= 0.1745$ (V) $- 0.0506$ (V) $*$ Log [v (mV/s)]; $R^2 = 0.987$ **(3.2)**

Based on Laviron's theory (equation 2.5 to 2.7) α and K_α for the rGO-MgONf/ITO

electrode were found to be 0.89 and 0.223 s^{-1}, respectively.
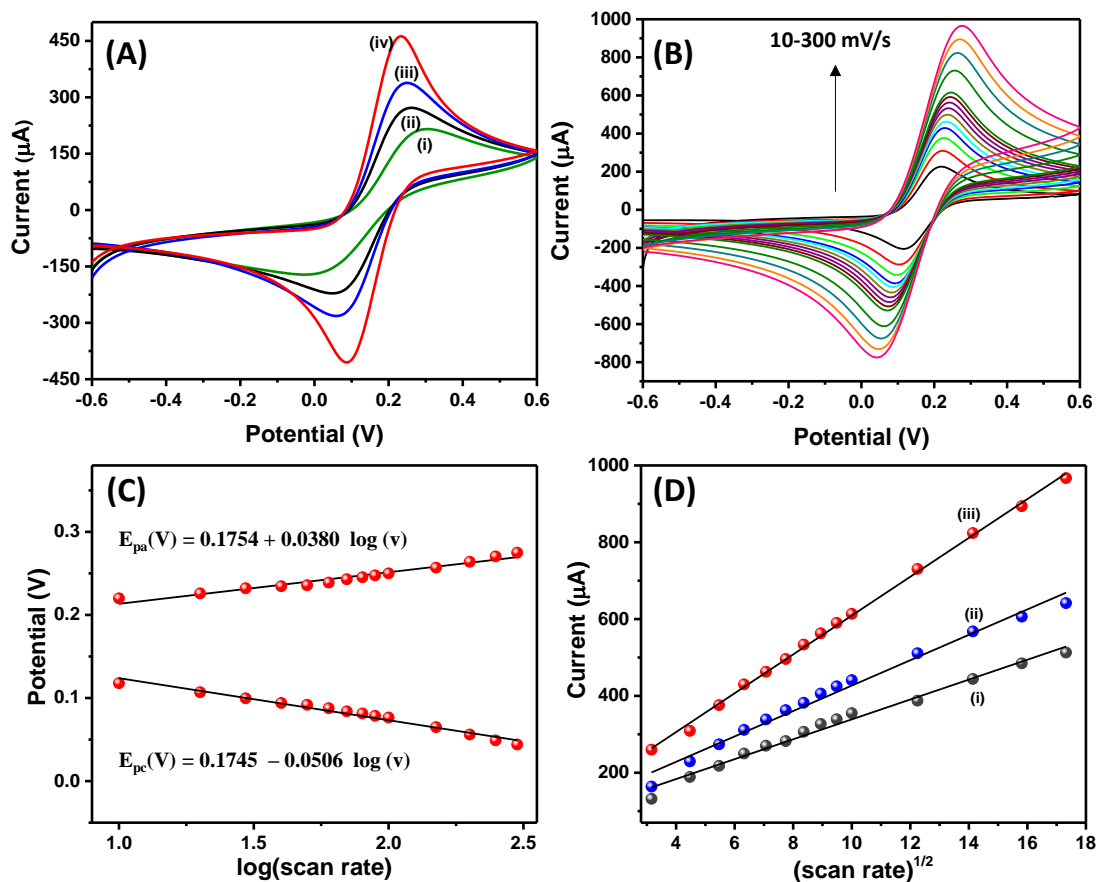
Fig. 3.5: **(A)** CV analysis of (i) ITO, (ii) GO/ITO, (iii) MgO/ITO and (iv) rGO-MgONf/ITO electrodes at 50 mV/sec **(B)** Scan rate studies (10-300 mV/s) of rGO-MgONf/ITO **(C)** Peak potential with log scan rate for rGO-MgONf/ITO electrodes and **(D)** Anodic peak current vs. square root of υ for (i) GO/ITO, (ii) MgO/ITO and (iii) rGO-MgONf/ITO electrodes in PBS (100mM, pH 7.0, 0.9% NaCl) consisting of 5mM [Fe(CN)$_6$]$^{3-/4-}$

Further, the plot of anodic peak current vs scan rate's square root depicts linear

dependency. The successive increase in oxidation peak to more positive values with

respect to scan rates signifies a diffusion control process that follows equations 3.3 to

3.5 (**Fig. 3.5D**).

77

$$I_{pa}(\mu A)\ [GO/ITO] = 79.9\ \mu A + 25.8\ \mu A\ (s/mV) * v^{1/2}\ (s/mV)^{1/2};\ R^2 = 0.975 \quad \textbf{(3.3)}$$

$$I_{pa}(\mu A)\ [MgO/ITO] = 96.1\ \mu A + 33.1\ \mu A\ (s/mV) * v^{1/2}\ (s/mV)^{1/2};\ R^2 = 0.986 \quad \textbf{(3.4)}$$

$$I_{pa}(\mu A)\ [rGO\text{-}MgONf/ITO] = 103.7\ \mu A + 50.5\ \mu A\ (s/mV) * v^{1/2}\ (s/mV)^{1/2};$$

$$R^2 = 0.993 \quad \textbf{(3.5)}$$

The electrochemical kinetics parameters were calculated based on the above equations and Randles–Ševčík equation (2.8 and 2.9). The Γ of the rGO-MgONf/ITO, GO/ITO, and MgO/ITO electrodes was calculated to be 20.53 nmol cm^{-2}, 11.98 nmol cm^{-2}, and 15.02 nmol cm^{-2}, respectively. The large values of kinetic parameters (Γ, D and A) in the case of rGO-MgONf/ITO as compared to GO/ITO and MgO/ITO indicates the efficacy of rGO-MgONf/ITO electrode for amperometric biosensing.

3.3.3. Optimization studies

The pH of solution greatly affects the electrochemical performance of Lac/rGO-MgONf/ITO electrodes has been carried out by varying the pH from 5.0 to 8.0. It has been noted that pH 7.0 had the maximum current response **(Fig. 3.6A)**. The concentration of the Lac enzyme has also been optimized by varying the enzyme concentration from 0.25 - 2 mg mL^{-1}. Electrochemical results implies an increase in current response on 0.25 - 1 mg mL^{-1} of enzyme concentration, while the current response was constant at 1 mg mL^{-1} **(Fig. 3.6B)**. Therefore, for the biosensing studies the concentration of enzyme used was 1 mg mL^{-1}.
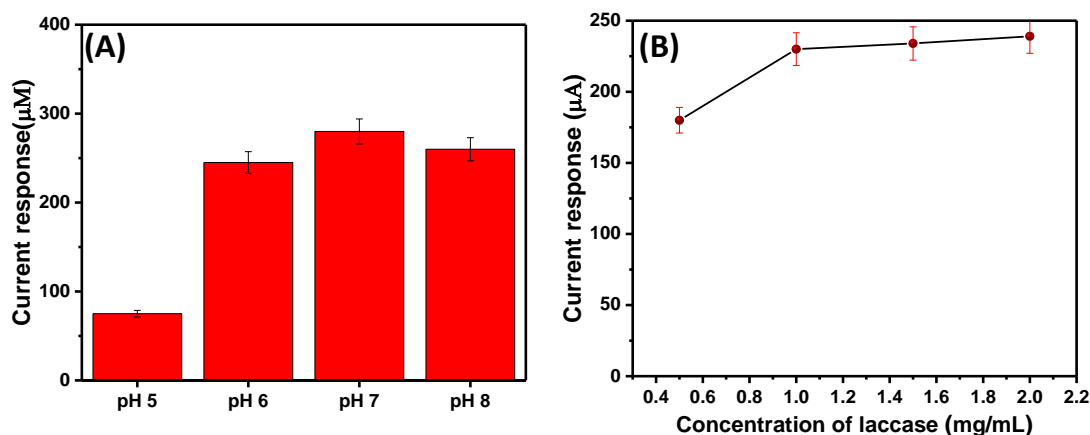
Fig. 3.6: (A) pH variation for PBS buffer to detect Hq (20 µM) and **(B)** Variation of Lac concentration for detection of 10µM Hq using Lac/rGO-MgONf/ITO electrode using Chronoamperometry

3.3.4. Electrochemical biosensing studies

The fabricated Lac/rGO-MgONf/ITO electrode has been used to study the electrochemical response towards different concentrations of Hq (1 µM -100 µM) in PBS (pH 7.0) using the chronoamperometric technique (Interval time > 0.1 s, applied potential 2 V). A decrease in current has been observed with a successive increase in Hq concentration **(Fig. 3.7A)**. The plot between saturated current responses with respect to different concentrations of Hq (C_{Hq}) shows linearity **(Fig. 3.7B)** and follows the following equation:

Current (µA) = 242.94 µA – 1.41 µA/µM × C_{Hq} (µM), R^2 =0.99 **(3.6)**

The limit of detection (equation 2.10) of Lac/rGO-MgONf/ITO electrode was found to be 0.15 µM and sensitivity (equation 2.11) was calculated to 10 µA µM^{-1} cm^{-2} respectively. It has been observed that the fabricated Lac/rGO-MgONf/ITO electrode shows an excellent sensing platform for detecting Hq in terms of LOD and linear range.
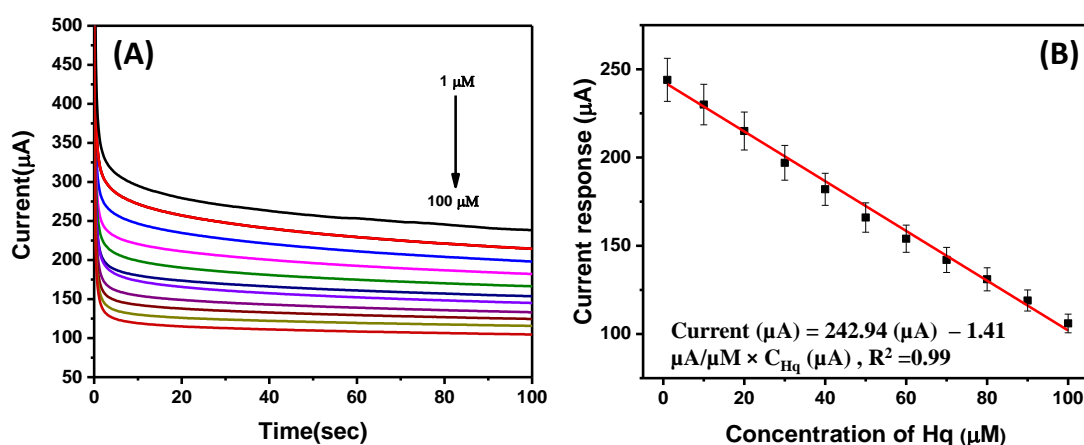
Fig. 3.7: (A) Chronoamperometric response Lac/rGO-MgONf/ITO electrode for detection of Hq (from top to bottom, 1μM- 100 μM) in PBS (pH 7.0) and **(B)** Plot depicting the linear relationship between saturation current and Hq concentration on Lac/rGO-MgONf/ITO bioelectrode.

3.3.5. Interference, reproducibility, reusability and stability studies

The specificity of fabricated biosensors was evaluated in the existence of many interfering analytes such as EDTA, sodium chloride, glucose, and uric acid. For the study, 5 folds concentration (500 μM) of each interfering analyte has been tested using the Lac/rGO-MgONf/ITO electrode.
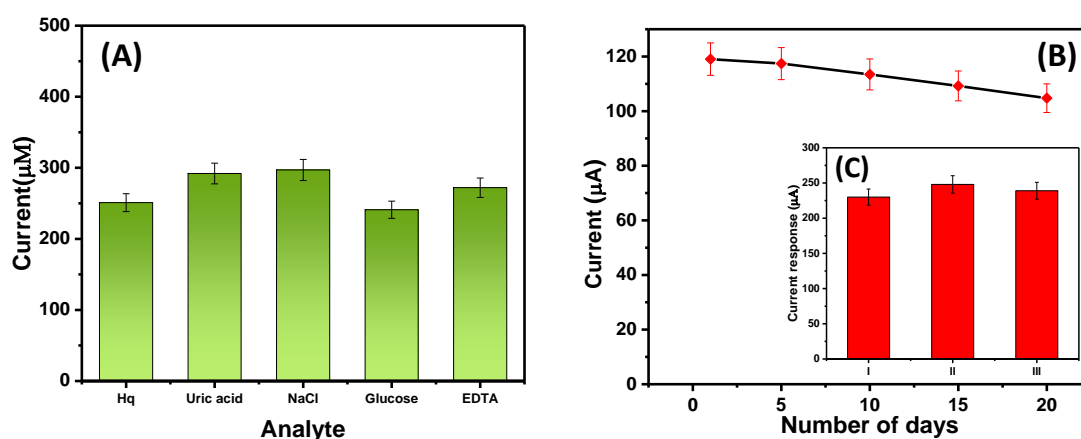
Fig. 3.8: (A) Interference study of different analytes with respect to Hq **(B)** Stability of biosensor for Hq (10 μM) detection checked for 20 days and **(C)** Reproducibility of the fabricated biosensor at 100 μM Hq**.**

It was observed that the Lac/rGO-MgONf/ITO electrode showed minimal deviation in the presence of other interfering analytes as compared to the Hq **(Fig. 3.8A)**, indicating the specificity of the Lac/rGO-MgONf/ITO electrode towards Hq detection. Further, the stability of the fabricated biosensor was measured after an interval of 5 days, and the current response was found to be reduced by 12 % after 20 days **(Fig. 3.8B)**. It indicates that the more research can be done to improve its shelf-life. To explore the reproducibility of Lac/rGO-MgONf/ITO electrode, three different electrodes of similar composition were fabricated and each electrode was subjected to 100 µM Hq concentration, the current response was then compared and resulted into a relatively low RSD of 3.21% **(Fig. 3.8C)** which signifies stability of electrode**.**

3.3.6. Real sample studies

In order to test the feasibility of the proposed Lac/rGO-MgONf/ITO electrode for on field applications, two sources of real water samples were used i.e., tap water and river water (The Ganga, U.P., India). Hq (20, 40, 60 and 80 µM) were spiked with Hq, the saturation current at each concentration was determined in both samples. The procedure was carried out three times, to determine the Hq concentration in various samples. The obtained recovery of Hq for the spiked water samples was found to be 98.4 % to 106.7 % (RSD value of 3.4 %), showing good recovery rate (**Table 3.1**). Therefore, the proposed biosensor shows promising applications for the electrochemical detection of PC.

Table 3.1: Comparative study of detection of Hq in tap water and river water using Lac/rGO-MoS$_2$/ITO electrode.

Sample	Added (µM)	Found (µM)	Recovery
Tap Water	20	20.08±0.13	100.4%
	40	41.19±0.23	102.9%
	60	59.03±0.34	98.4%
	80	79.74±0.72	99.7%
River Water	20	21.34±0.33	106.7%
	40	42.23±0.43	105.6%
	60	59.37±0.47	98.9%
	80	79.58±0.62	99.4%

3.4. Conclusions

In this chapter, we have successfully synthesized GO, MgO nanoparticles, and rGO-MgONf, which has been confirmed using structural and morphological techniques. The synergetic effect of MgO and GO has improved the conductivity and active surface area for rGO-MgONf compared to bare GO and MgO. The fabricated Lac/rGO-MgONf/ITO electrode showed good linearity, low detection limit (0.15 µM), wide linear range (1-100 µM) and high sensitivity (10 µA µM^{-1} cm^{-2}) for Hq detection. Additionally, the biosensor successfully detected Hq in river water and tap water with a remarkable recovery rate (98.4 % to 106.7 %).

The results of the present study have been published in "ChemsitrySelect" (2023), doi: 10.1002/slct.202302420

References

[1]   F. Parnianchi, M. Nazari, J. Maleki, and M. Mohebi, "Combination of graphene and graphene oxide with metal and metal oxide nanoparticles in fabrication of electrochemical enzymatic biosensors," *Int. Nano Lett.*, vol. 8, no. 4, p. 229–239, 2018.

[2]   X. Dong, M. Li, N. Feng, Y. Sun, C. Yang, and Z. Xu, "A nanoporous MgO based nonenzymatic electrochemical sensor for rapid screening of hydrogen peroxide in milk," *RSC Adv.*, vol. 5, no. 105, p. 86485–86489, 2015.

[3]   M. Patel, V. Agrawal, B. Malhotra, and S. G. Ansari, "Nanostructured Magnesium Oxide: A Suitable Material for DNA Based Biosensors," *Mater. Focus*, vol. 3, Feb. 2014.

[4]   J. Chen, B. Yao, C. Li, and G. Shi, "An improved Hummers method for eco-friendly synthesis of graphene oxide," *Carbon N. Y.*, vol. 64, p. 225–229, 2013.

[5]   R. Wahab, S. G. Ansari, M. Dar, Y. S. Kim, and H.-S. Shin, "Synthesis of Magnesium Oxide Nanoparticles by Sol-Gel Process," *Mater. Sci. Forum - MATER SCI FORUM*, vol. 558, p. 983–986, 2007.

[6]   S. K. Abdel-Aal, A. Ionov, R. N. Mozhchil, and A. H. Naqvi, "Simple synthesis of graphene nanocomposites MgO–rGO and Fe2O3–rGO for multifunctional applications," *Appl. Phys. A*, vol. 124, no. 5, p. 365, 2018.

[7]   R. Mahadevaiah, H. Lalithamba, S. B S, and R. Hanumanaika, "Synthesis of Nα-protected formamides from amino acids using MgO nano catalyst: Study of molecular docking and antibacterial activity," *Sci. Iran.*, vol. 24, 2017.

[8]   B. Sravani *et al.*, "A Pt-free graphenaceous composite as an electro-catalyst for efficient oxygen reduction reaction," *Nanoscale*, vol. 11, no. 28, p. 13300–13308, 2019.

[9]   A. H. Chowdhury, S. Ghosh, and S. M. Islam, "Flower-like AgNPs@m-MgO as an excellent catalyst for CO2 fixation and acylation reactions under ambient conditions," *New J. Chem.*, vol. 42, no. 17, p. 14194–14202, 2018.

[10] M. H. Zahir, K. Irshad, M. A. Aziz, M. Shafiullah, M. M. Rahman, and M. M. Hossain, "Shape-Stabilized Phase Change Material for Solar Thermal Energy Storage: CaO Containing MgCO3 Mixed with Polyethylene Glycol," *Energy & Fuels*, vol. 33, no. 11, p. 12041–12051, 2019.

[11] D. Thakur, C. M. Pandey, and D. Kumar, "Highly Sensitive Enzymatic Biosensor Based on Polyaniline-Wrapped Titanium Dioxide Nanohybrid for Fish Freshness Detection," *Appl. Biochem. Biotechnol.*, vol. 194, no. 8, p. 3765–3778, 2022.

[12] S. Paneru and D. Kumar, "A Novel Electrochemical Biosensor Based on Polyaniline-Embedded Copper Oxide Nanoparticles for High-Sensitive Paraoxon-Ethyl (PE) Detection," *Appl. Biochem. Biotechnol.*, vol. 195, p. 4485–4502, 2023.

CHAPTER 4

ENZYMATIC BIOSENSOR BASED ON GRAPHENE OXIDE/MoS2 NANOCOMPOSITE FOR PHENOLIC COMPOUNDS DETECTION

4.1. Introduction

In this chapter, a highly sensitive biosensing electrode has been developed using Lac enzyme supported by a hydrothermally synthesized rGO-Molybdenum disulfide (rGO-MoS$_2$) nanocomposite. Herein, an effective platform has been developed with the aim to detect Hq in tap water and river water samples **(Fig. 4.1)**. The details of the synthesis, characterization and electrochemical biosensing have been discussed in the following sections.
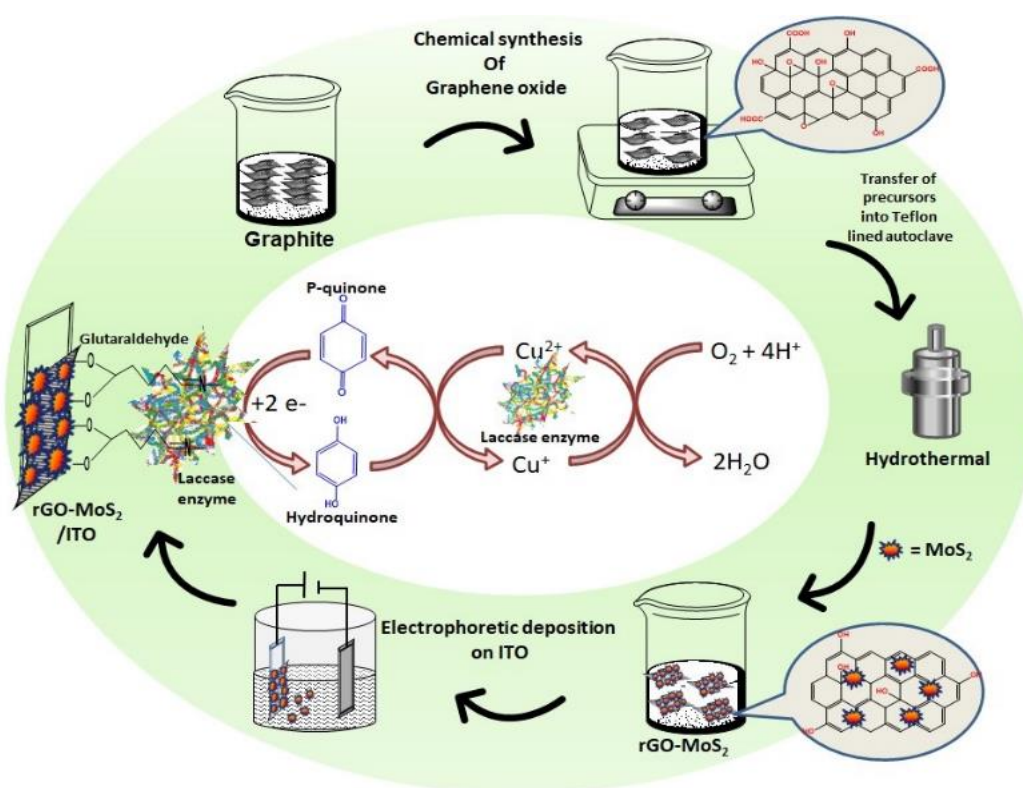
Fig. 4.1: Schematic representation showing the fabrication enzymatic biosensor based on rGO-MoS$_2$/ITO electrode for detection of Hq

4.2. Experimental Section

4.2.1. Synthesis of GO and rGO-MoS$_2$

Chapter 3 covered the process of synthesis of GO from graphite. rGO-MoS$_2$ nanocomposite, on the other hand, was synthesized utilizing a one-pot hydrothermal technique. For this, in 50 mL of DI water, GO powder (1 mg/mL) was ultrasonically shaken for one hour. Afterward, 0.825 g ammonium molybdate and 1.75 g thiourea (optimized to ~1:2 by mass of precursor of Mo and S) were added while the solution was constantly stirred for 2 h. Later, the stirring was continued while adding 25 mg of D-(+)-Glucose. The resultant suspension was then put into a hydrothermal autoclave (100 mL) with a Teflon liner and heated to 180 °C for 8 h [1]. When the hydrothermal autoclave was cooled to room temperature, the precipitate produced had been cleaned with a water/ethanol solution and centrifuged at 5000 rpm. The resulting product was dried for 12 h in an oven at 80 °C.

4.2.2. Electrophoretic deposition of rGO-MoS$_2$ nanocomposite

A pre-hydrolyzed ITO-coated glass substrate was used to deposit the synthesized rGO-MoS$_2$ nanocomposite. As of Chapter 3, Pt was employed as the counter electrode for the EPD, again at 1 cm distant to the working electrode. The rGO-MoS$_2$ nanocomposite (0.5 mg/mL) was ultrasonically sonicated in DI water prior to deposition. Several voltages were used to shorten the deposition period. It was found that a DC potential of 10 V applied for 8 s produced a uniform film on the ITO substrate. It was observed that, the application of a larger voltage caused the electrode to burn, but a lower potential resulted in no film development.

4.2.3. Fabrication of rGO-MoS₂ nanocomposite-based laccase biosensing electrode

The bioelectrode fabrication has been carried out by incubating the rGO-MoS$_2$/ITO electrode with 20 µL Lac enzyme (1 mg/mL). Prior to being utilized for biosensing application, the immobilized electrodes were preserved at 4°C.

4.3. Results And Discussion

4.3.1. Structural and morphological studies

Fig. 4.2A depicts the XRD pattern of GO and rGO-MoS$_2$ nanocomposite. XRD pattern of GO has been explained in Chapter 3. In curve (ii) belonging to rGO-MoS$_2$, the disappearance of peak at 10.4˚ gives evidence for reduction of GO under hydrothermal condition. The 002 planes of MoS$_2$ are represented by the strong peak at 14˚, but the broadening of the diffraction peak indicates the presence of layered MoS$_2$ with a lamellar structure [2]. The 100 and 006 planes of crystalline MoS$_2$ are represented by the diffraction peaks in rGO-MoS$_2$ at 32.8 and 57.3, respectively (JCPDS: 37-1492) [3].

The FT-IR spectra of the GO exhibit a peak in the range 3000-3500 cm^{-1}, associated with O-H stretching vibrations **(Fig. 4.2B(i))**. However, the stretching peak at 1397cm^{-1}, 1741 cm^{-1}, 1660 cm^{-1} and 899 cm^{-1} corresponds to O-H deformation, C=O carbonyl stretching vibrations, C=C (aromatic) vibrations and –C-H vibrations respectively. The strong peak at 1198 cm^{-1} and 1099 cm^{-1} depicts the presence of epoxy C-O-C stretching and C-O stretching vibrations. The presence of the peak at 1600 cm^{-1} and the absence of the epoxy peak in the curve (ii) indicated that GO have

undergone hydrothermal reduction **(Fig. 4.2B(ii)).** Further, the peak observed at 612

cm^{-1} in the spectra of rGO-MoS$_2$ is due to Mo-S vibration.
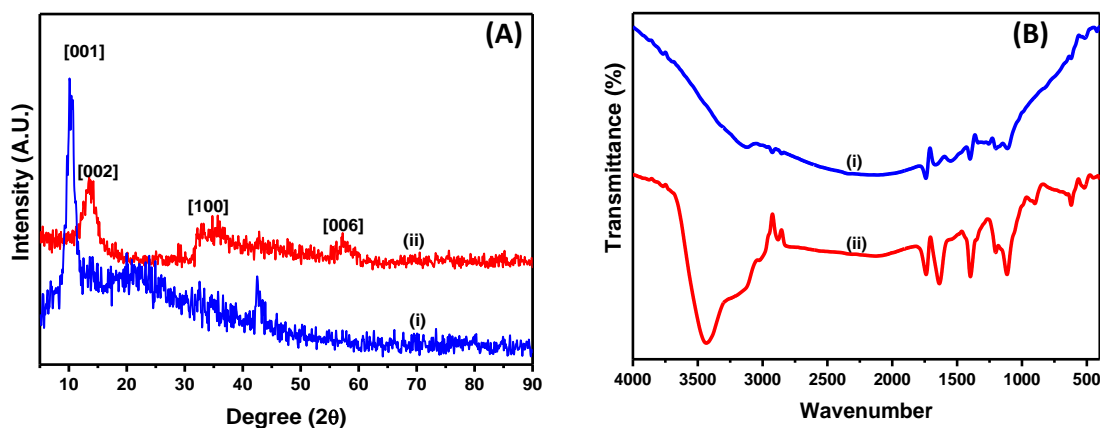
Fig. 4.2: (A) XRD and **(B)** FT-IR spectra for (i) GO and (ii) rGO-MoS$_2$ nanocomposite.

Investigation for successful synthesis of GO and rGO-MoS$_2$ nanocomposite was also

conducted using Raman spectroscopy. In the Raman spectrum **(Fig. 4.3A),** the

characteristic D band at 1349 cm^{-1}, and the G band at 1589 cm^{-1}, signifies physical

assembly of graphene which has been found correlated to the sp^2 carbon atom at E$_{2g}$

vibration mode [4]. The in-plane E$^1_{2g}$ and out-of-plane A^1_g vibrational modes of the

2H phase of MoS$_2$ are responsible for strong peaks at 335 cm^{-1} and 375 cm^{-1}

respectively in Raman spectra of rGO-MoS$_2$ nanocomposite. Even though the peaks

are a little relocated as compared to pure MoS$_2$. Mo-S bonding of MoS$_2$ has been

depicted by the presence of intense peaks at 817 cm^{-1} and 990 cm^{-1} [5]. The probable

existence of Molybdenum oxide, which results from the oxidation of MoS$_2$, may be

the cause of a tiny peak about 600 cm^{-1} [6]. Additionally, the I$_D$/I$_G$ ratio being less

than 1, reflects tiny flaws on graphene sheets.

In UV visible spectra of GO, an absorption band at around 225 nm and shoulder at 300

nm corresponds to on plane π-π* transition (C=C) and n–π* (C=O) absorption band

respectively. **(Fig. 4.3B(i))**. Whereas, in curve (ii) corresponding to rGO-MoS$_2$ peaks at 645 nm and 678 nm are due to the uninterrupted excitonic transitions lying in the Brillouin zone, referring to valence band spin-orbit splitting for MoS$_2$ **(Fig. 4.3B(ii))** [7].
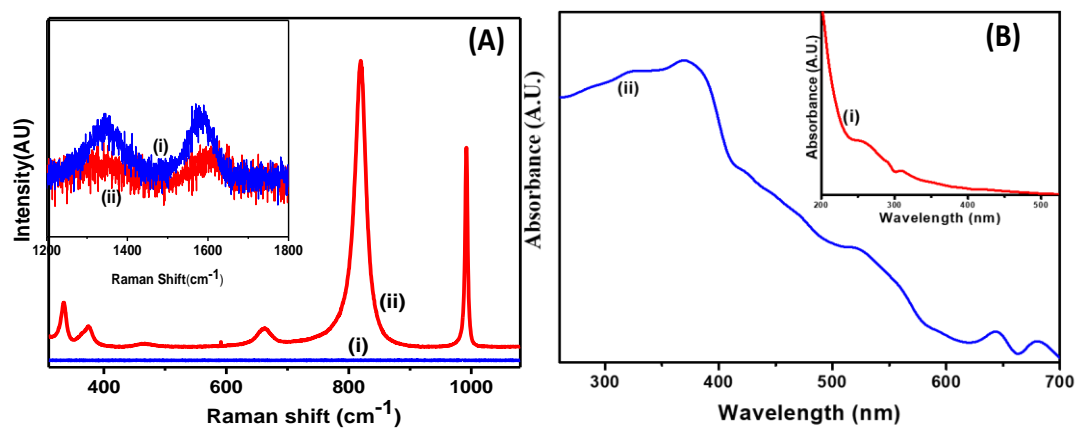
Fig. 4.3: **(A)** Raman spectra, **(B)** UV visible spectra for (i) GO and (ii) rGO-MoS$_2$ nanocomposite
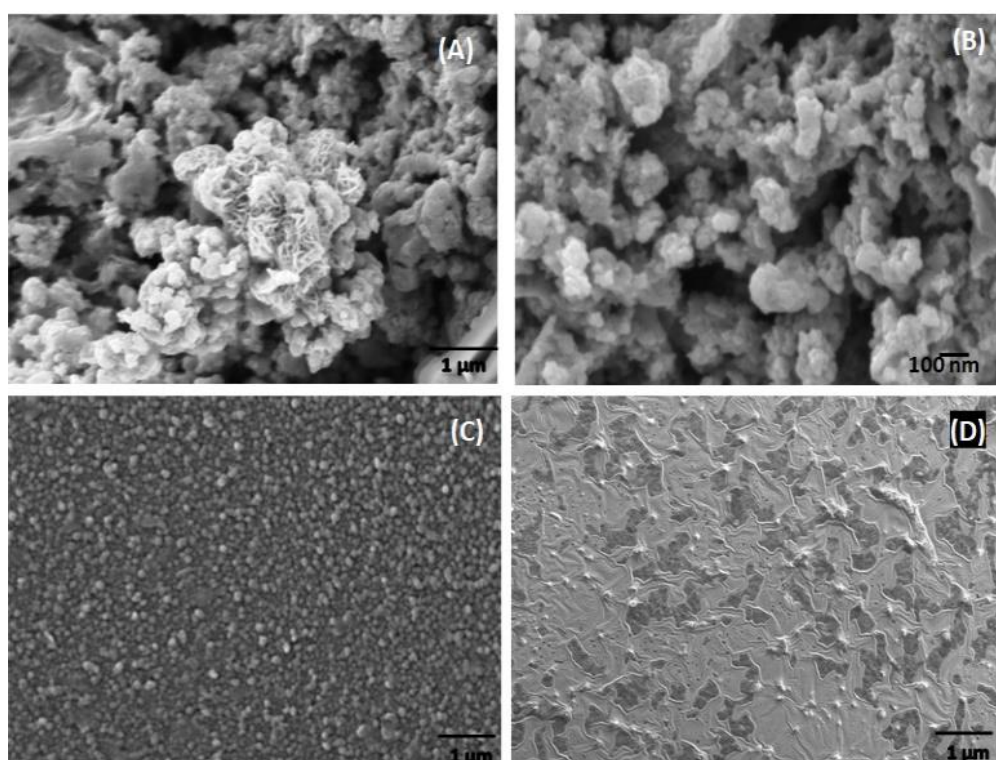
Fig. 4.4: FE-SEM images of **(A)** and **(B)** powdered rGO-MoS$_2$ nanocomposite **(C)** rGO-MoS$_2$/ITO electrode and **(D)** Lac/rGO-MoS$_2$/ITO electrode.

In **Fig. 4.4A and 4.4B**, the hierarchically intercalated structures, which have an average particle size of 100–300 nm depict the FESEM picture of the powdered rGO–MoS$_2$. The MoS$_2$ nanoparticles were found to be grown on sheets of rGO. Additionally, the ITO electrode with rGO-MoS$_2$ showed uniform rGO-MoS$_2$ deposition **(Fig. 4.4C)**. rGO-MoS$_2$ depicts highly stacked, crumpled spheres where MoS$_2$ is homogeneously dispersed onto flakes of rGO. A globular structure on the electrode surface **(Fig. 4.4D)** can be observed after the immobilization of the enzyme, which indicates that Lac was successfully immobilized.

4.3.2. Electrochemical Characterization

EIS in the frequency range 0.01-10^5 Hz (amplitude 0.01V, potential 0.01V) has been used to conduct electrochemical studies to investigate the interfacial properties of the various modified electrodes. The different parameters of the EIS have already been discussed in Chapter 3 [8]. The EIS curve **(Fig. 4.5A)** of ITO (curve iii), GO/ITO (curve ii) and rGO-MoS$_2$ /ITO (curve i) electrodes shows an R_{ct} of 415.17 Ω, 111.6 Ω, and 76.3 Ω, respectively. The reduction in the R_{ct} value for the rGO-MoS$_2$/ITO electrode is due to the synergistic properties of GO sheets and MoS$_2$, which improves the electrochemical behaviour of the electrode. On the basis of obtained R_{ct} values and equations 2.3, I$_o$ value for GO/ITO and rGO-MoS$_2$/ITO electrodes were calculated to be 4.7×10^{-4} A/cm^2 and 7.01×10^{-4} A/cm^2, respectively. Likewise, k$_o$ (equation 2.4) for the GO/ITO and rGO-MoS$_2$ /ITO electrode was calculated to 9.9×10^{-4} cm/s and 14.53×10^{-4} cm/s respectively. The greater I$_o$ and k$_o$ for the rGO-MoS$_2$/ITO electrode indicate that the electrode's conduction has increased after the modification of GO to rGO-MoS$_2$ nanocomposite [9].
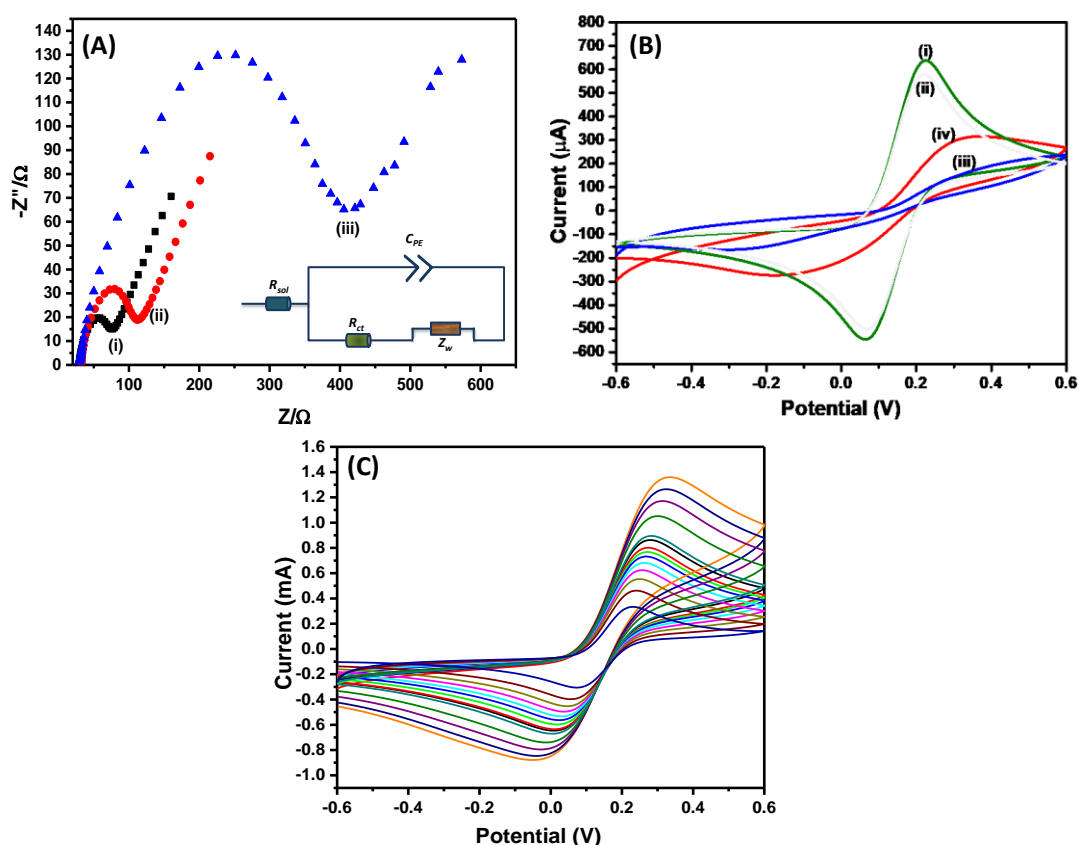
Fig. 4.5: (A) Nyquist diagram for (i) rGO-MoS$_2$/ITO electrode, (ii) GO/ITO electrode and (iii) ITO electrode (inset- circuit fit) **(B)** Comparison between CV scan (50 mV/s) of (i) rGO-MoS$_2$/ITO (ii) GO/ITO (iii) Lac/rGO-MoS$_2$/ITO electrode and (iv) Hq/Lac/rGO-MoS$_2$/ITO electrode and **(C)** Scan rate (10-300 mV/s) study of rGO-MoS$_2$/ITO electrode in PBS consisting of 5mM [Fe(CN)$_6$]$^{3-}$ and [Fe(CN)$_6$]$^{4-}$.

The CV studies performed at scan rate 50 mV/s suggests rGO-MoS$_2$/ITO electrodes shows maximum peak current (640 µA) **(Fig. 4.5B(i))** as compared to GO/ITO electrode (575.7 µA) **(Fig. 4.5B(ii))**. This enhanced peak current of rGO-MoS$_2$/ITO signify an surge in the conductivity which may be due to the superior specific surface area of the modified electrode. It has been observed that after immobilization of Lac enzyme, the peak current decreases, this can be attributed to the fact that Lac is a non-conducting protein **(Fig. 4.5B(iii))** [10]. Though, addition of Hq onto the enzymatic electrode, rises the peak current due to occurence redox activity at surface of electrode **(Fig. 4.5B(iv))**. Briefly, the redox behavior of the Lac/rGO-MoS$_2$/ITO

electrode in the presence of Hq is associated with its oxidation to p-quinone and reduction of O_2 to H_2O in the presence of the Lac [11]. The scan rate study of rGO-MoS₂/ITO electrode **(Fig. 4.5C)** results to a linear relationship between the redox peak current and square root of scan rate (υ), suggesting that the transfer of electron is a surface controlled process and follows equation 4.1 and 4.2 **(Fig. 4.6A)**. There is also a linear correlation between redox peak potentials with log υ for fabricated electrodes, referring to equations 4.3 and 4.4 **(Fig. 4.6B)**.

I_{pa}(µA) [rGO-MoS₂/ITO] = 166.1 µA + 70.6 µA (s/mV) $*$ υ $^{1/2}$ (s/mV)$^{1/2}$;

R^2 = 0.993 **(4.1)**

I_{pc}(µA) [rGO-MoS₂/ITO] = -247.4 µA – 39.07 µA (s/mV) $*$ υ $^{1/2}$ (s/mV)$^{1/2}$;

R^2 = 0.964 **(4.2)**

E_{pa}(V)[rGO-MoS₂/ITO] = 0.14029 (V) + 0.07399 (V) $*$ Log [υ (mV/s)];

R^2 = 0.996 **(4.3)**

E_{pc}(V)[rGO-MoS₂/ITO] = 0.1583 (V) – 0.0776 (V) $*$ Log [υ (mV/s)]; R^2 = 0.995 **(4.4)**
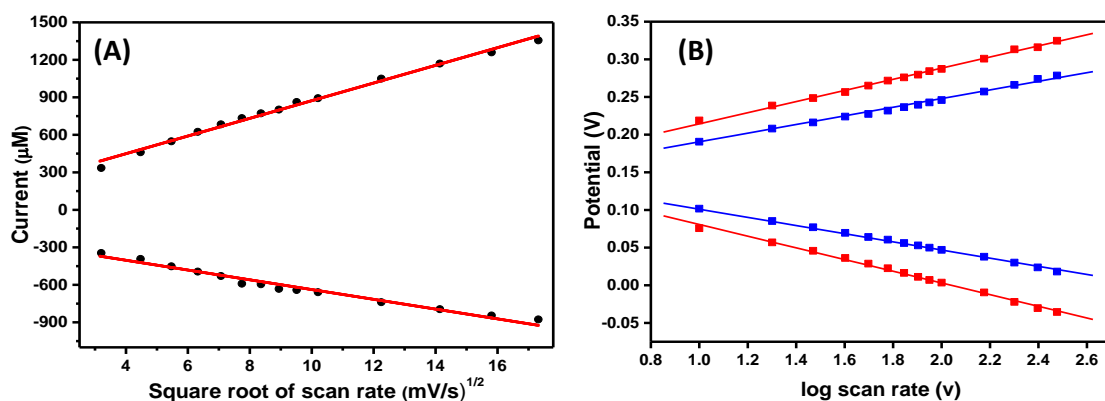
Fig. 4.6: **(A)** Peak current vs. square root of scan rate for rGO-MoS₂/ITO electrode and **(B)** Peak potential with log scan rate for (i) GO/ITO electrode and (ii) rGO-MoS₂/ITO electrode in PBS (100mM, pH 7.0, 0.9% NaCl) consisting of 5mM [Fe(CN)₆]$^{3-/4-}$

Based on the Laviron equation (2.5 to 2.7) and the linearity curve, the α for GO/ITO and rGO-MoS$_2$/ITO electrode has been found to be 0.887 and 0.901, respectively, while and K$_\alpha$ for GO/ITO and rGO-MoS$_2$/ITO is 0.146 and 0.1108 s^{-1} respectively.

A linear relationship [Eq. (4.1) and (4.2)] obtained from anodic and cathodic peak currents with square roots of respective scan rates for rGO-MoS$_2$/ITO can be used to calculate diffusion coefficient (D) using Randle-Sevick equation (equation 2.8 and 2.9). The Γ of rGO-MoS$_2$/ITO electrode was found to be 3.03×10^{-8} mol/cm^2 (D $= 25.72 \times 10^{-12}$ cm^2/s) while for GO/ITO electrode Γ was calculated to be 2.82×10^{-8} mol/cm^2 (D $= 23.04 \times 10^{-12}$ cm^2/s).

4.3.3. Optimization studies

The optimum concentration for Lac binding on the rGO-MoS$_2$/ITO electrode has been analysed using the chronoamperometry technique. Different concentration (0.5-3 mg/mL) of Lac enzyme was covalently immobilized on the rGO-MoS$_2$/ITO electrode. An increase in current was observed on the subsequent addition of Lac and reached a plateau after a concentration of 1 mg/mL **(Fig. 4.7A)**. So, the optimum concentration of 1 mg/mL has been used for further biosensing studies. On the other hand, the pH of the electrolytic solution impacts the biosensor's performance. Therefore, the Lac/rGO-MoS$_2$/ITO electrode was subjected to various pH (5.0 to 8.0) and at each pH, the change in current was measured. The results indicate that, at pH 7.0 the maximum current response was obtained, showing it to be the optimal pH for biosensing studies **(Fig. 4.7B).**
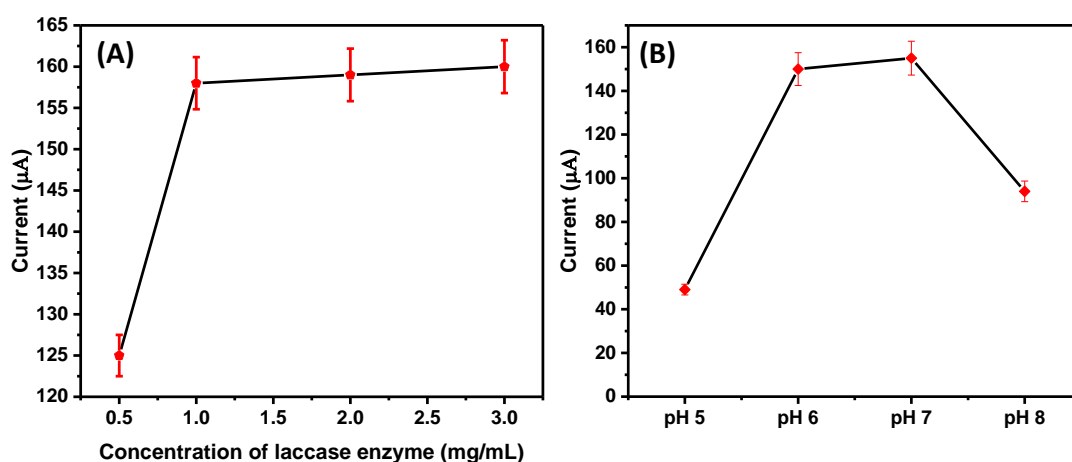
Fig. 4.7: (A) Variation of concentration of Lac enzyme immobilized onto rGO-MoS$_2$/ITO for 100 µM Hq and **(B)** Variation of pH for PBS buffer for biosensing of 100 µM Hq using Chronoamperometry

4.3.4. Electrochemical biosensing studies

The fabricated Lac/rGO-MoS$_2$/ITO electrode has been used to study the electrochemical behaviour of different concentrations of Hq, investigated using the chronoamperometry technique. The Lac/rGO-MoS$_2$/ITO electrode was subjected to an increasing concentration of Hq (1-100 µM) and it was observed that with an increase in the concentration of Hq, there was a decrease in the saturation current **(Fig. 4.8A)**. The plot between slope of saturated current vs. Hq concentrations depicts linearity in detection **(Fig. 4.8B)**. Whereas the sensitivity (S) of biosensing electrode (equation 2.11) was evaluated using the regression equation:

Current (µA) = 2.9158 µA – 0.013 µA/µM× C$_{Hq}$ (µM) having R^2 =0.991 **(4.5)**

was found to be 0.027 µA /(µMcm^2). Whereas, the limit of detection (LOD) was calculated to 0.1 µM using the equation 2.10.
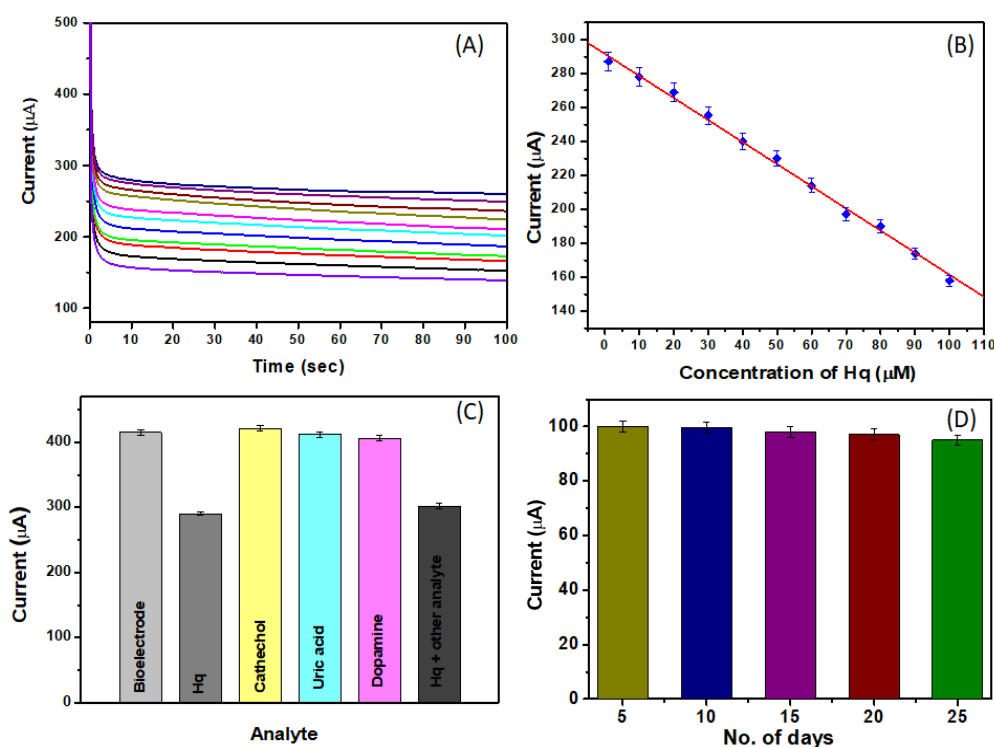
Fig. 4.8: **(A)** Chronoamperometric response of Lac/rGO-MoS$_2$/ITO electrode for detection of Hq (from top to bottom, 1 µM- 100 µM) in PBS (pH 7.0) **(B)** Plot depicting linearity between the magnitudes of saturation current and Hq concentration **(C)** Interference study of different analyte with respect to Hq (10 µM) **(D)** Stability of biosensor for Hq detection checked for 25 days.

4.3.5. Interference and reproducibility studies

The specificity of the biosensor was examined in the presence of other analytes (i.e., catechol, dopamine, and uric acid). An equal amount (10 µM) of the interfering analytes was incubated with Lac/rGO-MoS$_2$/ITO electrode and it was observed that there was no significant change in current with respect to Lac/rGO-MoS$_2$/ITO electrode **(Fig. 4.8C)**. Further, a mixture of the different interfering analyte-containing Hq was tested on the fabricated biosensor, which showed a positive response in detecting Hq. Based on the obtained results, it can be assumed that the biosensor is specific for detecting Hq even in the presence of other analytes.

The reproducibility of the biosensor was examined by using three different electrodes constructed using the same procedure. The result shows an RSD of 3.0 %, showing that the fabricated biosensor has acceptable reproducibility. Further, the long-term stability of the biosensor was also measured with the same electrode kept at 4 °C. The electrode retains 95 % of its initial response after 25 days, and after that, there was a decrease in the response, which may be due to the leaching of the Lac from the rGO-MoS$_2$/ITO electrode **(Fig. 4.8D)**.

4.3.6. Real sample analysis

The Lac/rGO-MoS$_2$/ITO electrode was exposed to water samples spiked with Hq to verify the feasibility of the developed biosensor for real sample analysis. The water sample was collected from two sources i.e., tap water and running river (Ganga) water (Bijnor, India). Both the water samples were spiked with equal concentrations of Hq (20, 40, 60 and 100 µM) and the saturation current was measured using chronoamperometry. The experiment was repeated 5 times and the calibration curve was employed to calculate the Hq concentration of different samples and the results are summarized in **Table 4.1**. The recovery of Hq for the spiked samples was 96 % to 106 %, with an RSD value of 3.2 %. Based on the result, the proposed biosensor shows promising applications for the electrochemical detection of phenolic compounds.

Table 4.1: Comparative study of detection of Hq in tap water and river water using Lac/rGO-MoS$_2$/ITO electrode using chronoamperometry.

Sample	Added (µM)	Found (µM)	Recovery
Tap Water	20	19.24±0.12	96.1%
	40	41.12±0.32	102.9%
	60	61.57±0.28	102.5%
	100	102.42±0.52	102.3%
River Water	20	21.24±0.32	106.1%
	40	42.16±0.46	105.3%
	60	61.37±0.80	102.1%
	100	103.22±0.72	103.1%

4.4. Conclusions

In this chapter, the successful synthesis of rGO-MoS$_2$ nanocomposite has been achieved using the one-pot hydrothermal method. The excellent conducting performance of rGO-MoS$_2$/ITO electrode can be attributed to the high surface area of rGO-MoS$_2$ nanocomposite and the synergistic effect of rGO and MoS$_2$, enabling an appropriate platform for enzyme immobilization. Afterward, biosensing electrode has been fabricated by immobilizing Lac onto the rGO-MoS$_2$/ITO. Furthermore, Lac/rGO-MoS$_2$/ITO electrode shows high sensitivity, specificity and reproducibility for detecting Hq. The fabricated biosensor successfully detected Hq in the tap and the river water with excellent recovery.

The results of the present study have been published in "New Journal of Chemistry" (2022), doi: 10.1039/D2NJ04285A

References

[1]   H. Liu, T. Li, Y. Liu, G. Qin, X. Wang, and T. Chen, "Glucose-Reduced Graphene Oxide with Excellent Biocompatibility and Photothermal Efficiency as well as Drug Loading," *Nanoscale Res. Lett.*, vol. 11, no. 1, p. 211, 2016.

[2]   A. Bahuguna *et al.*, "Nanocomposite of MoS2-RGO as Facile, Heterogeneous, Recyclable, and Highly Efficient Green Catalyst for One-Pot Synthesis of Indole Alkaloids," *ACS Sustain. Chem. Eng.*, vol. 5, no. 10, p. 8551–8567, 2017.

[3]   M. S. Raghu, Y. Kumar K, S. Rao, T. Aravinda, S. C. Sharma, and P. M K, "Simple fabrication of reduced graphene oxide -few layer MoS 2 nanocomposite for enhanced electrochemical performance in supercapacitors and water purification," *Phys. B Condens. Matter*, vol. 537, 2018.

[4]   J. Bao *et al.*, "Three-dimensional MoS2/rGO nanocomposites with homogeneous network structure for supercapacitor electrodes," *J. Mater. Sci.*, vol. 54, 2019.

[5]   K. Aujara, B. W. Chieng, N. Ibrahim, N. Zainuddin, and C. Ratnam, "Gamma-Irradiation Induced Functionalization of Graphene Oxide with Organosilanes," *Int. J. Mol. Sci.*, vol. 20, p. 1910, Apr. 2019.

[6]   B. C. Windom, W. G. Sawyer, and D. W. Hahn, "A Raman Spectroscopic Study of MoS2 and MoO3: Applications to Tribological Systems," *Tribol. Lett.*, vol. 42, no. 3, p. 301–310, 2011.

[7]   R. Kumar, N. Goel, R. Raliya, P. Biswas, and M. Kumar, "High-performance photodetector based on hybrid of {MoS}2 and reduced graphene oxide," *Nanotechnology*, vol. 29, no. 40, p. 404001, 2018.

[8]   Y. Liu, Y.-M. Wang, W.-Y. Zhu, C.-H. Zhang, H. Tang, and J.-H. Jiang, "Conjugated polymer nanoparticles-based fluorescent biosensor for ultrasensitive detection of hydroquinone," *Anal. Chim. Acta*, vol. 1012, p. 60–65, 2018.

[9]   O. Jalil, C. M. Pandey, and D. Kumar, "Electrochemical biosensor for the epithelial cancer biomarker EpCAM based on reduced graphene oxide modified with nanostructured titanium dioxide," *Microchim. Acta*, vol. 187, no. 5, p. 275, 2020.

[10] M. Sýs, R. Metelka, A. Frangu, K. Vytřas, and T. Arbneshi, "Electrochemical Study of Trametes Versicolor Laccase Compatibility to Different Polyphenolic Substrates," *Chemosensors*, vol. 5, no. 1. 2017.

[11] I. Zrinski *et al.*, "Evaluation of phenolic antioxidant capacity in beverages based on laccase immobilized on screen-printed carbon electrode modified with graphene nanoplatelets and gold nanoparticles," *Microchem. J.*, vol. 152, p. 104282, 2020.

CHAPTER 5

NON-ENZYMATIC ELECTROCHEMICAL DETECTION OF PHENOLIC COMPOUNDS USING MgO@rGO-MoS$_2$ NANOHYBRID

5.1. Introduction

Another attempt has been done to synthesize a novel nanohybrid to lower the detection limit for determining phenolic pollutants from water. Although GO is itself a remarkable material, however, to improve the electrochemical sensing performance of GO, it can be integrated with other metal chalcogenides, which can improve conductivity for electrochemical applications. One such metal chalcogenide is nanostructured MgO, which has been proven to show good catalytic activity and has been used to treat organic compounds from polluted water. MgO is a wide band gap semiconductor, which is non-toxic, easy to synthesize and economical [1],[2]. Additonally, it has been integrated with a highly conducting and well-explored material i.e., MoS$_2$ and finds its applications in diverse electrochemical and catalytic applications along with Chapter 4 [3].

In this chapter, we present the method of preparation, characterization and application of MgO grafted rGO-MoS$_2$ nanohybrid (MgO@rGO-MoS$_2$) for non-enzymatic detection of water-polluting phenolic compounds viz., hydroquinone (Hq) and catechol (Ctl) **(Fig. 5.1)**. Non enzymatic biosensors can be regarded as third generation biosensors under which reactions take place directly at the surface of the working electrode. Direct electrochemical detection of PC on the electrode's surface takes place via the formation phenoxy radicals and their oxidation to quinones. The

Electrode fabrication has been accomplished by optimized electrophoretic deposition of MgO@rGO-MoS$_2$ onto an ITO-coated glass substrate. All the biosensing parameters such as linear range (0.1-200 µM), detection limit, sensitivity and stability of MgO@rGO-MoS$_2$/ITO have been examined and reported in the following sections.
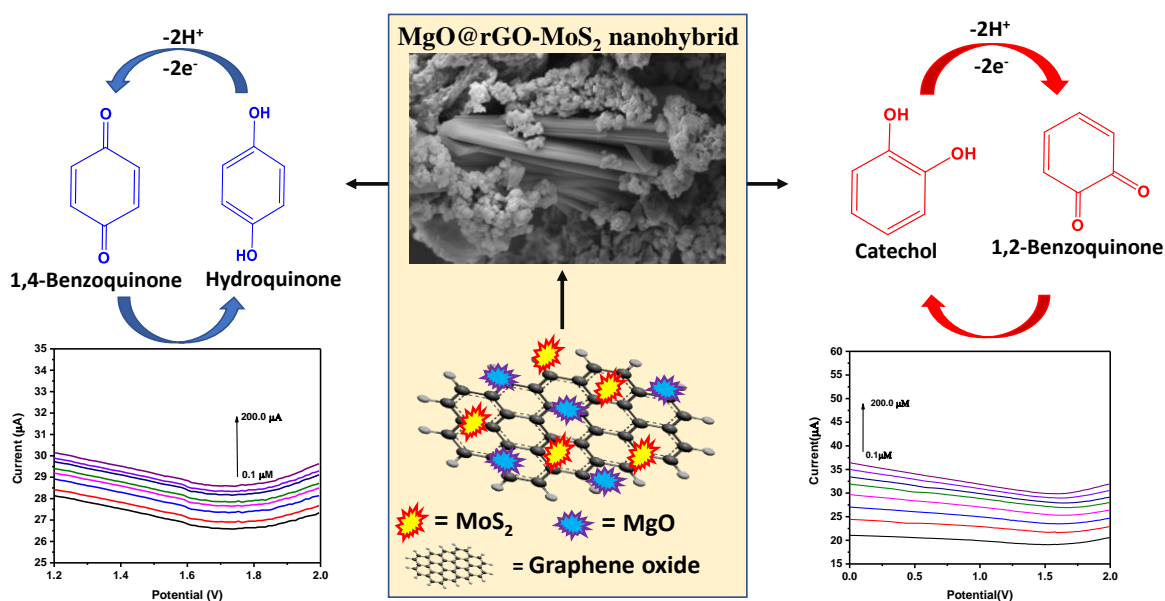
Fig. 5.1: Scheme depicting MgO@rGO-MoS$_2$ nanohybrid for detection of Hq and Ctl

5.2. Experimental section

5.2.1. Synthesis of MgO@rGO-MoS$_2$ nanohybrid

For synthesizing MgO@rGO-MoS$_2$, 0.5 mg/mL of synthesized GO was suplimented to DI water (50 mL) and ultrasonicated for 2 h. To the sonicated suspension, 1:1 molar ratio of ammonium molybdate and Magnesium nitrate hexahydrate (6.7 mM each) was added to make nanohybrid. Thereafter, 0.2 M thiourea and 30% hydrazine hydrate were added and magnetically stirred for 1 h while heating at 70 °C [5]. The obtained stagnant were then poured into Teflon-lined hydrothermal autoclave and heated at 180 °C for 8 hours. Afterwards, the hydrothermal Autoclave was left to cool

overnight and the resultant solution was washed in the water-ethanol mixture, followed by drying overnight in oven at 60 °C.

5.2.2. Fabrication of electrode

The synthesized nanohybrid was added to DI water (0.5 mg/mL) and sonicated for 2 h for electrode fabrication. The colloidal suspension so formed was used to electrophoretically deposit nanohybrid onto a pre-hydrolyzed ITO (Indium tin oxide) glass substrate using an electrophoretic deposition unit. The deposition was carried out using a two-electrode set-up where platinum was taken as a counter electrode. The deposition of GO and MgO@rGO-MoS$_2$ nanohybrid was carried out at an optimized DC potential of 10 V for 10 sec.

5.3. Results and Discussion

5.3.1. Characterization of nanohybrid

The XRD pattern of GO has been explained in Chapter 3 (**Fig. 5.2A (i)**). Whereas, the XRD pattern of MgO@rGO-MoS$_2$ nanohybrid has been shown in **Fig. 5.2A (ii)**. The sharp peaks at 14º, 33º and 57º correspond to the planes (002), (100) and (006), respectively, suggesting the formation of MoS$_2$. In contrast, the peak at 37º, 42º, 74º and 78º corresponds to the planes (111), (200), (311) and (222), respectively, suggesting the formation of MgO. The characteristic peak of GO (at 10º) vanishes due to the reduction of GO under hydrothermal conditions in the presence of hydrazine hydrate. The broadening of the diffraction peaks in spectra indicates the stacking of GO layers [5],[6].

The FTIR spectra of GO (curve i) and MgO@rGO-MoS$_2$ (curve ii) nanohybrid (**Fig. 5.2B)** shows a peak in the range 3000– 3500 cm^{-1} which can be attributed to O–H stretching vibrations. The spectra of GO show peaks at 1400 cm^{-1}, 1600 cm^{-1} and 1736 cm^{-1} corresponding to C–H vibrations, C=C aromatic vibrations and C=O carbonyl stretching vibrations, respectively. However, the same vibrations for C-H and C=C in the spectra of MgO@rGO-MoS$_2$ composite appear to shift from 1418 cm^{-1} to 1629 cm^{-1}. A peak at 1736 cm^{-1} disappears in MgO@rGO-MoS$_2$ nanohybrid due to the reduction of GO to rGO. The strong peaks at 1194 cm^{-1} and 1112 cm^{-1} shows the existence of C–O–C stretching and C–O stretching vibrations for GO and 1121 cm^{-1} and 1038 cm^{-1} for nanohybrid, respectively. The peaks near 900 cm^{-1} and 700 cm^{-1} represent Mg-O-Mg stretching, while a peak at around 600 cm^{-1} represents Mo-S vibration [7], [8].
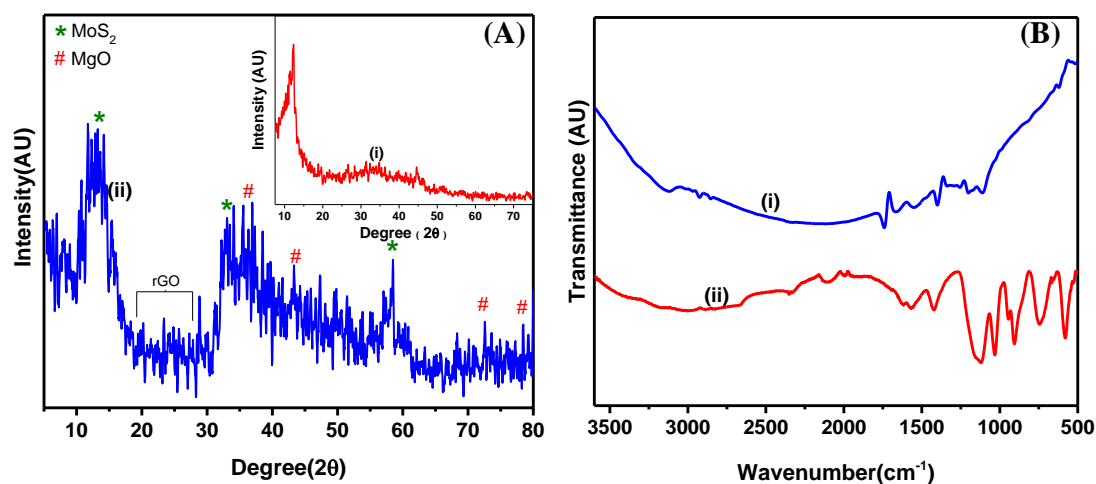
Fig. 5.2: (A) XRD and **(B)** FTIR spectra of (i) GO and (ii) MgO@rGO-MoS$_2$ nanohybrid
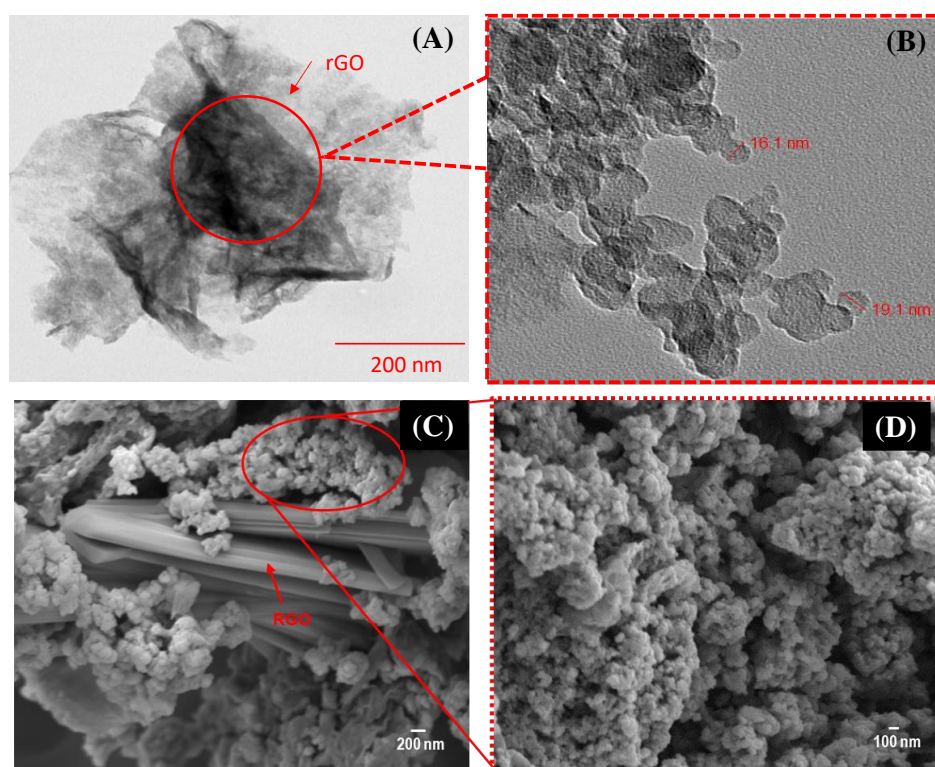
Fig. 5.3: (A) and (B) TEM images of MgO@rGO-MoS$_2$, **(C) and (D)** FE-SEM images of MgO@rGO-MoS$_2$ nanohybrid

The **Fig. 5.3A** represents TEM image of MgO@rGO-MoS$_2$ nanohybrid in which MoS$_2$ and MgO particles seems to be loaded on surface of rGO. However, on further magnification, **Fig 5.3B** reveals the size of such particles in 10 - 20 nm range. Whereas, the FESEM image of MgO@rGO-MoS$_2$ nanohybrid **(Fig. 5.3C)** indicates densely packed layers of rGO (thickness ~ 100 nm) with which metal chalcogen particles are intercalated in three-dimensional globular form. Each globular structure **(Fig. 5.3D)** appears to be comprised of a bunch of nanosheets (size ~ 70-100 nm). A magnified view of the globular structure reveals its rough surface and porous morphology. The EDX data for MgO@rGO-MoS$_2$ nanohybrid (Fig. 5.4) depicts the presence of C, O, Mo, S, and Mg on the Cu grid.
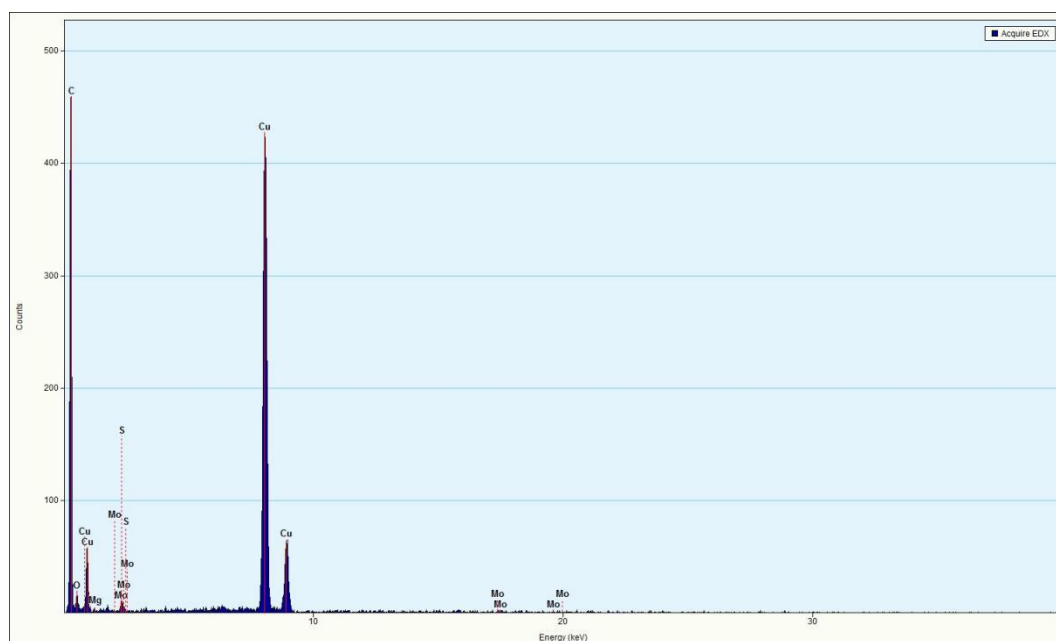
Fig. 5.4: EDX data of MgO@rGO-MoS$_2$ nanohybrid on Cu grid

5.3.2. Electrochemical Characterization of fabricated electrode

The electrochemical properties of fabricated electrodes has been conducted using CV technique. All the studies have been conducted in potential window of -0.6V to 0.6V in PBS (pH 7.0) consisting of 5mM [Fe(CN)$_6$]$^{3-}$ and [Fe(CN)$_6$]$^{4-}$. **Fig. 5.5A** represents a CV of bare ITO, GO/ITO and MgO@rGO-MoS$_2$/ITO electrodes at scan rate 50mV/s. The results indicate that MgO@rGO-MoS$_2$/ITO electrode shows enhanced redox peak currents compared to the pristine GO/ITO electrode. In the case of MgO@rGO-MoS$_2$/ITO electrode, this increment in current could be accounted for by adding MoS$_2$, which led to an increase in specific surface area and electron transfer rate.
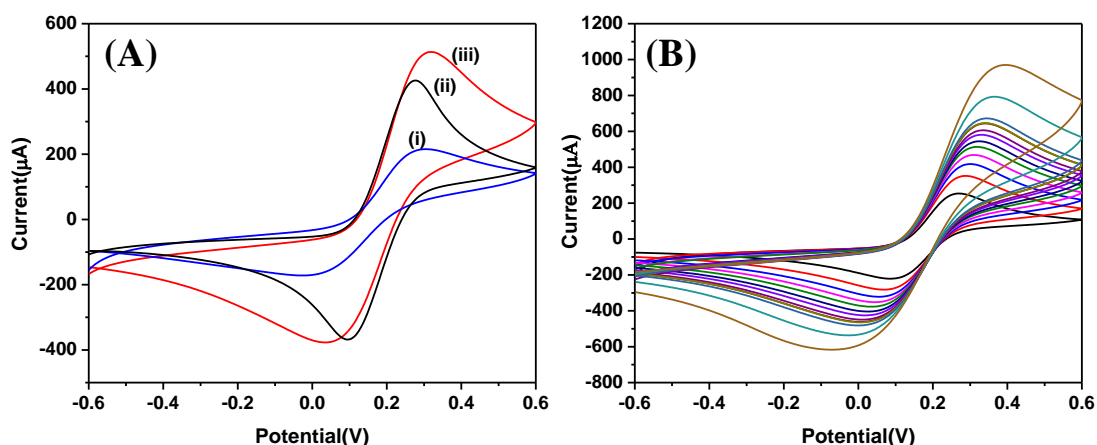
Fig. 5.5: (A) CV of (i) bare ITO (ii) GO/ITO and (iii) MgO@rGO-MoS$_2$/ITO electrode measured at 50 mV/s and **(B)** CV analysis of MgO@rGO-MoS$_2$/ITO electrode with varying scan rate (10-250 mV/s) in PBS consisting of 5mM [Fe(CN)$_6$]$^{3-}$ and [Fe(CN)$_6$]$^{4-}$.
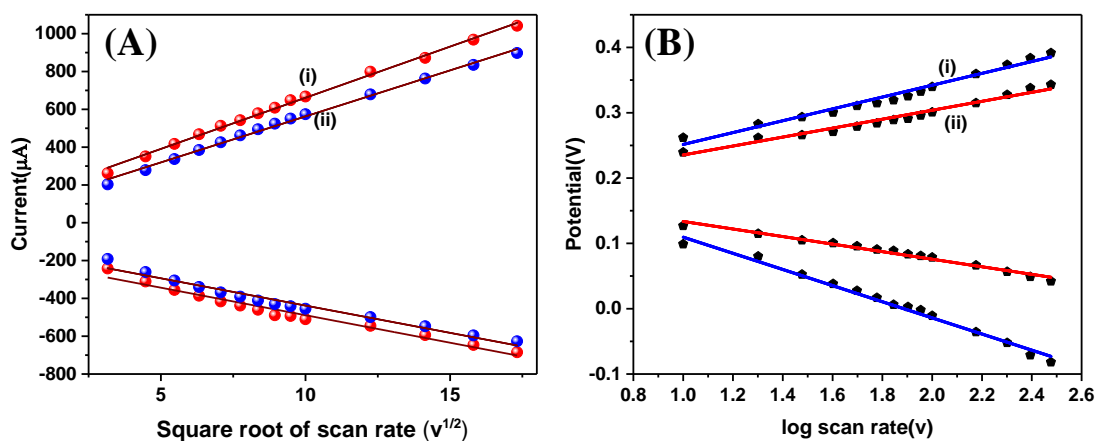
Fig 5.6: (A) Linearity plot for peak current vs. square root of scan rate and **(B)** Linearity plot for peak potential with log scan rate for (i) MgO@rGO-MoS$_2$/ITO and (ii) GO/ITO electrode in PBS (100mM, pH 7.0, 0.9% NaCl) consisting of 5mM [Fe(CN)$_6$]$^{3-/4-}$

The effect of scan rate (10-250 mV/s) for MgO@rGO-MoS$_2$/ITO electrode has been illustrated in **Fig. 5.5B**. With increases in scan rate (10 to 250 mV/s), the anodic (I$_{pa}$) and cathodic (I$_{pc}$) peak current drifts towards a higher and lower current value respectively and simultaneously. A plot between peak current and the square root of scan rate ($\upsilon^{1/2}$) (mV/s) shows a linear relationship which signifies that the transfer of electrons is diffusion controlled and follows equations 5.1 and 5.4 **(Fig. 5.6A)**. Also,

the obtained redox potential, when plotted with respect to log υ signifies linear relationship depicted by equations 5.5 and 5.8 **(Fig. 5.6B)**.

$I_{pa}(\mu A)[MgO@rGO-MoS_2/ITO] = 119.7\ \mu A + 54.1\ \mu A\ (mV/s) * υ^{1/2}; R^2 = 0.996$ **(5.1)**

$I_{pc}(\mu A)[MgO@rGO-MoS_2/ITO] = -197.2\ \mu A - 29.1\ \mu A\ (mV/s) * υ^{1/2};$

$R^2 = 0.973$ **(5.2)**

$I_{pa}(\mu A)\ [GO/ITO] = 75.4\ \mu A + 48.7\ \mu A\ (mV/s) * υ^{1/2}; R^2 = 0.995$ **(5.3)**

$I_{pc}(\mu A)\ [GO/ITO] = -149.3\ \mu A - 28.8\ \mu A\ (mV/s) * υ^{1/2}; R^2 = 0.972$ **(5.4)**

$E_{pa}(V)[\ MgO@rGO-MoS_2/ITO] = 0.161\ (V) + 0.0906\ (V) * Log\ υ; R^2 = 0.974$ **(5.5)**

$E_{pc}(V)[\ MgO@rGO-MoS_2/ITO] = 0.233\ (V) - 0.124\ (V) * Log\ υ; R^2 = 0.985$ **(5.6)**

$E_{pa}(V)[GO/ITO] = 1.667\ (V) + 0.068\ (V) * Log\ υ; R^2 = 0.971$ **(5.7)**

$E_{pc}(V)[GO/ITO] = 0.191\ (V) - 0.057\ (V) * Log\ υ; R^2 = 0.978$ **(5.8)**

Using the obtained data, α and K_α for surface-diffused electroactive species can be calculated using Laviron's equation (equation 2.5 to 2.7) for anodic and cathodic peak potentials, respectively [9]. For $[Fe(CN)_6]^{3-/4-}$, the value of α using GO/ITO and MgO@rGO-MoS_2/ITO electrode has been found to be 0.905 and 0.915, respectively, while the K_α using GO/ITO and MgO@rGO-MoS_2/ITO was found to be 0.111 and 0.045 s^{-1} respectively.

Moreover, the quantitative value of diffusion coefficient (D) and surface coverage of the electrode (Γ) were calculated using the Randles-Sevcik equation (equation 2.8 and 2.9) and the redox peak current obtained. The Γ of MgO@rGO-MoS_2/ITO electrode

was calculated to 44.4 nmol/cm^2 (D = 46.53×10^{-12} cm^2/s) whereas, for GO/ITO electrode Γ was calculated to 36.8 nmol/cm^2 (D = 32.04×10^{-12} cm^2/s). The electrochemically active surface area for MgO@rGO-MoS$_2$/ITO electrode was also calculated to 0.249 cm^2.

5.3.3. Optimization studies

The electrolytic solution's pH is the most important factor influencing electrochemical biosensing performance. The effect of pH of PBS on current was observed for pH ranging from 5.0 to 8.0 using the MgO@rGO-MoS$_2$/ITO electrode. Based on the result, pH 7.0 PBS has been used for all biosensing experiments (**Fig. 5.7A**). A comparison between the voltammetry curve of MgO@rGO-MoS$_2$/ITO electrode before and after adding 10.0 µM Hq has been depicted in **Fig. 5.7B**. It signifies the usefulness of the fabricated electrode for detecting Hq since no peak has been obtained in the former (curve i) compared to the latter (curve ii).
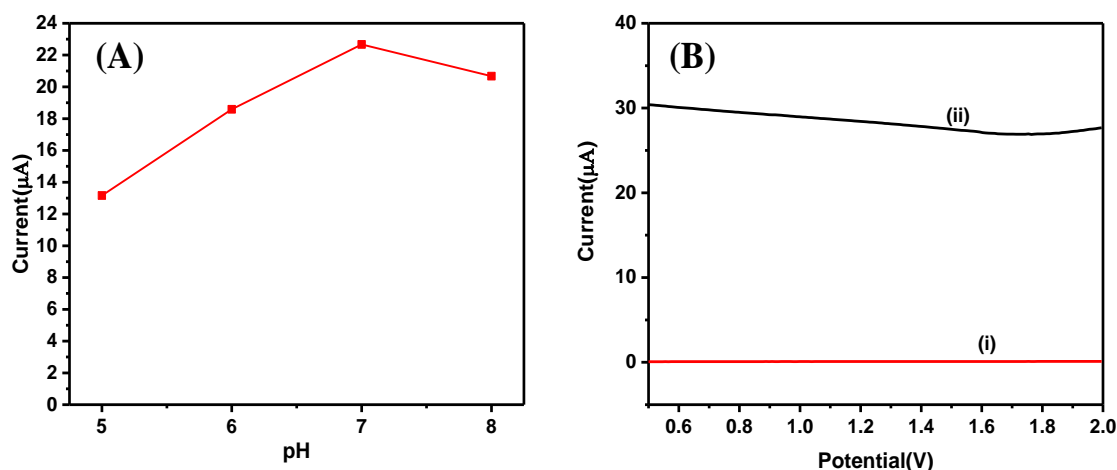
Fig. 5.7: (A) Variation of pH of buffer for MgO@rGO-MoS$_2$/ITO **(B)** Comparison of voltammetry curve for MgO@rGO-MoS$_2$/ITO (i) without analyte (ii) in the presence of Hq

5.3.4. Electrochemical biosensing response of phenolic water pollutants using fabricated electrode

Square wave voltammetry (SWV) has been applied to examine the amperomentric biosensing response of Hq. SWV is the fastest and most widely used large amplitude differential technique for the rapid and sensitive detection of different analytes [10]. The MgO@rGO-MoS$_2$/ITO electrode was subjected to an increasing concentration of Hq from 0.1–200.0 µM. It has been observed that with an increase in the concentration of analytes, the current response increases successively **(Fig. 5.8A)**. The calibration curve illustrates a linear dependence between the slope of the saturated current vs. analyte concentrations plot (**Fig. 5.8B**). The linearity equation is as follows:

Current (A) = 26.99 µA + 0.0091 µA M^{-1} * C$_{Hq}$ (µM), R^2 = 0.987   **(5.9)**

The limit of detection (LOD) was 0.086 µM (equation 2.10). However, the sensitivity of the MgO@rGO-MoS$_2$/ITO electrode (equation 2.11) was evaluated using the regression equation and was found to be 0.04 µA µM^{-1}cm^{-2} for Hq. The MgO@rGO-MoS$_2$/ITO electrode was found to have extremely high sensitivity and lower LOD as compared to enzymatic detection of Hq using laccase enzyme immobilized onto rGO-MoS$_2$/ITO electrode, which has a sensitivity of 0.027 µA µM^{-1} cm^{-2} and LOD of 0.1 µM LOD [5]. The effectiveness of synthesized material was also tested using Ctl as an analyte. It was observed that the detection of Ctl using MgO@rGO-MoS$_2$/ITO suggests 0.078 µM LOD in 0.1- 200.0 µM linear range with 0.18 µA µM^{-1} cm^{-2} sensitivity. **Fig. 5.8C** depicts the SWV results and linear relationship between the current and concentration of Ctl (**Fig. 5.8D**). It may be concluded that the production

of phenoxy radicals of Hq and Ctl takes place directly at the surface of MgO@rGO-MoS$_2$/ITO electrode, followed by their oxidation to 1,4-bezoquinone and 1,2-benzoquinone respectively [9],[11] leading to enhanced electrochemical properties.
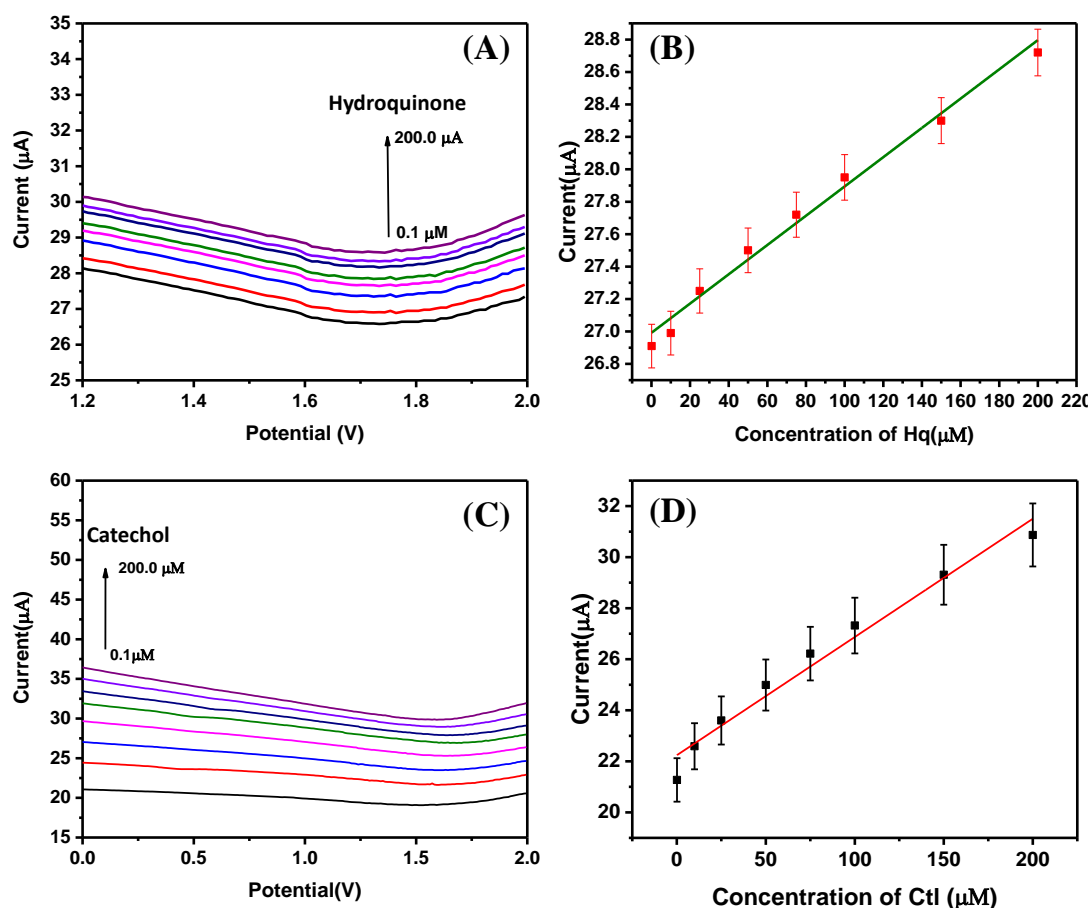
Fig. 5.8: SWV response of MgO@rGO-MoS$_2$/ITO electrode for the detection of **(A)** Hq (from bottom to top, 0.1 µM- 200.0 µM) **(B)** Plot depicting linearity between the current and concentration of Hq **(C)** Ctl (from bottom to top, 0.1 µM- 200.0 µM) **(D)** Plot depicts linearity between of current and concentration of Ctl.

5.3.5. Specificity, stability and shelf-life studies

Anti-interference ability of biosensing electrode was tested in the presence of interfering analytes such as glucose, NaCl, ethylenediaminetetraacetic acid and uric acid. For the study, 2 times the volume of concentration 0.1µM of each interfering analyte has been added along with Hq of same concentration and tested using the

MgO@rGO-MoS$_2$/ITO electrode. It has been observed that the MgO@rGO-MoS$_2$/ITO electrode showed minimal deviation in the presence of other interfering analytes as compared to the Hq **(Fig. 5.9A)**, indicating the specificity of the MgO@rGO-MoS$_2$/ITO electrode towards Hq detection. Further, in order to verify the stability of the fabricated biosensing electrode, the pre-fabricated MgO@rGO-MoS$_2$/ITO electrode was tested initially after two days and then upto 25 days, and the current was found to be decreased approximately by 8 % for Hq after 25 days **(Fig. 5.9B).** The reproducibility of the MgO@rGO-MoS$_2$/ITO electrode was tested by repeating the experiment using three different electrodes, and the results indicate relatively low RSD of 2.1% for Hq **(Fig. 5.9C).**
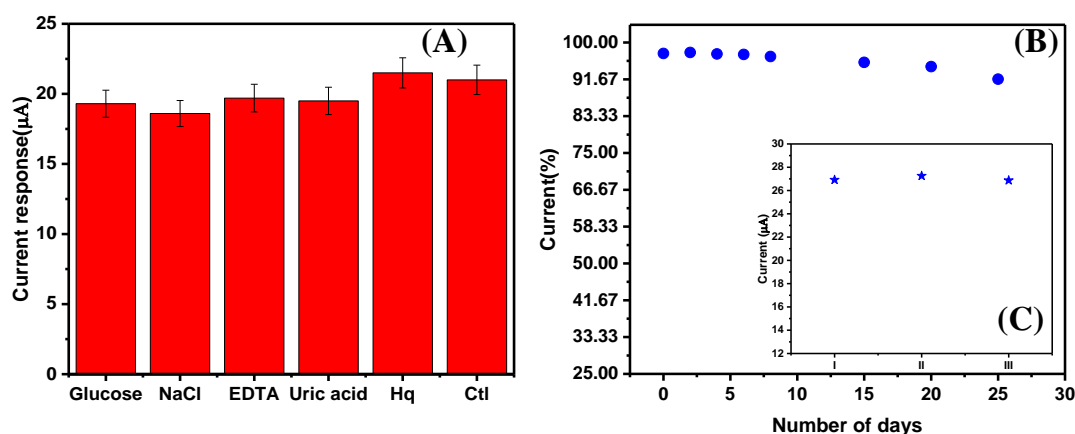
Fig. 5.9: (A) Interference study of different analytes with respect to Hq **(B)** Stability of biosensor for Hq (10 µM) detection checked for 25 days and **(C)** Reproducibility of the fabricated biosensor at 10 µM Hq using MgO@rGO-MoS$_2$/ITO electrode

5.3.6. Real sample analysis

The real sample analysis of the MgO@rGO-MoS$_2$/ITO electrode was done by spiking water samples with Hq and Ctl. In brief, the tap and river water were spkied Hq resulting to the samples with concentration 0.1µM, 10µM, 25µM and 50µM containing no PBS. The change in current obtained from real samples analysis was

used to evaluate the recovery rate of Hq in real water samples using SWV. For the spiked samples, the recovery of Hq ranged from 98.2% to 104.1% **(Table 5.1)** and the recovery of Ctl ranged from 97.8 % to 103.9% **(Table 5.2).** This suggests that the MgO@rGO-MoS$_2$/ITO electrode is a promising material for effectively detecting PC in water samples.

Table 5.1: Comparative analysis of the MgO@rGO-MoS$_2$/ITO electrode's ability to detect Hq in river and tap water using SWV.

Sample	Added (μM)	Found (μM)	Recovery
Tap Water	0.1	0.098	98.2%
	10	10.15	101.5%
	25	27.95	102.6%
	50	50.95	101.9%
River Water	0.1	0.102	102.7%
	10	10.33	103.3%
	25	28.54	103.6%
	50	52.05	104.1%

Table 5.2: Comparative analysis of the MgO@rGO-MoS$_2$/ITO electrode's ability to detect Ctl in river and tap water using SWV.

Sample	Added (μM)	Found (μM)	Recovery
Tap Water	0.1	0.097	97.8%
	10	10.07	100.7%
	25	25.23	101.6%
	50	50.6	101.2%
River Water	0.1	0.102	102.2%
	10	10.27	102.7%
	25	25.97	103.9%
	50	51.8	103.6%

5.4. Conclusion

This work reports the facile synthesis of MgO@rGO-MoS$_2$ nanohybrid using the hydrothermal method. Electrochemical characterization of MgO@rGO-MoS$_2$/ITO nanohybrid shows a highly effective surface area with excellent diffusion coefficient and high surface coverage compared to pristine GO/ITO electrodes. Further, MgO@rGO-MoS$_2$/ITO has been used for the non-enzymatic detection of Hq and Ctl. MgO@rGO-MoS$_2$/ITO offered good linearity in the concentration range 0.1 -200.0 µM with an excellent limit of detection 0.086 µM and 0.078 µM for Hq and Ctl, respectively. This non-enzymatic biosensor was found to have superior, sensitivity, stable and showed an uninterrupted current response in the presence of other analytes. The reliability of the biosensor with spiked Hq and Ctl also shows its applicability detection of phenolic compounds in tap and river water. With such advantages, the MgO@rGO-MoS$_2$-based biosensor can be used to detect other water pollutants.

The results of present study have been published in "Applied Organometallic Chemistry" (2023), doi: 10.1002/aoc.7325

References

[1] B. Wang, X. Xiong, H. Ren, and Z. Huang, "Preparation of MgO nanocrystals and catalytic mechanism on phenol ozonation," *RSC Adv.*, vol. 7, no. 69, p. 43464–43473, 2017.

[2] L. Zhou *et al.*, "Efficient degradation of phenol in aqueous solution by catalytic ozonation over MgO/AC," *J. Water Process Eng.*, vol. 36, p. 101168, 2020.

[3] G. Zhang, H. Liu, J. Qu, and J. Li, "Two-dimensional layered MoS2: rational design, properties and electrochemical applications," *Energy Environ. Sci.*, vol. 9, no. 4, p. 1190–1209, 2016.

[4] J. Chen, B. Yao, C. Li, and G. Shi, "An improved Hummers method for eco-friendly synthesis of graphene oxide," *Carbon N. Y.*, vol. 64, p. 225–229, 2013.

[5] S. Verma, C. M. Pandey, and D. Kumar, "A highly efficient rGO grafted MoS2 nanocomposite for dye adsorption and electrochemical detection of hydroquinone in wastewater," *New J. Chem.*, vol. 46, no. 44, p. 21190–21200, 2022.

[6] G. Balakrishnan, R. Velavan, K. Mujasam Batoo, and E. H. Raslan, "Microstructure, optical and photocatalytic properties of MgO nanoparticles," *Results Phys.*, vol. 16, p. 103013, 2020.

[7] R. Vinoth *et al.*, "Synergistically Enhanced Electrocatalytic Performance of an N-Doped Graphene Quantum Dot-Decorated 3D MoS 2 −Graphene Nanohybrid for Oxygen Reduction Reaction," *ACS Omega*, vol. 1, p. 971–980, 2016.

[8] M. H. Zahir, K. Irshad, M. A. Aziz, M. Shafiullah, M. M. Rahman, and M. M. Hossain, "Shape-Stabilized Phase Change Material for Solar Thermal Energy Storage: CaO Containing MgCO3 Mixed with Polyethylene Glycol," *Energy & Fuels*, vol. 33, no. 11, p. 12041–12051, 2019.

[9]   D. Cheng and X. Kan, "Simultaneous determination of dihydroxybenzene isomers based on gold dendritic/pEDOT electrochemical sensor," *J. Electroanal. Chem.*, vol. 857, p. 113741, 2020.

[10] A. Chen and B. Shah, "Electrochemical sensing and biosensing based on square wave voltammetry," *Anal. Methods*, vol. 5, no. 9, p. 2158–2173, 2013.

[11] R. Sha, S. K. Puttapati, V. V. S. S. Srikanth, and S. Badhulika, "Ultra-sensitive phenol sensor based on overcoming surface fouling of reduced graphene oxide-zinc oxide composite electrode," *J. Electroanal. Chem.*, vol. 785, p. 26–32, 2017.

CHAPTER 6

SUMMARY AND FUTURE PROSPECTS

6.1 Summary

There is a strong correlation between environmental pollution and human health, which highlights the significance of using dependable tools like biosensors to monitor pollutants in the real world. Phenols have been regarded as leading water pollutants by several health monitoring organizations. Hq and Ctl are a major threat due to their excessive use in chemical industries, leading to adverse effects on humans and aquatic animals.

The present thesis reveals the structural, morphological, and electrochemical characteristics of graphene oxide-based nanocomposites (MgO and MoS_2) and their potential for use in enzymatic and non-enzymatic biosensing applications. An ultrasensitive electrochemical biosensing platform has been developed to effectively detect such water-polluting phenolic compounds. For synthesizing nanocomposites, efforts have been made to follow eco-friendly and cost-efficient methods, which can lead to improved sensing performance. A highly active enzyme, i.e., laccase, has been chosen to be immobilized onto the electrode for enzymatic electrochemical biosensing.

In the foremost study, laccase immobilized rGO-MgONf/ITO has been used for the electrochemical detection of hydroquinone. MgO is chemically stable, environmentally friendly, and a conducting metal oxide. It has a wide band gap that allows it to bind with GO to exhibit electrocatalytic behavior. EIS and CV studies

suggest better electron transfer ability and higher surface concentration for rGO-MgONf than pristine GO. The fabricated Lac/rGO-MgONf/ITO electrode showed good linearity, low detection limit (0.15 µM), wide linear range (1-100 µM), and high sensitivity (10 µA µM^{-1} cm^{-2}) for Hq detection. Additionally, the biosensor successfully detected Hq in spiked river water and tap water with a remarkable recovery rate (98.4 % to 106.7 %).

The enzymatic transducing electrode has been fabricated by introducing MoS$_2$ onto GO. MoS$_2$ is made up of stacks of Mo atoms stacked between a few layers of sulfur atoms. Therefore, it stacks with rGO sheets, giving rise to the synergetic effect of MoS$_2$ and rGO thereby improving the electronic properties of both nanomaterials. A biosensor has been proposed by immobilizing Lac onto the rGO-MoS$_2$ nanocomposite, which shows acceptable sensitivity, specificity, and reproducibility. The excellent analytical performance of this biosensor can be attributed to the high surface area of rGO-MoS$_2$ nanocomposite that provides a suitable environment for enzyme immobilization. The lac/ rGO-MoS$_2$/ITO offers a linear 1 -100 µA range with 0.1 µM LOD. The fabricated biosensor detected Hq in the tap and the river water with good recovery.

In Chapter 5, a novel biosensing platform has been constructed using MgO@rGO-MoS$_2$/ITO electrodes for stable non-enzymatic detection of water-polluting PhC. The non-enzymatic electrode has been found to offer the least LOD, which can be attributed to better electrode sensitivity as enzymes are temperature and pH-sensitive. MgO@rGO-MoS$_2$/ITO has been used for non-enzymatic Hq and Ctl detection. MgO@rGO-MoS$_2$/ITO offered good linearity in the concentration range 0.1 -200.0

µM with an excellent LOD of 0.086 µM and 0.078 µM for Hq and cat, respectively. This non-enzymatic biosensor was found to have superior sensitivity, stability and showed an uninterrupted current response in the presence of other analytes. The validity of the biosensor with spiked Hq and Ctl also shows its applicability for the reliable detection of phenolic compounds in tap and river water. With such advantages, the MgO@rGO-MoS$_2$-based biosensor can be used to detect other water pollutants.

6.2. Future prospects

Biosensors have become a dynamic technology for diverse analytes' qualitative and quantitative determination for environmental applications, medicine, agriculture, food, or defense applications. Despite having much greater potential than laboratory-based analytical methods, a number of issues still need to be resolved. Numerous biosensors have demonstrated outstanding capabilities for pristine laboratory samples and synthetic samples; however, they are not sufficiently durable for use in the real world. The biological receptors' and the physical transducers' operational and long-term stability are tied to the current constraints. Poor sensor repeatability and selectivity in complicated matrices could be the cause of additional drawbacks. The biggest challenges for practical applications arise when the sensor is employed for in-situ actual sample monitoring outside of laboratory settings. Immobilization methods, nanotechnology, downsizing, and multisensory array conclusions are the areas of development that are anticipated to have an impact on biosensor technology.

Despite successfully detecting hydroquinone in real water samples, it is still possible to explore more about it because it's uncertain for a biosensor to ideally satisfy all the

requirements for sensing PhCs. Further, fabricated biosensing electrodes can also be explored for the detection of other phenolic compounds in wine (as antioxidants), pesticides, fruits, vegetables, and body fluids. The use of synthesized nanocomposites in conjunction with other sensing technologies, such as optoelectronic sensors, can be explored.

Future advancements in biosensor technology could focus on microfluidics-based water quality monitoring systems. The major tools used in conventional water monitoring are laboratory devices or expensive, complex handheld probes for on-site examination. Microfluidics has become an effective technology that can take the place of traditional analytical systems as an alternative. Very recently research has been done on reliable water-monitoring microfluidic devices, a platform that is both affordable and readily available on the market. Therefore, synthesized materials can be used for microfluidics-based water quality monitoring systems in the future.

Wearable sensors and artificial intelligence (AI) are two crucial areas for achieving the objective of customizing the optimal detection of analytes. Combining these two sectors allows it to effectively collect information and build wearable sensors that can track the wearer's fitness, health, and environment. AI biosensors with the necessary technical features are currently confronted with new opportunities and problems as the Internet of Things (IoT), unmanageable data, and huge health advances. Material innovation, biorecognition components, signal gathering and data processing, and intelligence decision systems are the most crucial areas that need to be explored in the future.

PUBLICATIONS

1. **S. Verma**, C.M. Pandey, D. Kumar, "A highly efficient rGO grafted MoS_2 nanocomposite for dye adsorption and electrochemical detection of hydroquinone in wastewater", New Journal of Chemistry, vol. 46, p. 21190, 2022

2. **S. Verma,** C.M. Pandey, D. Kumar, "Enzymatic biosensor based on MgO nanoparticle grafted GO nanoflakes for ultrasensitive detection of phenolic compounds from wastewater", ChemistrySelect, vol. 8, p. e202302420, 2023.

3. **S. Verma**, C.M. Pandey, D. Kumar, "Non-enzymatic electrochemical biosensor based on $MgO@rGO-MoS_2$ nanohybrid for phenolic compounds detection", Applied Organometallic Chemistry, vol. e7325, 2023.

4. **S. Verma**, D. Thakur, C.M. Pandey, D. Kumar, "Recent Prospects of Carbonaceous Nanomaterials-Based Laccase Biosensor for Electrochemical Detection of Phenolic Compounds", Biosensors, vol. 13, p. 305, 2023.

5. G. Paul, **S. Verma**, O. Jalil, D. Thakur, C.M. Pandey, D. Kumar, "PEDOT: PSS-grafted graphene oxide-titanium dioxide nanocomposite-based conducting paper for glucose detection", Polymers for Advanced Technologies, vol. 32, p. 1774-1782, 2021.

6. P. Garg, D. Thakur, **S. Verma**, O. Jalil, C.M. Pandey, D. Kumar, "Biosynthesized rGO@ZnO-based ultrasensitive electrochemical immunosensor

for bovine serum albumin detection", Journal of Applied Electrochemistry, vol. 53, p. 1449–1459, 2023.

7. O. Jalil, **S. Verma**, C.M. Pandey, D. Kumar, "Electrochemical biosensor based on TiO_2/rGO/MoS_2 nanocomposite for ultrasensitive detection of cancer biomarkers". **(Manuscript under preparation)**

# POSTER/ORAL PRESENTATION IN SYMPOSIA/CONFERENCES

- Presented Poster at 2nd International Conference on "Recent Trends in Environment Sustainable Development" held on 17th and 19th October 2019 at Vivekananda Global University, Jaipur, India on 'Competent removal of dye from wastewater using graphene oxide@molybdenum disulfide nanocomposite'.

- Presented Poster at Virtual International Conference on "Surface Chemistry" held on 27th and 28th August 2020 at Annamalai University, Annamalai Nagar, Tamil Nādu, India on 'Kinetic studies of dye adsorption using hydrothermally assisted MoS_2 functionalized graphene oxide nanocomposite'.

- Presented poster at 7th International Conference on Nanoscience and Nanotechnology (ICONN) held on 27th to 29th March 2023 at SRM Institute of Science & Technology, Chennai, India on 'rGO grafted MoS_2 nanocomposite for enzymatic electrochemical detection of hydroquinone in wastewater'.

- Attended a Virtual International Conference on "Advanced Materials Behaviour & Characterization" held from 18th to 22nd July 2020 at Mattest Research Academy, Chennai, India.

- Attended a One Day Virtual Workshop on "Accelerators/Incubation – Opportunities for Students & Faculties- Early Stage Entrepreneurs" held on 19th June 2021 at Department of Applied Chemistry, Delhi Technological University , Delhi, India .

- Attended a One Day National Seminar on "Recent Advancement in Semiconductor Devices and Materials" RASDM-2023 held in Departm-ent of Applied Physics, Delhi Technological University , Delhi, India on 30th Jan 2023.

- Attended a One Day National Seminar on " Implementation of NEP-2020 in special reference to Innovation & Entrepreneurship" held in the Department of Applied Physics, Delhi Technological University , Delhi, India on 24th Feb 2023.

- Attended a One Day National Seminar "Implementation of NEP-2020 in special reference to innovation & entrepreneurship" held on 24th Feb, 2023 organised by the Applied Physics Department, Delhi Technological University , Delhi, India.

- Attended a International Conference on "Chemical & Allied Science and their Applications" organised by Department of Applied Chemistry, Delhi Technological University , Delhi, India on 20th Jan 2023 .

NJC

PAPER
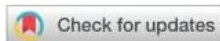
A highly efficient rGO grafted MoS$_2$ nanocomposite for dye adsorption and electrochemical detection of hydroquinone in wastewater†

Sakshi Verma,[a] Chandra Mouli Pandey [iD] *[b] and D. Kumar [iD] *[a]

A reduced graphene oxide–molybdenum disulfide (rGO–MoS$_2$) nanocomposite has been synthesized using a hydrothermal method, which has been further used to remove water pollutants and for electro-chemical detection of polyphenol compounds. The synthesized nanocomposite showed excellent adsorption efficiency and can effectively adsorb methylene blue dye (97%) from an aqueous solution using minimal adsorbent in a few minutes. A biosensing electrode has been fabricated by depositing the synthesized nanocomposite electrophoretically onto an indium tin oxide-coated glass substrate, fol-lowed by the covalent immobilization of the laccase (Lac) enzyme. The Lac/rGO–MoS$_2$ bioelectrode showed a high sensitivity (0.027 μA μM^{-1} cm^{-2}), a wide detection range (1–100 μM), and a low detection limit of 0.1 μM for hydroquinone (Hq) detection in real water (tap and river) samples with excellent recovery rate. Moreover, the proposed biosensor was found to be stable, reusable, and can potentially be used as an efficient platform for the detection of phenolic pollutants.

1. Introduction

Organic chemicals are being regressively used for development, modernization, and urbanization for industries and domestic purposes. There is always a considerable quantity of untreated effluents which run into the water system.[1] Hydroquinone (Hq) is one of the most widely used chemicals in industries and is the main constituent in photography, stabilizers in paints, dye intermediates, *etc.* However, even low concentration acquain-tance with Hq in water reservoirs can cause skin irritation and affect the nervous system.[2] It is extremely harmful to living organisms due to poor degradability. Different techniques used for Hq detection include chromatography, spectrophotometry, electrochemistry and chemiluminescence.[3,4] Among the various techniques, enzymatic electrochemical biosensors based on the laccase (Lac) enzyme are the most reliable for detecting phenolic compounds.[5] Lac consists of multi-copper atoms that can per-form oxido-reductase reactions by catalyzing phenolic com-pounds to their oxidized form and simultaneously reducing the molecular oxygen to water.[6] These laccase-based enzymatic

biosensors are accurate, sensitive, user-friendly, selective, and offer low response time, on-site monitoring of even very low concentrations of the analytes.[5]

Recently, many matrices such as graphene oxide (GO), multi-walled CNT, conducting polymers, carbon quantum dots *etc.* have been explored for immobilization of the laccase enzyme.[7–9] Among all matrices, GO has been found to be a promising nanomaterial due to its extraordinary characteristics such as large surface area, excellent conductivity, appreciable tensile strength and biocompatibility. The enhanced conductivity of reduced graphene oxide (rGO) and oxygen-containing groups helps in binding the enzymes more efficiently onto the transdu-cer surface.[10] On the other hand, metal derivative nanoparticles have diverse morphologies that provides catalytic advancement and biocompatibility.[11] In this context, metal chalcogen nano-particles can modify the surface parameters and electrochemical behavior with a tunable band-gap, thereby becoming a potential candidate for many biomedical applications.[12]

Nanostructured molybdenum disulfide (MoS$_2$) has the requisite potential to be used in biosensors as it comprises stacks of hexagonally attached layers of Mo atoms packed between a couple of layers of sulfur atoms. It posseses the capability of enhancing the electrochemical activity by stacking with rGO due to the synergetic effect of MoS$_2$ and rGO.[13,14] Although MoS$_2$ is a p-type semiconductor, restacking it with GO overcomes the gaps and improves the electronic properties of both nanomaterials.[15] rGO–MoS$_2$ nanocomposites have been

[a] *Department of Applied Chemistry, Delhi Technological University, Delhi-110042, India. E-mail: dkumar@dce.ac.in*

[b] *Department of Chemistry, Faculty of Science, SGT University, Gurugram, Haryana-122505, India. E-mail: cmp.npl@gmail.com*

Research Article

An Enzymatic Biosensor Based on MgO Nanoparticles Grafted on Reduced Graphene Oxide Nanoflakes for the Ultrasensitive Detection of Phenolic Compounds from Wastewater

Sakshi Verma, Dr. Chandra Mouli Pandey ✉, Prof. Devendra Kumar ✉

Graphical Abstract

An ultrasensitive and stable Enzymatic electrochemical biosensor based on graphene oxide-magnesium oxide nanoflakes has been fabricated to detect phenolic compound (hydroquinone) from wastewater. The synergetic effect of MgO and rGO serves as a highly conducting platform and provides a large surface area for the immobilization of the enzyme.
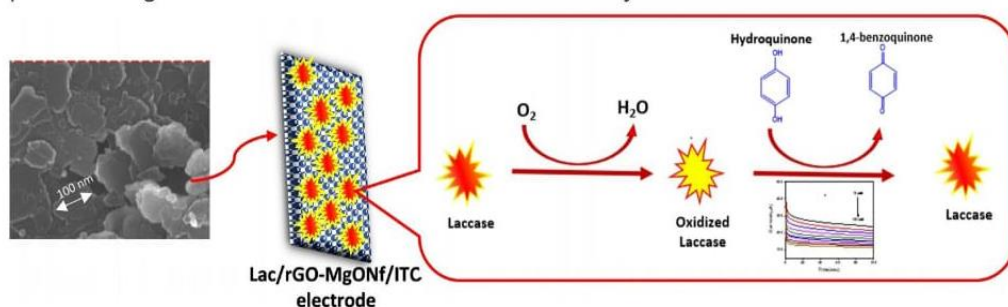
Abstract

In the present work, an enzymatic biosensor has been fabricated using reduced graphene-magnesium oxide nanoflakes (rGO-MgONf). For the fabrication of the bioelectrode, the synthesized rGO-MgONf were electrophoretically deposited onto indium tin oxide (ITO) coated glass substrate, followed by the covalent immobilization of the Laccase (lac) enzyme. Electrochemical studies show an enhanced diffusion coefficient (10.29×10^{-12} cm^2 s^{-1}), and exchange current per geometric unit area (3.66 µA cm^{-2}) on using the rGO-MgONf/ITO electrode compared to the GO/ITO and MgO/ITO electrode. Further, the fabricated biosensor (lac/rGO-MgONf/ITO) displayed excellent performance towards hydroquinone (Hq) detection, with a low limit of detection (0.15 µM), wide linear range (1.0–100.0 µM), and high sensitivity (10.0 µA µM^{-1} cm^{-2}). The selectivity study suggests that the fabricated biosensor efficiently detects Hq in wastewater. Additionally,

RESEARCH ARTICLE

Applied Organometallic Chemistry **WILEY**

Non-enzymatic electrochemical biosensor based on MgO@rGO-MoS₂ nanohybrid for phenolic compounds detection

Sakshi Verma[1] | **Chandra Mouli Pandey**[2] | **Devendra Kumar**[1]

[1]Department of Applied Chemistry, Delhi Technological University, Delhi, India

[2]Department of Chemistry, Faculty of Science, SGT University, Gurugram (Haryana), India

Correspondence

Chandra Mouli Pandey, Department of Chemistry, Faculty of Science, SGT University, Gurugram (Haryana) 122505, India.
Email: cmp.npl@gmail.com

Devendra Kumar, Department of Applied Chemistry, Delhi Technological University, Delhi 110042, India.
Email: dkumar@dce.ac.in

In the present work, efforts have been made to fabricate a non-enzymatic electrochemical biosensor based on MgO nanoparticles modified graphene oxide-molybdenum disulfide (MgO@rGO-MoS₂) nanohybrid for ultra-sensitive detection of water-polluting dihydroxy benzene compound. The one-pot hydrothermal method has been used to synthesize MgO@rGO-MoS₂ nanohybrid followed by electrophoretic deposition of the nanohybrid onto ITO-coated glass substrate. The excellent conducting and catalytic ability of MoS₂ and MgO facilitates the superior electroanalytical ability of fabricated electrodes, as revealed by the electrochemical studies, whereas the non-enzymatic approach boosts the stability and sensitivity of the transducing matrix. The fabricated biosensor exhibits linear response in the 0.1 to 200.0 μM concentration range for hydroquinone (Hqn) with a detection limit of 0.086 μM and 0.04 μA μM⁻¹ cm⁻² sensitivity. The validation of the biosensor with tap and running river water shows an outstanding recovery rate.

KEYWORDS

electrochemical biosensor, graphene, MgO, MoS₂, wastewater

1 | INTRODUCTION

Hydroquinone (Hqn) is the most commonly used dihydroxy benzene isomer in several industries, such as cosmetics, plastics, oil, pharmaceuticals, dyes, tanning, and rubber manufacturing.[1] These dihydroxy benzene isomers have been considered highly toxic compounds with poor degradability, which become one of the reasons for water pollution when these pollutants run off into waterbodies without prior treatment. The maximum permissible limit of such phenolic derivatives is 0.001 ppm in natural water and 1 ppm in inland surface water.[2] The excessive discharge of these compounds into water bodies has been found risky to human health as it leads to toxicity in soil microbes, causes skin irritation, may damage chromosomes and DNA, and so forth.[3,4] Conventional analytical techniques such as chemiluminescence,

fluorescence, chromatography, advanced oxidation, and capillary electrophoresis have been used to detect such pollutants.[5–7] However, these techniques are efficient but time-consuming, expensive, and complex.[8]

Electrochemical biosensors have been considered one of the finest approaches for detecting phenolic compounds (PhC) as they offer benefits like accuracy, real-time monitoring, quick response and are economical as well as user-friendly.[9] Various enzymatic approach has been frequently used for the specific recognition of these PhCs. However, these enzymatic biosensors possess limitations, including short-term stability due to leaching, sensitivity with respect to temperature, high cost, and require time-consuming complicated immobilization stages. Therefore, to overcome such shortcomings, the non-enzymatic approach is becoming relatively popular.[10,11]

CONTACT

PHONE:
8791593818

EMAIL:
vsakshi937@gmail.com
sakshiverma.95@gov.in

FATHER'S NAME
Mr. Dinesh Verma

ADDRESS

Current- Sagar residential complex, Naval and Physical Oceanography Laboratory, DRDO, Kochi, Kerela- 682021

Permanent- Shambha bazar, Bijnor, Uttar Pradesh- 246701

DATE OF BIRTH
20-02-1995

NATIONALITY
Indian

MARITAL STATUS
Married

LANGUAGE KNOWN
Hindi, English

SAKSHI VERMA

Scientist 'B'
Naval Physical and Oceanographic Laboratory, Kochi
Defence Research & Development Organisation

EDUCATION

AISSE (CGPA 9.4), CBSE Board, Bijnor (U.P.)
2010

AISSCE – PCM (85 %), CBSE Board, Bijnor (U.P.)
2012

B.Sc. – PCM (73 %), MJP Rohilkhand University, Bareilly (U.P.)
2016

M.Sc. – Chemistry (72 %), MJP Rohilkhand University, Bareilly (U.P.)
2018

ACHIEVEMENTS

CSIR NET SRF- Chemical Science
June 2017

GATE- Chemistry
2018, 2019, 2020, 2021, 2023

JOURNAL PUBLICATIONS

Published 5 research and 1 review paper

AWARDS

5th Research Excellence award presented for excellence in research to published a paper "PEDOT: PSS-grafted graphene oxide-titanium dioxide nanocomposite-based conducting paper for glucose detection" by Delhi Technological University on March 3, 2022.

INSTRUMENTAL SKILLS

Potentiostat/Galvanostat: Cyclic Voltammetry, Square Wave Voltammetry, Chronoamperometry, Electrochemical Impedance Spectroscopy, X-Ray Diffractometer, Fourier Transform Infrared and UV-Visible spectrophotometer